Insights into the ATP-dependent Reductive Activation of the Corrinoid/Iron-Sulfur Protein of *Carboxydothermus hydrogenoformans*

D i s s e r t a t i o n

zur Erlangung des akademischen Grades

d o c t o r r e r u m n a t u r a l i u m

(Dr. rer. nat.)

im Fach Biologie

eingereicht an der

Mathematisch-Naturwissenschaftlichen Fakultät I

der Humboldt-Universität zu Berlin

von

Diplom-Chemikerin Sandra Elisabeth Hennig

Präsident der Humboldt-Universität zu Berlin

Prof. Dr. Jan-Hendrik Olbertz

Dekan der Mathematisch-Naturwissenschaftlichen Fakultät I

Prof. Dr. Stefan Hecht

Gutachter/innen: 1. Prof. Dr. Holger Dobbek

2. Prof. Dr. Erwin Schneider

3. Prof. Dr. Peter Hildebrandt

Tag der Abgabe: 17.12.2013

Tag der mündlichen Prüfung: 12.05.2014

„Das Schönste,
was wir entdecken können,
ist das Geheimnisvolle.“

Albert Einstein

Diese Arbeit wurde von Dezember 2009 bis März 2010 an der Universität Bayreuth und von April 2010 bis Dezember 2013 an der Humboldt Universität zu Berlin angefertigt. Teile der im zeitlichen Rahmen dieser Dissertation erzielten Ergebnisse sind in folgenden Publikationen veröffentlicht:

This study was performed from december 2009 until march 2010 at the university of Bayreuth and from april 2010 to december 2013 at the Humboldt university of Berlin. Parts of the results have been published in the following publications:

S. E. Hennig, J.-H. Jeoung, S. Goetzl, H. Dobbek, Redox-dependent complex formation by an ATP-dependent activator of the corrinoid/iron-sulfur protein. *Proc. Natl. Acad. Sci. U.S.A.* **109**, 5235 (2012).

W. Meister, S. E. Hennig, J.-H. Jeoung, F. Lendzian, H. Dobbek, P. Hildebrandt, Complex Formation with the Activator RACo Affects the Corrinoid Structure of CoFeSP. *Biochemistry* **51**, 7040 (2012).

J.-H. Jeoung, S. Goetzl, S. E. Hennig, J. Fesseler, C. Wörmann, J. Dendra, H. Dobbek, The Extended Reductive Acetyl-CoA Pathway: ATPases in Metal Cluster Maturation and Reductive Activation. *Biol. Chem.* **395**, 545 (2014).

S. E. Hennig, S. Goetzl, J.-H. Jeoung, M. Bommer, F. Lendzian, P. Hildebrandt, H. Dobbek, ATP-induced protein-protein electron transfer by redox-selective partner recognition. *Submitted.*

TABLE OF CONTENTS

ZUSAMMENFASSUNG

Die Verknüpfung einer exergonischen mit einer endergonischen Reaktion zur Ermöglichung der letzteren ist eine in biologischen Systemen weit verbreitete Strategie. Energetisch benachteiligte Elektronenübertragungsreaktionen im Rahmen der reduktiven Aktivierung von Nitrogenasen, Radikal-abhängigen β,α-Dehydratasen, der zu diesen verwandten Benzoyl-CoA-Reduktasen und diversen Cobalamin-abhängigen Methyltransferasen sind gekoppelt an die Hydrolyse von ATP. Der Methylgruppentransfer des reduktiven Acetyl-CoA-Weges von *Carboxydothermus hydrogenoformans* erfordert den Co(I)-Zustand des Corrinoid/Eisen-Schwefel Proteins (CoFeSP). Um diese superreduzierte Form nach einer oxidativen Inaktivierung zu regenerieren ist ein „Reparaturmechanismus“ erforderlich. Ein offenes Leseraster (*orf7*), welches möglicherweise für eine reduktive Aktivase von Corrinoid Enzymen (RACE) kodiert, wurde in dem Gencluster der am reduktiven Acetyl-CoA-Weg beteiligten Proteine entdeckt. Im Rahmen dieser Arbeit wurde dieses potenzielle RACE Protein biochemisch und strukturell charakterisiert.

Die Übertragung eines Elektrons durch das *orf7*-Produkt ist ATP-abhängig (Rate = 1,27 ± 0,23 min^{-1} in Anwesenheit von 1 mM ATP) und stuft das Protein als ATP-abhängigen, reduktiven Aktivator von CoFeSP (RACo) ein. Analytische Gelfiltration und ITC zeigten, dass RACo – unabhängig vom eigenen Redoxzustand und der Anwesenheit von Nukleotiden – ausschließlich mit der inaktiven Co(II)-Form von CoFeSP einen stabilen Komplex bildet (K_D von 18,1 ± 2,8 nM). In dem RACo:CoFeSP-Komplex wurde eine um ca. 25-fach erhöhte spezifische ATPase-Aktivität von RACo gemessen. Mittels spektroskopischer Methoden (Resonanz-Raman- und EPR-Spektroskopie) konnte demonstriert werden, dass die Komplexbildung ausschließlich die Koordination und elektronische Struktur des Cobalamin-Kofaktors beeinflusst, während die Struktur der beiden [FeS]-Zentren nicht beeinträchtigt wird. Das Redoxpotential des Elektronenakzeptors wird durch Wechselwirkungen mit RACo um mehr als -150 mV verschoben, was durch Redoxtitrationen in Verbindung mit EPR-Spektroskopie gezeigt werden konnte. Die Kristallstruktur des RACo:CoFeSP-Komplexes, die in dieser Arbeit bis zu einer Auflösung von 2.5 Å gelöst wurde, zeigte große Umlagerungen der beweglichen N – und C–terminalen Domänen von CoFeSP. Des Weiteren deckte die Struktur auf, dass RACo in zwei verschiedenen Konformationen vorliegen kann. Die im Komplex beobachtete geöffnete Konformation liefert eine Erklärung für die im Komplex gemessene erhöhte ATPase-Aktivität. Das Kobalt des Cobalamin-Kofaktors wird

im Komplex von einem Serinrest von RACo (Ser398) koordiniert. Dieser spielt vermutlich für die oxidationsstufenabhängige Partnererkennung eine wichtige Rolle.

Auf Grundlage der in dieser Arbeit gewonnenen Ergebnisse wurde ein Mechanismus für die ATP-abhängige Aktivierung entworfen. Dieser gibt Einblicke wie die durch ATP-Hydrolyse bereitgestellte Energie einen energetisch ungünstigen Elektronentransfer ermöglichen kann. Hierzu kombiniert RACo das Ausgleichen von Bindungsenergien mit Modulationen am Elektronenakzeptor. Eine vergleichbare Strategie wurde bisher in keinem anderen ATP-abhängigen Elektronenübertragungssystem wie dem von Nitrogenasen, Radikal-abhängigen β,α-Dehydratasen oder Benzoyl-CoA-Reduktasen beobachtet und könnte ein für RACE Proteine allgemein gültige Eigenschaft darstellen.

SUMMARY

The principle of coupling an exergonic to an endergonic reaction to enable the latter is a widespread strategy in biological systems. Unfavoured electron transfer reactions in the reductive activation of nitrogenases, radical-dependent β,α-dehydratases and the related benzoyl- CoA reductases, as well as different cobalamin-dependent methyltransferases are coupled to the hydrolysis of ATP. The reductive acetyl-CoA pathway of *Carboxydothermus hydrogenoformans* relies on the superreduced Co(I)-state of the corrinoid/iron-sulfur protein (CoFeSP) that requires a "repair mechanism" in case of incidental oxidation. An open reading frame (*orf7*) coding for a putative reductive activase of corrinoid enzymes (RACE) was discovered in the gene cluster of proteins involved in the reductive acetyl-CoA pathway. In this study, this putative RACE protein was biochemically and structurally characterised.

The one-electron activation of Co(II)-CoFeSP by the *orf7* product strictly depends on ATP (rate = 1.27 ± 0.23 min^{-1} in the presence of 1 mM ATP) and classifies this protein as the ATP-dependent reductive activator of CoFeSP (RACo). RACo forms a tight complex only with the inactive Co(II) state of CoFeSP irrespective of its own redox state and the presence of nucleotides, as determined by analytic gel filtration and ITC (K_D of 18.1 ± 2.8 nM). The specific ATPase activity of RACo was enhanced approximately 25-fold upon formation of the RACo:CoFeSP complex. By spectroscopic methods (resonance Raman and EPR spectroscopy) it could be shown that complex formation affected the coordination and the electronic structure of the cobalamin cofactor exclusively but none of the present [FeS] clusters. The midpoint potential of the electron accepting cofactor is shifted by more than -150 mV by the interactions with RACo demonstrated by redox titrations combined with EPR. The crystal structure of the RACo:CoFeSP complex, which was solved to a resolution of 2.5 Å, gave further insights. Besides large movements of the flexible N- and C-terminal domain of CoFeSP, the structure revealed that RACo could exist in two different conformations. The open conformation of RACo within the complex offers an explanation for the higher ATPase activity measured for the RACo:CoFeSP complex. In the complex a serine residue (S398) of RACo directly coordinates the cobalt ion and is probably responsible for the oxidation-state dependent partner recognition.

Based on the results of this study, a mechanism for the ATP-dependent reactivation of CoFeSP was deduced providing insights into how the energy provided by ATP could trigger

this unfavourable electron transfer. The reductive activator of CoFeSP combines balance of binding energies and modulations of the electron acceptor to promote the uphill electron transfer to CoFeSP. A comparable strategy has not been observed in other ATP-dependent electron transfer systems like nitrogenases, radical-dependent β,α-dehydratases and benzoyl-CoA reductases and could be a universal feature of RACE proteins.

I. INTRODUCTION

1. Energy Transduction

"The living cell *avoids direct utilization of external energy sources in the performance of useful work. It transforms energy of these sources to a convertible energy currency, i.e. ATP,* $\Delta\mu H^+$ *or* $\Delta\mu Na^+$*, which is then spent to support various types of energy consuming processes."* (*1*)

As early as in 1941, Fritz Lipmann mint the concept of ATP being the cellular energy currency (*2*). The "first law" of bioenergetics (*1*) had to be extended later by including the protonic and sodium potentials (*3, 4*). Energy provided by those is used chemically in biosynthetic reactions (ATP synthesis, reverse electron-transfer), "osmotically" (uphill transport of solutes) and mechanically (motility of transport and other metabolic processes (*1, 5*). Or short, life depends on the interplay of energy production and consumption. How organisms convert environmental sources of light and redox energy to cellular energy sources in the form of high energy compounds like adenosin-5´-triphosphate (ATP), ion gradients or conformational energy of proteins (*6*) remains partially elusive despite intensive research. It is the discipline of bioenergetics that refers to the study of energy transformation in living organisms. Milestone in the investigation of the energy balance of organisms, e.g. of energy transduction, is the discovery of the chemi-osmotic mechanism of the coupling of electron and hydrogen transfer to phosphorylation reaction in the respiratory chain during ATP synthesis (*7*). Electron transfer reactions mediated by metal containing cofactors bound to proteins are generally important processes in nature (*8*). Whereas spontaneous electron transfer reactions occur thermodynamically "downhill" and profit energy, nature has developed different strategies to perform less favourable redox processes. The transduction of energy, e.g. the combination of one exergonic (favoured) and an endergonic (unflavoured) reaction in the manner that the overall reaction is exergonic, is achieved by connecting uphill electron transfer reactions to catalysis, atom and/or ion transfer (*1, 8*). How two energetic processes are efficiently coupled has been the main focus in (structural) bioenergetics (*5*). Electron transfer systems coupled to the hydrolysis of ATP are abundant and will be introduced in the following chapters.

2. ATP-Dependent Electron Transfer Systems

Electron donors with moderate reduction potentials are often used for the reduction of low-potential clusters. Beside flavin-based electron bifurcation (*9, 10*), less favoured electron transfer reactions are thermodynamically driven by the direct or indirect coupling to an energy providing reaction like the hydrolysis of ATP (*11*).

Over the last decades, ATP-dependent electron transfer reactions have been investigated as important parts of biological relevant reactions in the carbon and nitrogen cycle. Activators or reductases reducing low-potential metal clusters are found in nitrogenases, β,α-dehydratases and corrinoid enzymes among others (*12–17*). The by far most intensively investigated ATP-dependent electron transfer system is the reduction of dinitrogenase by the dinitrogenase reductase (*18–24*), but in the last years studies on similar systems have gained attraction. The next chapter gives a short introduction to different types of ATP-dependent activation systems found in the global carbon and nitrogen cycle.

2.1. Nitrogenase

For the synthesis of essential biological building blocks like nucleic acids, amino acids and amino sugars, all organisms require dinitrogen (N_2). Even though it is the most frequent element in the atmosphere (approximately 80 vol.%), the bioavailability of molecular nitrogen is limited due to the stable triple bond (945 kJ/ mol) (*25*). Under physiological conditions (25 °C, 1 atm) dinitrogen can be converted into ammonia, the only form of N_2, which can be transformed into biomass but the cleavage of the triple bond is a highly energy consuming reaction. The reaction within the biogeochemical nitrogen cycle is known as nitrogen fixation (*26*). It is catalysed by the oxygen sensitive protein complex nitrogenase (*12, 18, 23, 27*).

$$N_2 + 8H^+ + 8e^- + 16ATP + 16H_2O \rightarrow 2NH_3 + H_2 + 16ADP + 16P_i \quad (1)$$

Nitrogenase consists of two components, the Fe-protein (dinitrogen reductase) and the MoFe-protein (dinitrogenase) where the reduction of nitrogen takes place. Under and only under turnover conditions the two proteins assemble to form the nitrogenase complex (*12, 24, 28, 29*).

The Fe-protein or dinitrogenase reductase is a γ_2-homodimer. A [4Fe4S] cluster is located at the interface of the two subunits (Figure 1A) (*30, 31*). Every monomer of the Fe-protein contains one nucleotide-binding site with structural motifs found in nucleotide-binding switch and G-proteins, which classify the Fe-protein as a P-loop NTPase (*32*). The Walker A or P-loop motif (GXXXXGKS/T) is a widespread structural unit and triggers conformational changes upon nucleotide-binding (*20, 33–35*). The Fe-protein is the only known physiological electron donor for the MoFe-protein.

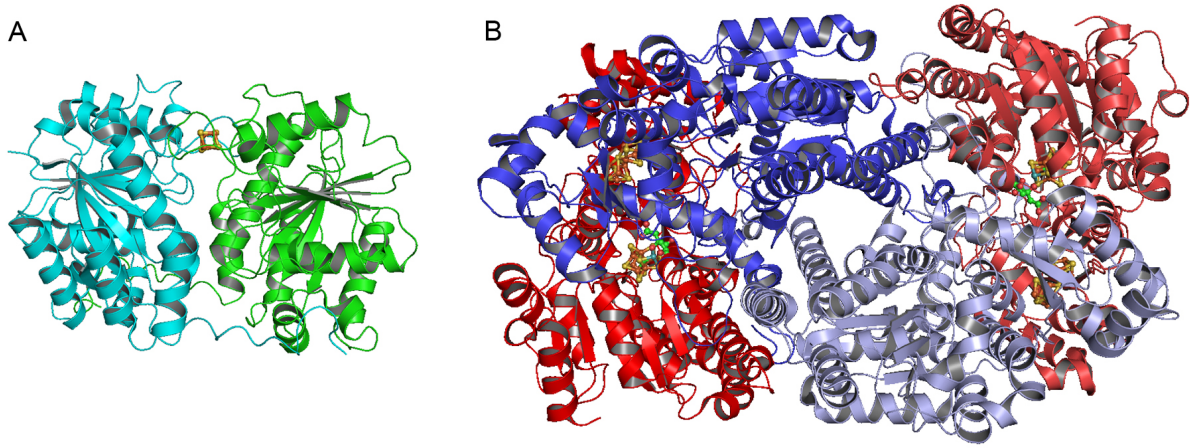

Figure 1: Nitrogenase components. (A) The two γ-subunits (cyan and green cartoon) of the Fe-protein are bridged by a [4Fe4S] cluster (stick model), which is located in the interface of the two monomers (B). The FeMo-protein is a $\alpha_2\beta_2$-heterotetramer. The α-subunits are coloured in red and the β-subunits in blue. The catalytic unit consists of one αβ-heterodimer and contains one P-and FeMo-cofactor, respectively (stick models). The figure is based on the PDB entries 1G5P (*31*) and 3U7Q (*36*).

The FeMo-protein, also called dinitrogenase, is a $\alpha_2\beta_2$-heterotetramer binding two unique metal centres, named P-cluster and FeMo-cofactor (Figure 1B). Each catalytical unit, the αβ-heterodimer, contains one P-cluster ([8Fe:7S]) and one FeMo-cofactor ([7Fe:Mo:9S:X:R-homocitrate] where the reduction of nitrogen takes place (*37, 38*). The interstitial ligand X was assigned recently as a carbon atom by analysis of a high-resolution structure and ESEEM spectroscopy (*36*).

The crystal structure of the MgADP·AlF_4^- stabilised nitrogenase complex, composed of one MoFe-protein and two Fe-proteins ($\alpha_2\beta_2(\gamma_2)$-composition), which contains two catalytic units

for the nitrogen reduction, gave first insights into the transition state during turnover conditions (Figure 2) (*28, 39*).

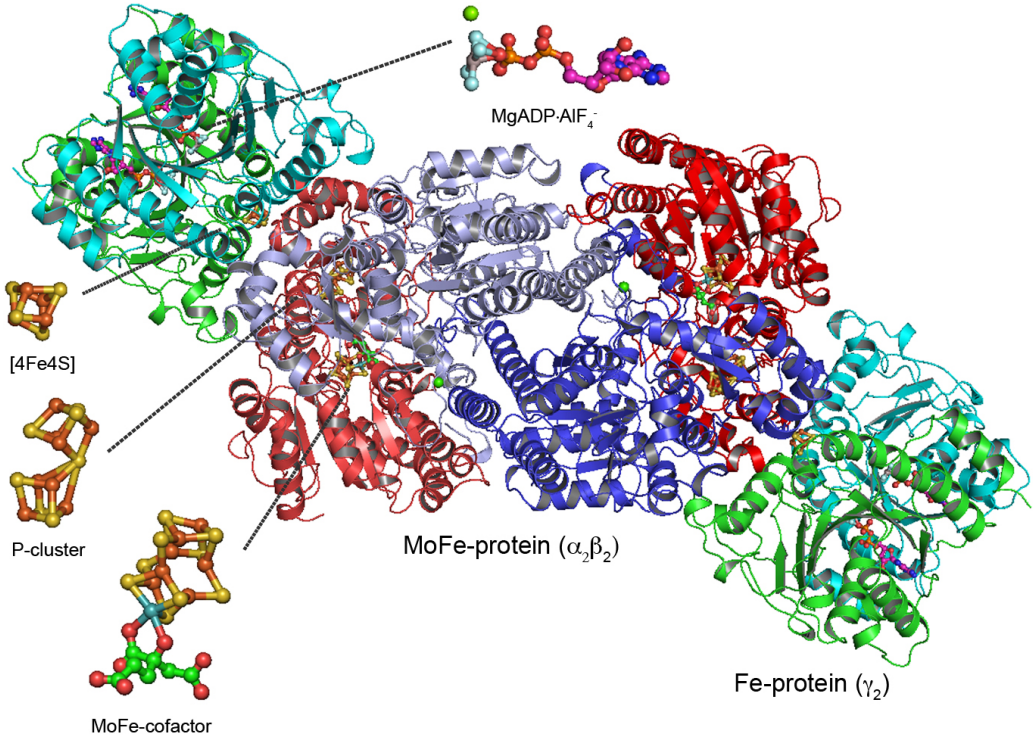

Figure 2: The nitrogenase complex. Cartoon presentation along the 2-fold symmetry axis of the nitrogenase complex based on the PDB entry 1N2C (*28*). The Fe-protein and MoFe-protein are coloured as in Figure 1. The cofactors are shown as stick models. Ca-ions are presented as green spheres.

In the complex, the [4Fe4S] cluster of the Fe-protein is located in the interface between the two proteins. An edge-to-edge distance to the P-cluster of about 14 Å was determined, which is a reasonable distance for electron transfer (Figure 3) (*40, 41*). The transfer is proposed from the reduced [4Fe4S] cluster of the Fe-protein to the P-cluster coupled to the hydrolysis of ATP. The electron is then transferred from the P-cluster to the FeMo-cofactor and is utilised in the reduction of nitrogen (*28*). Recently, a different model for the electron transfer was suggested. In the "deficit-spending" model, first an electron is transferred from the P-cluster to the active site, e.g. the FeMo-cofactor. The oxidised P-cluster shows a "deficit" and "backfill" electron transfer from the [4Fe4S] cluster of the Fe-protein to the P-cluster is necessary to fill the electron gap (Figure 3) (*22, 42, 43*).

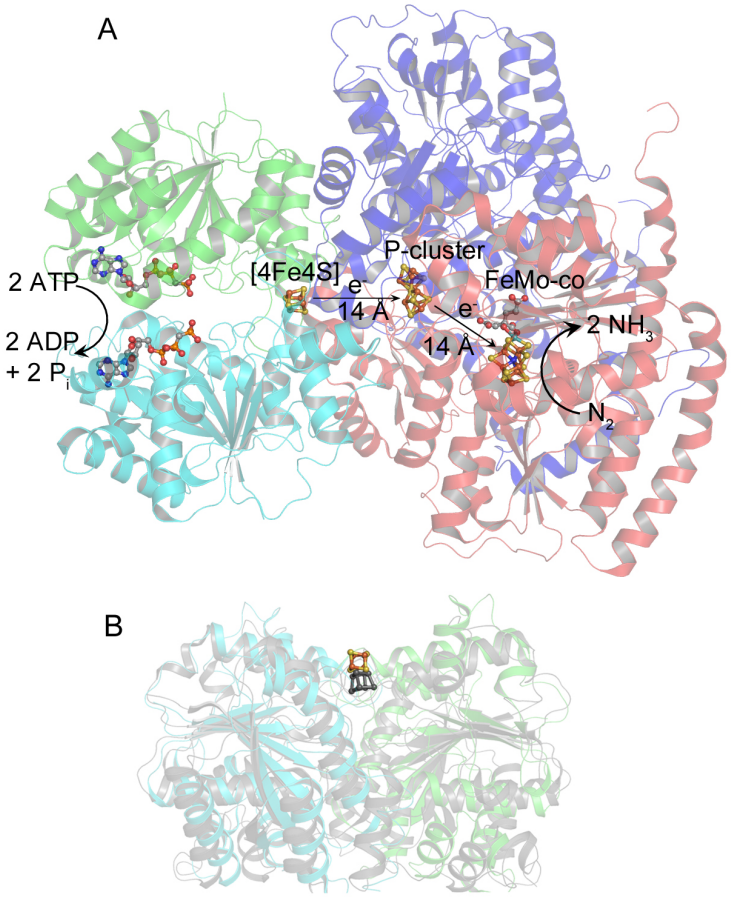

Figure 3: The nitrogenase proteins with cofactors. (A) The Fe-protein (green and cyan, left), one αβ-unit of the MoFe-protein (red and blue, right) and all cofactors are shown. The Fe-protein has two ATP molecules bound. The [4Fe4S] cluster of the Fe-protein, as well as the P-cluster and FeMo-cofactor of the MoFe-protein are represented as ball and stick models. Fe-atoms are coloured in orange, sulfur in yellow, C-atoms in grey, O-atoms in red, N-atoms in blue and the Mo-atom in cyan. This figure was prepared from the PDB file 2AFK (*29*). (B) Changes of the Fe-protein of nitrogenase. Superimposition of both Fe-protein structures (ribbon presentation) demonstrates the 5 Å-displacement of the [4Fe4S] cluster. Free Fe-protein (1G5P) (*31*) is shown in grey. The monomers of the Fe-protein in the complex (1N2C) (*28*) are coloured in green and cyan; the [4Fe4S] cluster in yellow and orange.

In all models, conformational changes of the Fe-protein act as a switch for the association and dissociation of the Fe-protein:MoFe-protein complex (*22, 35, 42*). In the complex, the [4Fe4S] cluster is displaced by 5 Å towards the surface (Figure 3B) resulting in a shortening of the edge-to-edge distance to the P-cluster (*19, 21, 22, 28, 35*).

The investigation of the electron transfer within the nitrogenase complex and of the overall mechanism of the nitrogen conversion to ammonia at the MoFe-cofactor has been fostered in the last decades. A detailed understanding of the biological nitrogen fixation, meaning the

understanding of the nitrogenase mechanism and its active site, are of common interest to promote the development of a sustainable technical process replacing the Haber-Bosch technique.

2.2. (*R*)-2-Hydroxyacyl-CoA-Dehydratase and the Related Benzoyl-CoA Reductase

2.2.1. (R)-2-Hydroxyacyl-CoA-Dehydratase

In the absence of electron acceptors such as oxygen, nitrate or sulfate, only few anaerobes, "*fusobacteria*" and *clostridia* are able to profit from α-amino acids as energy substrates. Several *Clostridia* and *Fusobacterium nucleatum* are able to ferment 12 of the 20 proteinogenous amino acids by deamination to the corresponding (*R*)-2-Hydroxyacyl-CoA derivatives (*44*). They are converted to enoyl-CoAs in an atypical dehydration reaction catalysed by the two-component system (*R*)-2-Hydroxyacyl-CoA dehydratases. The β,α-dehydration is a chemically challenging reaction due to the high pK of 40 of the β-proton, which is too high to be abstracted by a protein residue. The reaction depends on the reductive generation of ketyl radicals on the substrate (*45*). Thereby, a single highly energetic electron functions as a cofactor (Figure 4A) (*44–46*).

The 2-hydroxyacyl-CoA-dehydratases are two-component systems similar to nitrogenase and consist of component A, a reductive activator, and of component D, the dehydratase. The reductive activator is a homodimer with one [4Fe4S] cluster bridging the two monomers (Figure 4C). Like in the Fe-protein of nitrogenase, a nucleotide-binding site is present in each monomer. Its structural fold classifies the activator as a member of the ASKHA (acetate and sugar kinases, heat shock 70 protein / actin fold) protein family (*47, 48*). The dehydratase, or component D, is a heterodimer containing one or two [4Fe4S] clusters depending on the organism. The crystal structure of the (*R*)-2-hydroxyisocaproyl-CoA dehydratase from *C. difficile* revealed two [4Fe4S] clusters at a distance of 12 Å (Figure 4B). The cluster of the α-subunit belongs to the active site whereas the second cluster bound to the β-subunit, serves as a "reservoir" and protects the electron from unwanted side reactions (*49*).

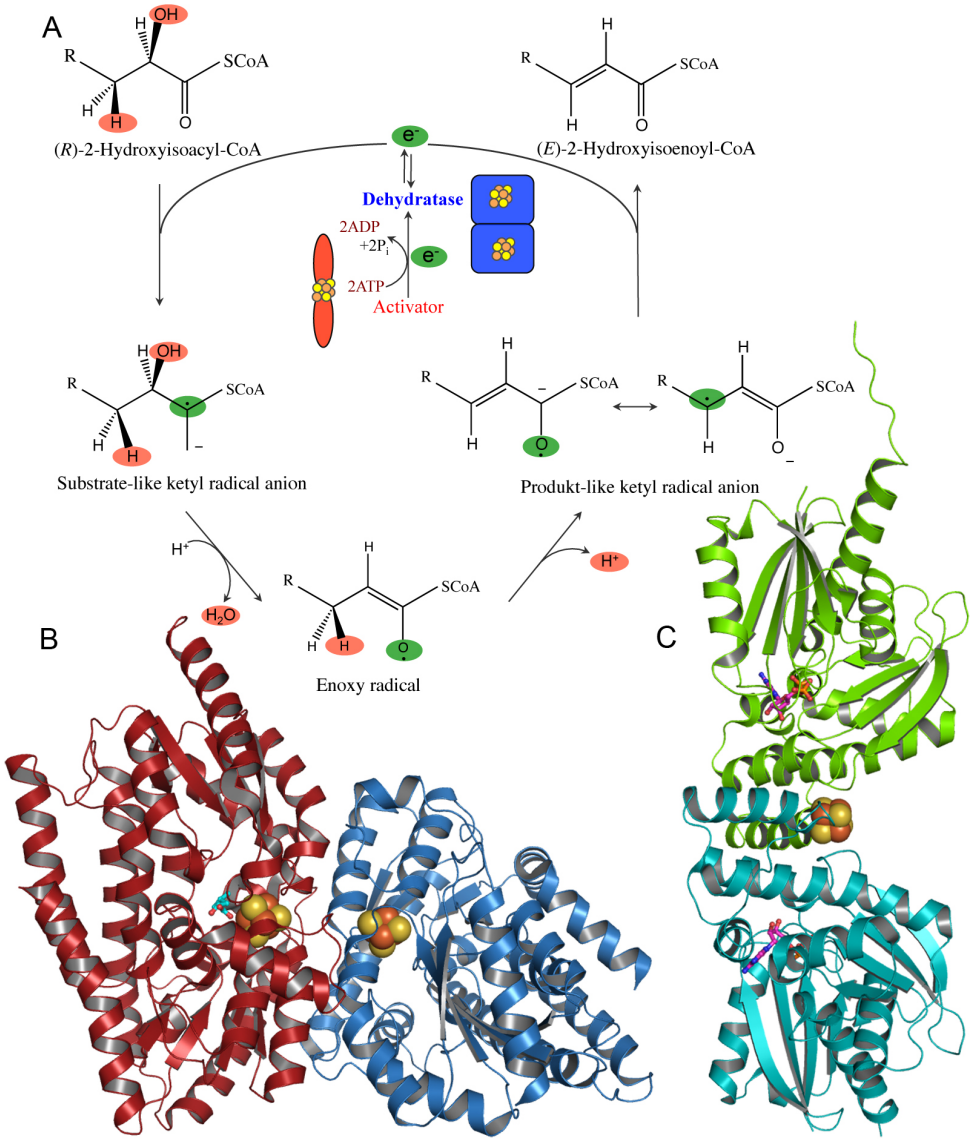

Figure 4: (*R*)-2-Hydroxyisocaproyl-CoA-Dehydratase components. (A) Proposed mechanism for the dehydration of (*R*)-2-hydroxyacyl-CoA via a ketyl radical anion including the ATP-dependent activation of the dehydratase by its activator. The scheme was adapted from Kim *et al.* (*44*). (B) The (*R*)-2-Hydroxyisocaproyl-CoA-dehydratase (component D) in its substrate bound state. The α-subunit where the 2-hydroxyisocaproyl-CoA binds in direct proximity to the α-cluster (cyan stick model) is shown in red. The β-subunit with the "reservoir"-[4Fe4S] cluster is coloured in blue. The figure was prepared based on the PDB entry 3O3M (*49*) (C) The homodimer of the activator of (*R*)-2-hydroxyisocaproyl-CoA-dehydratase is shown in its ADP-bound state. The [4Fe4S] cluster (yellow and orange spheres) bridges the two monomers (displayed in cyan and green). The nucleotide is shown as violet stick model. The figure was prepared based on the PDB 4EHT (*50*).

Crystal structures of the activator with and without bound nucleotides, indicate that the protein is able to adapt two different conformational states (Results and Discussion Figure 45) (*50*). In the nucleotide-free state, it adapts an open conformation. The binding of the nucleotide prepares component A for the formation of the dehydratase complex by switching

to the closed conformation. Complexes of 2-hydroxyisocaproyl-CoA dehydratase and its activator as well as between the activator and the (*R*)-2-hydroxyisocaproyl-CoA dehydratase from *Clostridium difficile* were observed in gel filtration experiments in the presence of the ATP-transition state analogue AMP-PNP (*50, 51*). Electron transfer from the reduced [4Fe4S] cluster of the activator within the activation complex is induced by the hydrolysis of ATP. Once activated, the dehydratase is able to fulfil about 10,000 turnovers before the electron is lost by oxidation and another ATP-dependent activation by its activator is necessary (*51, 52*).

2.2.2. Benzoyl-CoA Reductase

Benzoyl-CoA reductase from the denitrifying bacterium *Thauera aromatica* acts in the reductive dearomatisation of benzoyl-CoA. The reduction of the aromatic benzoyl-CoA to cyclohexa-1,5-diene-1-carbonyl-CoA is driven by a stoichiometric ATP hydrolysis (Figure 5A) and is catalysed by a heterotetramer with a ABCD composition (Figure 5B) (*14, 53, 54*). The complex can be divided into several heterodimeric units according to their function. The subunits A and D resemble the activator and dehydratase of 2-hydroxyglutaryl-CoA dehydratase and represent the activating module. Subunits B and C form the substrate reduction module. The activating module contains two ATP-binding sites of the ASKHA-type and a [4Fe4S] cluster is coordinated by both monomers at the interface. Benzoyl-CoA is bound to the substrate reduction module binding two additional [4Fe4S] clusters (*14, 53, 54*). The reduction of benzoyl-CoA can be described as an enzymatic Birch-like reduction (*55*). A thioester ketyl radical emerges as intermediate like in the homologous R-hydroxyacyl-CoA dehydratases. Electron transfer from the activating module to the substrate is coupled to stoichiometric ATP hydrolysis (*14, 53–55*).

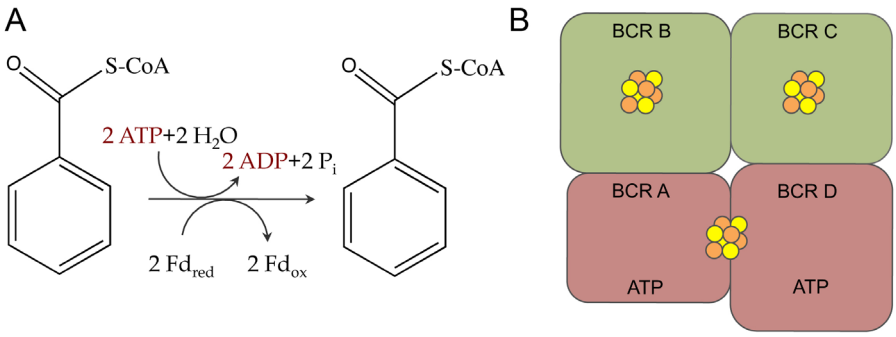

Figure 5: Reaction and composition of benzoyl-CoA reductase of *T. aromatica*. (A) ATP-dependent conversion of benzoyl-CoA catalysed by benzoyl-CoA reductase is an enzymatic Birch-like reduction. (B) Postulated subunit and cofactor composition. Subunits belonging to the same functional module are coloured equally. The substrate reduction unit is shown in green, the activating unit with two ATP-binding sites in brown, respectively. The figure was adapted from *Unciuleac et al.* (*14*).

2.3. Reductive Activators of Corrinoid-Dependent Methyltransferases: RACE Proteins

Cobalamin and the relative corrinoids act in methyl transfer reactions. Beside the well-studied cobalamin-dependent methionine synthase (*56–58*), methyltransferase systems, depending on corrinoid proteins, have been described for anaerobic bacteria and archaea (*59–62*).

Methanogenic methyltransferases catalyse the transfer of a methyl group from methanol, methylamines or dimethylsulfides to coenzyme M (*63, 64*). In their function these methyltransferases conform the *O*-demethylases found in acetogenic bacteria like *Acetobacterium dehalogenans*. *O*-demethylases mediate the cleavage of phenyl methyl ethers providing a methyl group utilised as carbon and energy source. The inducible four-component system consists of methyltransferase I and II (MT I and II), a corrinoid protein (CP) and an activating enzyme (AE) (*65, 66*). MT I and II as well as the corrinoid protein act in the methyl transfer from the substrate (for example vanillate, veratrol) to tetrahydrofolate. The MT I binds the phenyl methyl ether, catalyses the cleavage of the ether bond and transfers the methyl group to the reduced CP protein (in the reduced Co(I) state). In the second methyl transfer reaction mediated by MT II, tetrahydrofolate is converted to methyl-tetrahydrofolate, which is needed for the production of acetate in the acetogenic catabolism (Figure 6) (*65, 66*). The redox potential of the cob(II)alamin/cob(I)alamin couple is very negative (E_{SHE} < -500 mV) (*67–69*) and inactivation by incidental oxidation to Co(II) may occur in the cells

(*70*). The activating enzyme is able to regain the superreduced Co(I) state in an ATP-dependent reaction (Figure 6) (*16, 17, 65, 71–74*).

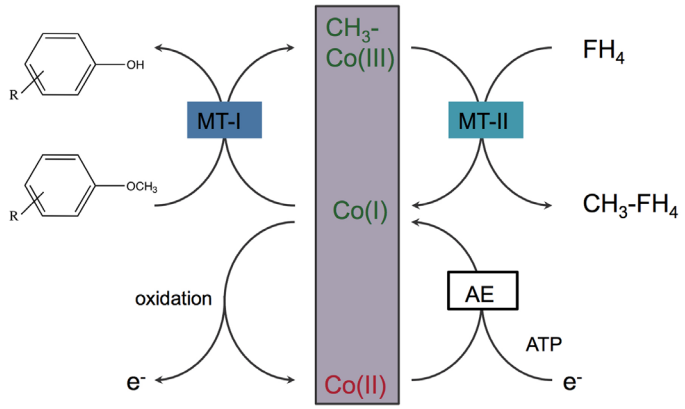

Figure 6: Scheme of the methyl transfer reactions mediated by the components of the *O*-demethylases. Methyltransferase I (MT-I) transfers the methyl group from the phenyl methyl ethers to the reduced corrinoid protein (Co(I) state) resulting in methylated corrinoid (CH_3-Co(III) state). The two active states are shown in green. MT-II catalyses the conversion of tetrahydrofolate (FH_4) to methyl-tetrahydrofolate (CH_3-FH_4). The fourth component of the *O*-demethylase, the activating enzyme, provides a "repair" mechanism in case oxidation inactivates the corrinoid protein to the Co(II) state (red). The overview was adapted from *Kaufmann et al.* (*66*).

In numerous operons of methanogenic MTs a gene, often of unknown function, is located in proximity to the genes encoding methyltransferases. RamA or MapA of the methanogenic *Methanobrevibacter smithii* and *Methanosarcina bakeri* for example code for an activating enzyme similar to the AE of *O*-demethylase (*15*). Schilhabel and co-workers compared the operons of the *O*-demethylase with operons of methanogenic MT systems as well as with operons of other anaerobic methyltransferases and CODH/ACS complexes (*17*). The majority of hits with sequence identities between 20 and 41 % are metal binding proteins of unknown function that are grouped in the Cluster of Orthologous Groups (COG) database as COG3894. Whereas the bacterial proteins show motifs of a N-terminally bound [2Fe2S] cluster, patterns of 2x [4Fe4S] cluster were identified in archaeal sequences (Figure 7) (*17*).

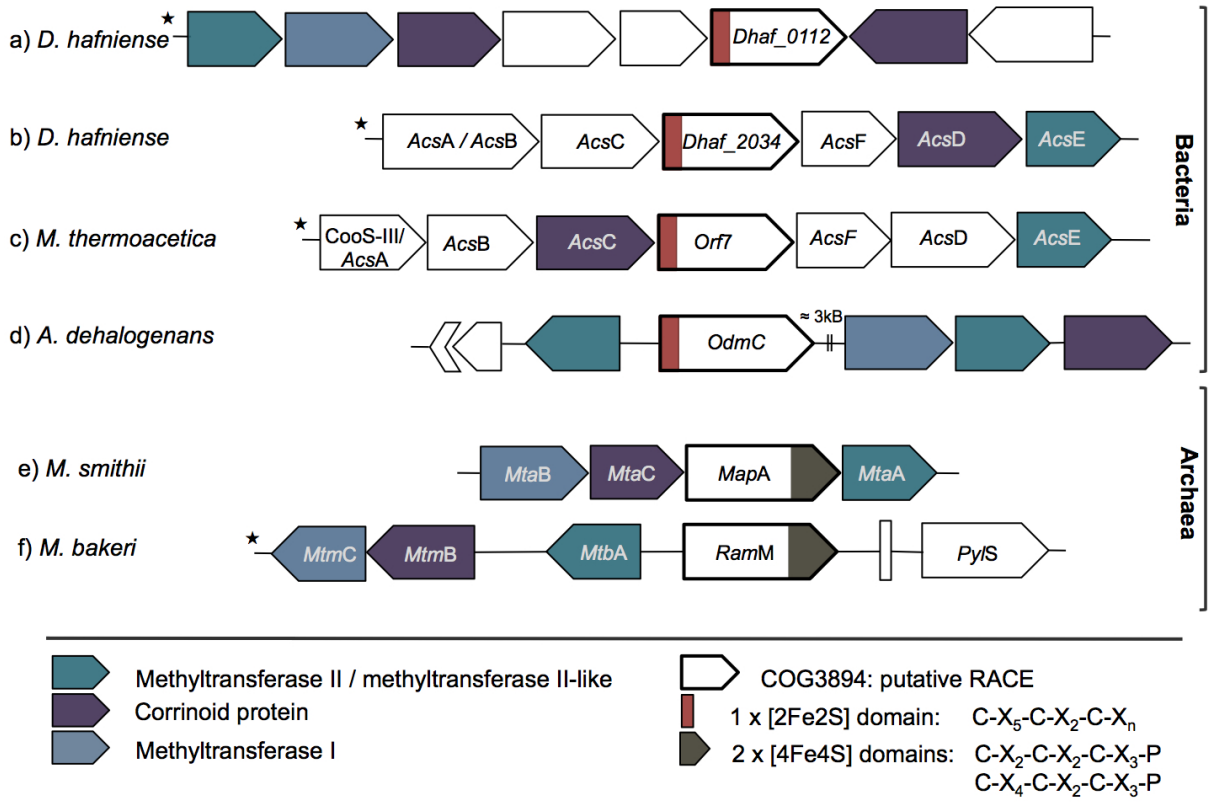

Figure 7: Comparison of orthologous gene clusters involved in the activation of corrinoid proteins. The gene clusters of four bacteria (a-d) and two archaea (e-f) containing the COG3894 genes are shown. The trimethylamine MT (a) and CODH/ACS (b) of *Dehalobacter hafniense* DCD-2, CODH/ACS of *Moorella thermoacetica* (c), the activating enzyme (OdmC) of *Acetobacterium dehalogenans* (d), the methanol:coenzyme M (CoM) MT of Methanobrevibacter *smithii* (e) and the monomethylamine:CoM Mt of *Methanosarcina barkeri*. Some gene clusters have been orientated in reverse direction for the comparison of the orthologs and are marked with an asterisk. This figure was adapted from *Schilhabel et al*. (*17*).

As in all methyltransferases and CODH/ACS complexes the superreduced Co(I) state of the corrinoid protein plays a crucial role in the catalytic cycle, the genes probably code for FeS proteins participating in the activation and reduction of protein bound corrinoids. The products of these genes likely code for reductive activases of corrinoid enzymes and the term RACE was introduced for this protein family recently (*17*). Biochemical characterisation of members of this protein family is still in the early stage of development and includes predominantly the activating enzyme of *O*-demethylases (*15, 16, 73, 74*).

3. Reductive Activation in the Reductive Acetyl-CoA Pathway

3.1. Carbon Fixation via the Reductive Acetyl-CoA Pathway in Anaerobic Bacteria

The fixation of inorganic carbon and its conversion to organic compounds can be considered as the starting point of biological evolution (*75*). Plants and the majority of prokaryotes fix approximately 10^{17} g of carbon dioxide into biomass in the reductive pentose phosphate (Calvin-Benson) cycle (*76*). Beside the Calvin-Benson cycle five alternative autotrophic pathways of CO_2-fixation exist, namely the reductive citric acid cycle, the 3-hydroxypropionate bicycle, the hydroxypropionate-hydroxybutyrate cycle, the dicarboxylate-hydroxybutyrate cycle and the reductive acetyl-CoA pathway (Wood-Ljungdahl pathway) (*75, 76*). Approximately 10 % of the annually produced 10^{13} kg of acetic acid derive from acetogens (*77*) and this pathway can be considered as a bacterial version of the Monsanto process. The importance of microbial carbon fixation to maintain a viable atmosphere is also obvious as every year 10^{11} t of carbon dioxide – corresponding to 10 % of the CO_2 content of the air – and approximately 10^{8} t of the greenhouse gas carbon monoxide are fixed autotrophically (*76, 78*). The reductive acetyl-CoA pathway is the most ancient C1 carbon fixation pathway and is assumed to be the closest to the ancestral autotrophic carbon fixation pathway (*75, 79*).

Figure 8 gives an overview of the reductive acetyl-CoA pathway used by anaerobic bacteria (acetogens) as main mechanism for energy conservation and for the synthesis of acetyl-CoA spent in cell carbon (*80*) .

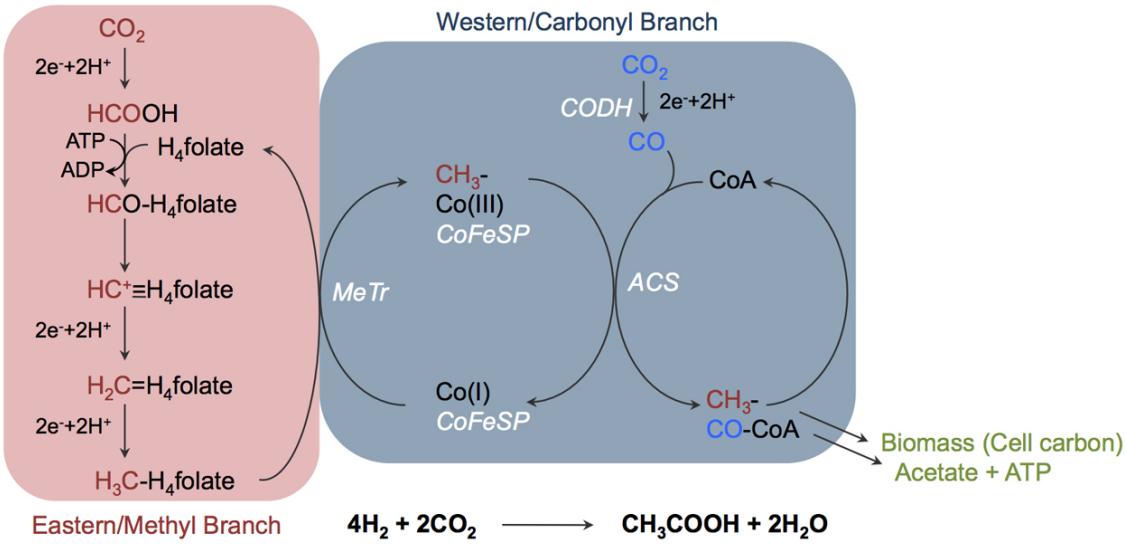

Figure 8: The reductive acetyl-CoA or Wood-Ljungdahl pathway of *Moorella thermoacetica*. The two branches of the pathway are highlighted in red (Methyl/Eastern branch) and blue (Western/Carbonyl branch). In total, two molecules of carbon dioxide are fixed to acetyl-CoA, which is used in the cell carbon cycle or for the production of energy. The metalloenzymes acting in the carbonyl branch are given in white. The scheme was adapted from *Ragsdale and Pierce* (*77*).

The reductive acetyl-CoA pathway is divided into two branches. One molecule of CO_2 is stepwise reduced in the eastern/methyl branch to a methyl group bound to tetrahydrofolate (Figure 8, red box). The methyl group from CH_3-tetrahydrofolate is transferred to the corrinoid/iron-sulfur protein (CoFeSP) by methyltransferase (MeTr). CO-Dehydrogenase (CODH) in the western/carbonyl branch reduces another molecule of CO_2 to carbon monoxide. Condensation of the CO and the bound methyl group catalysed by acetyl-CoA-synthase (ACS) yields acetyl-CoA, which is incorporated into cell carbon or used for energy production in the cell (Figure 8, blue box) (*77, 78, 81*) . The eastern branch of the reductive acetyl-CoA pathway equals the folate-dependent one-carbon metabolic pathway found in humans and bacteria but the western branch with highly oxygen-sensitive metalloenzymes is unique to acetogens, methanogens and sulfate reducers (*77, 81*).

The extremely thermophilic and strictly anaerobic, gram-positive eubacterium *Carboxydothermus hydrogenoformans* was isolated from a hot spring in Kunashir Island. It was considered to be an obligate CO autotroph (*82*), which gains energy fermentatively by performing the water shift reaction at lower temperatures than technical catalysts do. Hence the application of microorganisms like *C. hydrogenoformans* in the production of hydrogen gas at low CO concentrations has gained attraction in the field of biotechnology (*83, 84*).

Microbes using CO as carbon source depend on carbon monoxide dehydrogenases (CODH), which catalyse the oxidation of CO to CO_2. In the genome of *C. hydrogenoformans* five genes encoding for CODH homologs are present (named CODH I-V) and act in energy conservation and oxidative stress response amongst others (*83, 85*). CODH-III is located in the gene cluster coding for the enzymes involved in carbon fixation via the reductive acetyl-CoA pathway (Figure 9, red box) (*83*).

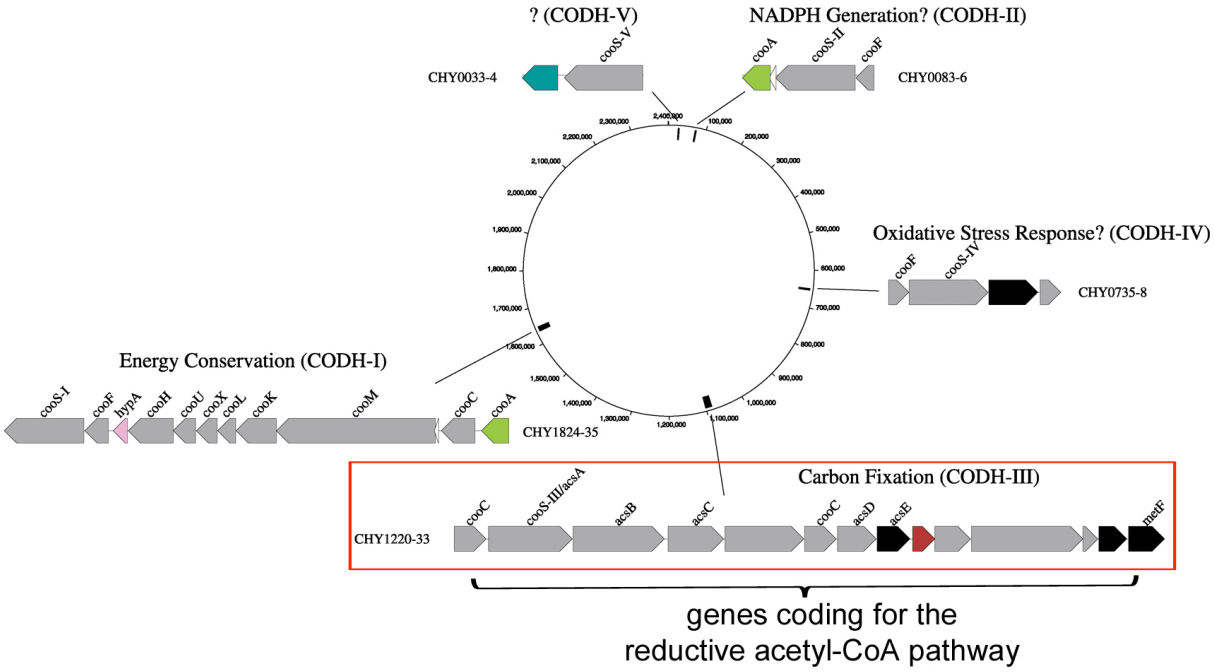

Figure 9: Genes encoding CODHs and their location in the genomic DNA of *C. hydrogenoformans*. The gene cluster including CODH-III and genes coding for enzymes acting in carbon fixation via the reductive acetyl-CoA pathway is highlighted with a red box. This figure was adapted from Wu *et al.* (*83*).

The investigation of enzymes acting in the reductive acetyl-CoA pathway of *M. thermoacetica* has intensively been performed in the last 30 years (*81, 86, 87*). Most of these enzymes including ACS, CODH II, the Ni-binding ATPase CooC1 and CoFeSP of the hydrogenogenic bacterium *C. hydrogenoformans* (Figure 9) have been functionally and structurally investigated (*33, 88–94*).

3.2. The Corrinoid/Iron-Sulfur Protein of *Carboxydothermus hydrogenoformans* at the Heart of the Reductive Acetyl-CoA Pathway

The corrinoid/iron-sulfur protein is a heterodimer consisting of two subunits, the large subunit CfsA and the small CfsB subunit, respectively. As the name indicates, CoFeSP binds two cofactors with both of them located in the large subunit, CfsA; namely a Coβ-aqua(5,6-dimethylbenzimidazolylcobamide) or cobalamin, and a cubane type [4Fe4S] cluster (*95, 96*). The structure of CoFeSP of *C. hydrogenoformans* was solved some years ago and demonstrates that the large subunit, CfsA, is divided into different domains (*89, 94*). The [4Fe4S] cluster is bound to the N-terminal domain with a four-helix-bundle-like architecture which is connected to the middle domain composite of a $(\beta\alpha)_8$-barrel, by a flexible linker (*94*). The C-terminal domain is linked to the middle domain by a proline-rich linker and binds the cobalamin cofactor, which is sandwiched between the C-terminal part of CfsA and CfsB (Figure 10) (*89, 94*). CfsB contains a Rossmann-like fold consisting of a parallel four-stranded β-sheet framed by two α-helices. A "cap-helix" is in van-der-Waals distance and interacts with the lower side of the corrin macrocycle (*89, 94*). On the upper face of the corrin moiety, a water molecule directly coordinates the cobalt ion. In contrast to other B_{12}-dependent proteins like methionine synthase (MetH), the cobalamin cofactor is bound base-off, e.g. neither the dimethylbenzimidazole chain nor a protein side chain coordinates the cobalt (Figure 10, inset). The base-off / His-off conformation results probably in a stabilisation of the cob(I)amide by about +100 mV compared to the base- or His-on states (*68*). The structures solved in 2006 (*89*) and 2011 (*94*) show both the inactive Co(II)-state of CoFeSP.

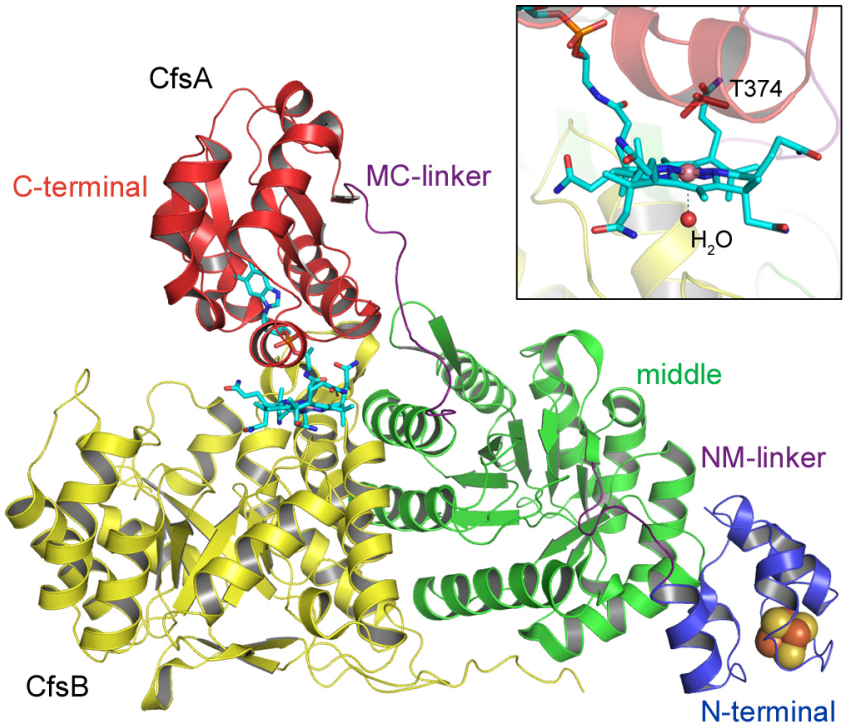

Figure 10: Overall structure of CoFeSP of *C. hydrogenoformans*. The structure including the N-terminal [4Fe4S] cluster domain is shown as cartoon. The small subunit (CfsB) is coloured in yellow. The large subunit CfsA contains three domains. The N-terminal domain is illustrated in blue, the middle domain in green and the C-terminal domain in red. The linker connecting the N-terminal and C-terminal domain to the middle domain, respectively, is shown in purple. The [4Fe4S] cluster is presented as spheres (iron atoms in orange, sulfur in yellow). The cobalamin cofactor is shown as cyan stick model. The coordination environment of the cobalamin cofactor is illustrated in the inset. The cobalt ion (shown as pink sphere) binds a water molecule on the upper face of the corrin ring. On the lower side T374 of the cap-helix is in van-der-Waals distance. The subunits are coloured as in the main figure. The figure was prepared using the PDB entry 2YCL (*94*).

CoFeSP is at the heart of the reductive acetyl-CoA pathway by bridging the methyl and the carbonyl branch and functions as a methyl group carrier (Figure 8). The protein accepts a methyl group from CH_3-H_4folate in a reaction catalysed by MeTr (reaction 2) (*97*).

$$CH_3 - H_4 folate + Co(I)FeSP + H^+ \leftrightarrow CH_3 - Co(III)FeSP + H_4 folate \qquad (2)$$

Methylated CoFeSP transfers the methyl group to the A-cluster of ACS (*88*). Acetyl-CoA is synthesised at the Ni–Ni–[4Fe4S] site in a condensation reaction of CoA, CO (from CO_2 reduction by CODH) and the methyl group (*81*).

$$CH_3 - Co(III)FeSP + CO + CoA \leftrightarrow CH_3(CO)CoA + Co(I)FeSP \quad (3)$$

As shown in previously reported structures of CoFeSP (*89, 94*) and CoFeSP in complex with its methyltransferase (*98*), the protein exists in several conformations depending on the environment and its interaction partners. The MC- and NM-linker connecting the cofactor carrying domains to the middle domain of CfsA, provide the basis for its flexibility (Figure 10) (*89, 94, 9*).

The function of the [4Fe4S] cluster was described as the conduit for an electron transferred from an external donor to the cobalamin (*99, 100*). A distance of approximately 60 Å between the two centres (*94*) contradicts direct electron transfer. Large conformational changes in the protein would be required to reduce the distance of the cofactors to 14 Å or less in order to enable the transfer of an electron (*40*). However, activation by interactions with another protein has not been described so far.

3.3. An Open Reading Frame in the Gene Cluster of the Reductive Acetyl-CoA Pathway – Coding for a Putative RACE Protein?

During the catalytic cycle of CoFeSP, the cobalamin cofactor cycles between two active states: the superreduced Co(I) state accepting the methyl group from MeTr and the methyl-bound Co(III)-CoFeSP interacting with ACS (*81*). The Co(I) state is highly sensitive to incidental oxidation and inactivation to Co(II) occurs approximately every 100 turnovers (*100*), which indicates the existence of a reductive activation system for the reduction of the Co(II) state.In the gene cluster coding for the proteins acting in the reductive acetyl-CoA pathway of *M. thermoacetica* an open reading frame is situated in proximity to the *acsC* and *acsD* genes coding for the two subunits of the corrinoid/iron-sulfur protein (*101*). This open reading frame, annotated *orf7*, is also located between the genes coding for CoFeSP in the genome of *C. hydrogenoformans* (Figure 11) (*83*).

Figure 11: Gene cluster of proteins of the reductive acetyl-CoA pathway of *C. hydrogenoformans*. The genes of the enzymes of the reductive acetyl-CoA pathway are organised in one gene cluster. An open reading frame (*orf7*) is located between the genes coding for the subunits of CoFeSP.

With the definition of the RACE protein family an alternative reductive activation mechanism for corrinoid enzymes in general (*17*) and for CoFeSP in particular, has been proposed. Like the activating enzyme of *O*-demethylases of *A. dehalogenans* the gene product of *orf7* belongs to COG3894 and contains a [2Fe2S] cluster binding motif at its N-terminus (*17, 83*).

Dr. Jae-Hun Jeoung (Strukturbiologie / Biochemie, Humboldt Universität zu Berlin) was able to isolate the gene product for crystallisation and solved the structure by SAD-MAD techniques.

The *orf7* product is a homodimer; each monomer is composed of four domains (Figure 13A). A plant-ferredoxin like [2Fe2S] cluster is bound to the N-terminal domain (residues 1 – 94), which is connected by a long linker (residues 95 – 125) to the middle domain (residues126 – 205). This domain is the contact interface responsible for the dimerisation of the monomers (Figure 13A) (*102*).

The largest domain, the C-terminal domain (residues 206 – 631), shows a fold common in members of the ASKHA (acetate and sugar kinases/heat shock protein 70/actin) superfamily (*47, 48*). The domain is composed of two subdomains, I and II, consisting of a five-stranded β-sheet surrounded by three α-helices with βββαβαβα topology (Figure 13B) (*102*). A nucleotide-binding site is suggested to be located in a cleft between subdomain I and II. A phosphate ion associated with magnesium was modelled into the active site (Figure 13C) (*102*).

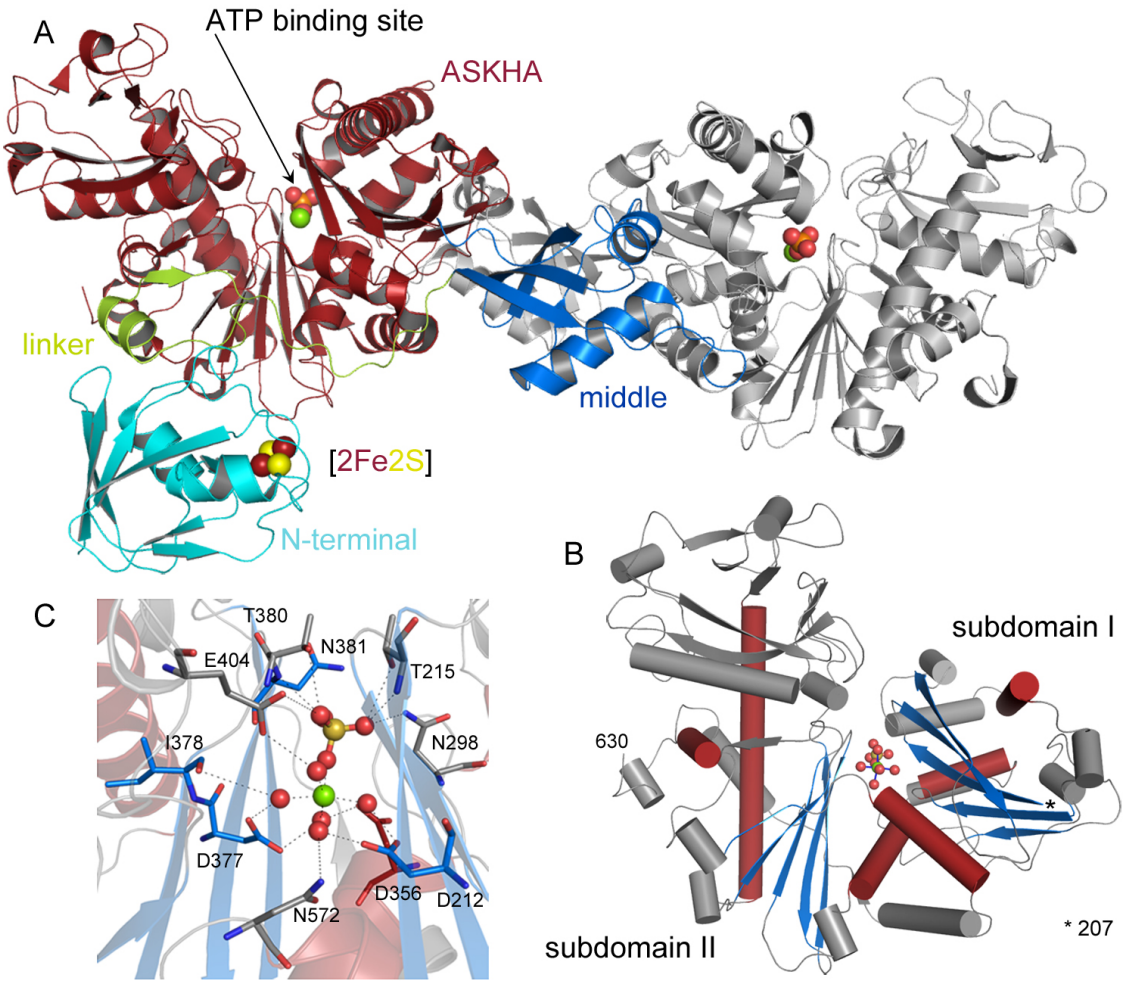

Figure 12: The overall structure of the gene product of *orf7*. (A) Shown is the homodimer in cartoon presentation. In the first monomer all domains are visible. The N-terminal domain is coloured in cyan with the [2Fe2S] cluster illustrated as spheres (iron atoms in red, sulfur in yellow). The middle domain is shown in blue and the big C-terminal domain with the ATP-binding site (ASKHA domain) in red. $MgPO_4$ was modelled into the active site. The second monomer is coloured in grey. The N-terminal domain is disordered in this molecule. (B) Illustration of the subdomains I and II of the ASKHA domain (residues 207-630) with the for ASKHA family typical ββββαβαβα topology. The α-helices are coloured in red, β-sheets in blue. (C) Nucleotide-binding site with Mg^{2+} and PO_4^{3-} bound (spheres and stick model with Mg^{2+} in green, PO_4^{3-} in yellow for phosphor and red for oxygen, water molecules are presented as red spheres). Residues in H-bonding distance are labelled. The figure was prepared from the PDB entry 3ZYY (*102*).

Ensuing from the structure and the location of the open reading frame within the gene cluster of the proteins participating in the reductive acetyl-CoA pathway, a biochemical characterisation of the gene product appeared promising. The question, if a reductive activator of CoFeSP exists within the reductive acetyl-CoA pathway of *C. hydrogenoformans* and its characterisation as a member of the young RACE protein family, have been the driving force of this study.

4. Scope of the Study

Electron transfer between proteins is at the heart of numerous biological processes including respiration and photosynthesis. To drive an energetically unfavourable electron transfer and keep it unidirectional, another energetic process such as an ATPase reaction needs to be coupled to it. This kind of energy transduction is found in the carbon and nitrogen cycle, in particular in the reductive activation of nitrogenase, radical-dependent β,α-dehydratases, the related benzoyl-CoA reductases, and different cobalamin-dependent methyltransferases (*12, 15, 17, 44, 53*). General aspects of the reductive activation of corrinoid enzymes by a RACE protein were recently reported for the first time (*16, 17, 73, 74*), but a detailed characterisation of a RACE protein has had a long time in the coming.

Aim of this work is the investigation of the gene product of *orf7* found in the gene cluster coding for the enzymes of the reductive acetyl-CoA pathway of *Carboxydothermus hydrogenoformans*. The protein should be biochemically characterised with regard to its possible role in the reactivation of the inactive / oxidised corrinoid/iron-sulfur protein to prove that a RACE protein acts in this hydrogenic organism. The establishment of an activation assay demonstrating the need of ATP for interprotein electron transfer and the analysis of a possible complex formation as observed in nitrogenases and / or dehydratases by analytical gel filtration and isothermal titration calorimetry are one objective. The influence of a hypothetical complex formation on the single proteins and their cofactors should be considered and investigated by different spectroscopic methods.

The biochemical characterisation of the putative RACE protein and its interactions with the target protein, CoFeSP, would be the first of its kind. The structural investigation of the putative activation complex is the main goal of this study to provide insights into the mechanism of activation of corrinoid containing proteins.

Comparison with other activation systems is expected to reveal differences and / or common features of the three types of ATP-dependent activation systems found in the global carbon and nitrogen cycle and expand the understanding of how nature has devised different ways of translating the energy stored in the pyrophosphate bond of ATP to allow an energetically unfavourable electron transfer.

II. MATERIALS AND METHODS

1. Chemicals

All chemicals were of analytical purity grade (p.a.) and purchased from Applichem (Darmstadt, Germany), Merck (Darmstadt, Germany), Roth (Karlsruhe, Germany) and Sigma-Aldrich (Deisenhofen, Germany).

Pure nitrogen (N_2, 99.99 %) and nitrogen gas mixed with hydrogen (95 %N_2/5 %H_2) were provided by Air Liquide (Berlin, Germany).

Enzymes used in microbiology were obtained from Thermo Fisher Scientific Biosciences GmbH (St. Leon-Rot, Germany) or New England Biolabs (Frankfurt/Main, Germany). Plasmid preparation kit, PCR product purification kit and Gel extraction kit were purchased from Thermo Fisher Scientific Biosciences GmbH as well as size markers for agarose and SDS gel electrophoresis. Bradford solution was supplied by BioRad (Munich, Germany).

Chromatography columns and all materials used in the purification of proteins were purchased from GE Healthcare (Munich, Germany).

Anaerobic reaction tubes (15 ml), EPA (Environmental Protection Agency) vials (20 ml), glass vials (2 ml), butyl and silicon septa and other anaerobic glass equipment were purchased from Supelco (Sigma-Aldrich) and OCHS (Bovenden / Lenglern, Germany).

2. Working under Anoxic Conditions

If not mentioned explicitly, all experiments were carried out under oxygen-free conditions in an anaerobic chamber (Coy Laboratory Products Inc., Michigan, USA) with a 95 % N_2/ 5 % H_2 atmosphere. ITC experiments were done under a N_2 atmosphere inside a glove box (Braun, LabStar).

Solutions and buffers for purification, activity assays and crystallisation were prepared in bottles with butyl rubber septa by evacuating and flushing with N_2 (at least 5 cycles) at a vacuum gas line to remove dioxygen.

3. Molecular Biology

3.1. *Escherichia coli* Strains

For the cloning of genes *Escherichia coli* DH5α {F^- *.80 /lacZ/M15/(lacZYA-argF)U169, deoR, recA1, end A1,hsdR17(*rk^-*,* mk^+*), phoA, supE44,*0^-*, thi-1, gyrA96, relA1*} was used.

3.2. Cloning and Mutagenesis of the *orf7* Gene Product

3.2.1. Deletion of the N-terminal Domain (Residues 1-100)

For the deletion of the first 100 amino acids of the N-terminal domain of the putative reductive activator of CoFeSP (RACo) the PIPE (Polymerase incomplete primer extension) cloning method (*103*) modified by Dr. Martin Bommer (Strukturbiologie / Biochemie, Humboldt Universität zu Berlin) was used. The gene, lacking the base pairs of the first 100 amino acids to be deleted, was amplified by PCR using *Phusion* DNA polymerase, the primers RACo100^+_fwd and RACo100^+_rev with specific overlaps for the pET28aTEV-vector (Appendix Table 10) and genomic DNA of *C. hydrogenoformans*, respectively (Appendix Table 11). The conditions for the PCR are given in Appendix Table 12. The reaction was verified by loading a sample on a 1 % (w/v) agarose gel. The PCR product was purified and mixed with vector pET28a-TEV (prepared for PIPE cloning (*103*), provided by Dr. M. Bommer). After incubation on ice for five minutes, the plasmid was directly transformed into chemically competent *E. coli* DH5α cells. Positive clones were isolated and identified by DNA sequencing (Eurofins MWG Operon, Ebersberg) and named pPKCo28aTEV-Δ100.

3.2.2. Active Site Mutants (QuickChange Method)

The residues (D212, T215, D377, T380 and E404) considered to be responsible for binding of the nucleotide into the ATP binding pocket of RACo (Figure 13B) were mutated into alanines. For the insertion of point mutations the QuickChange Method (Stratagene Europe,

Amsterdam, Netherlands) was used. The plasmid pPKCoDuet1-TEV was amplified with the corresponding primers (Appendix Table 10) using *Pfu* DNA polymerase according to the manufacturer´s protocol. Mutagenesis primers and PCR conditions are listed in Appendix Table 13 and Table 14. Positive clones were isolated and identified by DNA sequencing (Eurofins MWG Operon, Ebersberg, Germany).

3.2.3. Mutation of Ser398 by Combining PIPE Cloning and QuickChange Method

The gene *orf7* coding for RACo was amplified using the primer orf7-fwd and S398X-rev in a first PCR. The PCR product was used in a second PCR reaction with primer orf7-rev and a forward primer carrying the point mutation for S398. The primers R_S398X-fwd and R_398X-rev contained the specific overlaps for the pET28a-TEV vector used for PIPE cloning (*103*) (Appendix Table 10). The same conditions were chosen for both PCRs (Appendix Table 15 and Table 16). The product of the second reaction was mixed with vector pET28a-TEV and subsequently treated as described in section 3.1.1.

3.3. Cloning and Mutagenesis of CoFeSP

3.3.1. Deletion of Entire Domains of CfsA

For the deletion of the entire C- or N-terminal domain of the large subunit CfsA of CoFeSP (Δ_N60-CoFeSP and) the PCR:Religate:Transform method of Dr. Martin Bommer (Strukturbiologie / Biochemie, Humboldt Universität zu Berlin) was used (*104*). The template pPKCD was amplified by PCR (Appendix Table 18 and Table 19) with the primers given in Appendix Table 17. The purified linear vector was incubated with phosphokinase for 30 min at 37 °C and then re-ligated for 10 min at room temperature using T4 DNA ligase. The ligation product was further purified and transformed into chemically competent cells. To identify positive clones plasmid samples of pPKCD_MC (Δ_N60-CoFeSP) and pPKCD_NM (Δ_C128-CoFeSP) were sent for sequencing (Eurofins MWG Operon, Ebersberg, Germany).

3.3.2. Site Directed Mutagenesis of Cysteines Coordinating the [4Fe4S] Cluster

The exchange of single cysteines coordinating the four irons of the [4Fe4S] cluster of CoFeSP was performed using the QuickChange protocol from Stratagene (Stratagene Europe, Amsterdam, Netherlands) with pPKCD as template. The primers and conditions of the PCR are listed in Appendix Table 17, Table 20 and Table 21, respectively. Positive constructs were identified by sequencing (Eurofins MWG Operon, Ebersberg, Germany) for the residues C20A, C20P and C25P.

3.4. Agarose Gel Electrophoresis

For the isolation of DNA or the analysis of PCR products 1 % (w/v) agarose gels containing GelRed™ (Biotium Inc.) were prepared routinely. Samples were mixed with 6-fold Loading Dye and loaded onto gels. DNA marker (Thermo Fisher Scientific Biosciences GmbH) was applied. Electrophoresis procedure was carried out in a horizontal gel system (PEQLAB Biotechnologie GmbH, Erlangen) at 90 V.

3.5. Transformation of *Escherichia coli* Competent Cells

Chemically competent cells of *E. coli* were transformed by adding 1 µL of plasmid DNA (20–400 ng/µL) to 200 µL cells refrigerated on ice. After incubation for 30 min on ice the samples were exposed to 42 °C for 45 s and subsequently chilled on ice for 10 min. 900 µL of LB medium were added and the samples were incubated at 37 °C while shaking for one hour. The samples were centrifuged at 14,000 g, supernatant was discarded and the pellets were resuspended in 100 µL LB medium. The transformed cells were plated onto LB agar plates containing the corresponding antibiotics or grown as overnight cultures in LB medium.

4. Expression and Purification of Proteins

4.1. Heterologous Expression

Genes were routinely expressed in *E. coli* strain BL21(DE3) with genotype *E. coli* {F^- ompT hsdSB(rB^- mB^-) gal dcm (DE3)}. Composition of the modified Terrific Broth (mTB) medium (*93*) with the antibiotics used for protein expression is shown in the following tables.

Table 1: Composition of expression medium.

mTB medium	
12 g/L	Tryptone
24 g/L	Yeast extract
10 mL/L	Glycerol

Table 2: Antibiotics used for expression.

Antibiotic	Stock concentration	Final concentration in the media
Carbenicillin (Cb)	50 mg/mL in ddH_2O	50 µg/mL
Kanamycin (Km)	50 mg/mL in ddH_2O	50 µg/mL

4.1.1. Expression of RACo (Variants)

The plasmids pPKCoDuet1-TEV or pPKCo28a-TEV and all modified vectors of RACo were transformed into the *E. coli* expression strain BL21(DE3). All strains were cultivated by shaking at 37 °C in mTB medium (*93*) supplemented with 0.3 mM $FeSO_4$, 0.3 mM Na_2S and the appropriate antibiotics. Gene expression was induced by the addition of 0.5 mM IPTG at an OD_{600} of 0.6 and 0.3 mM $FeSO_4$ and 0.3 mM Na_2S were added to the culture which was further cultivated at 32 °C. Six hours after induction cells were harvested by centrifugation at 7,000 rpm and 12 °C. Cell pellets were stored at –20 °C until use.

The RACo variant missing the [2Fe2S] cluster domain (Δ100-RACo) was expressed as described above without addition of iron and sulfur sources.

4.1.2. Expression of CoFeSP (Variants)

All plasmids coding for CoFeSP and CoFeSP variants (pPKCD, pPKCD_MC, pPKCD_NM and pPKCD_C25P) were transformed into *E. coli* BL21(DE3). The strains were cultivated by shaking at 37 °C. 0.2 mM $FeSO_4$, 0.2 mM Na_2S and the appropriate antibiotics were added to the mTB media (*93*). When an OD_{600} of 0.7 was reached 0.4 mM IPTG was added to induce the expression and the culture was supplemented with 0.3 mM $FeSO_4$ and 0.3 mM Na_2S. The culture was further cultivated at 32 °C and harvested 8 h after induction as described above.

The strain harbouring the plasmid pPKacsCD_MC (Δ_N60-CoFeSP) was cultivated without supplementation of iron or sulfur.

4.2. Protein Purification

All protein purification steps were performed inside a glove box (model B, COY Laboratory Products Inc., Michigan, USA) under an atmosphere of 95 % N_2 / 5 % H_2. Δ100-RACo was purified aerobically but buffer exchange was performed under anoxic conditions.

Homogeneity and concentrations of purified proteins were routinely analysed by SDS-PAGE (*105*) and the Bradford method (*106*) (Materials and Methods 5.1 and 5.2).

4.2.1. Purification of RACo, RACo Mutants and Δ100-RACo

4.2.1.1. Purification of RACo without Affinity Tag (Native Purification)

Table 3: Buffers used in native purification of RACo.

RACo purification without affitnity tag	
Buffer A	50 mM Tris/HCl, pH 8.0
Buffer B	50 mM Tris/HCl, pH 8.0 1 M NaCl
Buffer C	50 mM Tris/HCl, pH 8.0 1 M $(NH_4)_2SO_4$
Buffer D	50 mM Tris/HCl, pH 8.0 150 mM NaCl

The cell pellet was thawed on ice and resuspended in buffer A containing catalytic amounts of DNase I and lysozyme. The cell suspension was stirred for 10 minutes at room temperature. Cells were further disrupted by sonication using an ice-cooled rosette cell (Branson sonifier, 3 cycles of 5 min sonication, 50 % duty cycle). The suspension of broken cells was cleared from cell debris by ultracentrifugation at 35,000 rpm and 8 °C for 1 h. The supernatant was loaded onto DEAE sepharose material (50 mL, GE Healthcare) equilibrated in buffer A. After washing with buffer A, the protein was eluted with a linear gradient over 500 mL from 0 – 1 M NaCl using buffer B. Red coloured fractions were pooled and suspended in ammonium sulphate to a final concentration of 1 M. The suspension was stirred for 30 min at room temperature and centrifuged for 15 min at 12,000 rpm and 12 °C. The supernatant was applied to a phenyl sepharose column (25 mL, GE Healthcare) equilibrated in buffer C. After washing, the column was developed with a linear gradient of 1 – 0 M ammonium sulfate. Fractions containing RACo were pooled and concentrated to a volume less than 5 mL using a Vivaspin 70 spin concentrator (50 kDa molecular weight cutoff; Vivascience GmbH) equipped with a rubber-sealed screw cap followed by load of the concentrate onto a Superdex^{TM} 200 prep-grade gel filtration column (120 mL, GE Healthcare) equilibrated in buffer D. Protein fractions corresponding to the size of the RACo homodimer were collected and concentrated. A sample was taken for SDS-PAGE analysis (Materials and Methods 5.1), iron quantification (Materials and Methods 5.3) (*107*) and concentration determination by Bradford (Materials and Methods 5.2). The protein was frozen in glass vials equipped with a butyl-rubber septum in liquid nitrogen and stored at –80 °C.

4.2.1.2.Purification of RACo, RACo Mutants and Δ100-RACo by Removable Affinity Tag

Table 4: Purification buffers of the affinity tag purification of RACo.

RACo purification	
Buffer A	50 mM Tris/HCl, pH 8.0
Buffer B	50 mM Tris/HCl, pH 8.0
	200 mM NaCl
	20 mM Imidazole
Buffer C	50 mM Tris/HCl, pH 8.0
	200 mM NaCl
	250 mM Imidazole
Buffer D	50 mM Tris/HCl, pH 8.0
	1 M NaCl
Buffer E	50 mM Tris/HCl, pH 8.0
	150 mM NaCl

Cell free soluble supernatant was prepared as described above. The supernatant was loaded onto Ni-SHP material (5 mL, GE Healthcare) equilibrated in buffer B. The column was washed with buffer B and subsequently developed with a 450 mL linear gradient from 20 to 250 mM imidazole (buffer C). Coloured fractions were pooled and loaded onto a Source 30Q or Q-Sepharose column (30-50 mL, GE Healthcare) equilibrated in buffer A. RACo was eluted by applying a linear salt gradient from 0 to 1 M using buffer D. The His_6 tag was removed by overnight incubation at room temperature with His_6-tagged TEV protease in the same buffer supplemented with 5 mM β-mercaptoethanol. To separate RACo from TEV protease the mixture was applied to the Ni-SHP material. The flow-through containing RACo was pooled and concentrated to a volume less than 5 mL using an Amicon Ultra-15 30 K spin concentrator (Millipore). The concentrate was loaded onto a 120 mL Superdex^{TM} 200 prep-grade gel filtration column (GE Healthcare) equilibrated in buffer E. Fractions containing the RACo dimer were collected and concentrated. A sample was taken for SDS-PAGE analysis. The iron content was measured via the Fish method and the concentration was determined (Materials and Methods 5.1, 5.2 and 5.3). Aliquots of 100 µL were frozen in glass vials equipped with butyl rubber septa in liquid N_2 and stored at –80 °C.

4.2.1.3.Purification of CoFeSP, ΔN60-CoFeSP, ΔC128-CoFeSP and C25P-CoFeSP

Table 5: Purification buffers used in the purification of CoFeSP.

CoFeSP purification	
Buffer A	50 mM Tris/HCl, pH 8.0
Buffer B	50 mM Tris/HCl, pH 8.0 1 M NaCl
Buffer C	50 mM Tris/HCl, pH 8.0 1 M $(NH_4)_2SO_4$
Buffer D	50 mM Tris/HCl, pH 8.0 150 mM NaCl

Preparation of soluble supernatant was done as described in Materials and Methods 4.1.1. The soluble fraction was loaded onto a Q-Sepharose column (50 mL, GE Healthcare), which was equilibrated in buffer A. The column was washed with buffer A and developed with a 450 mL linear gradient from 0 to 0.8 M NaCl (buffer B). Fractions containing CoFeSP were pooled, suspended in a 1 M ammonium sulphate solution and incubated for 30 min. The suspension was applied to phenyl sepharose material (25 mL, GE Healthcare) equilibrated in buffer C. After washing, CoFeSP was eluted applying a linear gradient from 1 to 0 M ammonium sulphate. Fractions containing equimolar amounts of large and small subunit were pooled and reconstituted by adding equimolar amounts of hydroxocobalamin. The solution was incubated overnight at 25 °C. Reconstituted CoFeSP was further purified using a Source 30Q column (30 mL, GE Healthcare) equilibrated in buffer A. CoFeSP was eluted by a linear increasing concentration from 0 to 0.8 M NaCl (buffer B). As a last purification step, size exclusion chromatography was carried out using a Superdex^{TM} 200 prep-grade gel filtration column (120 mL, GE Healthcare) equilibrated in buffer D. The protein was analysed by SDS-PAGE and concentration was determined by the Bradford method (Materials and Methods 5.1 and 5.2). Aliquots of 100 µL were frozen in glass vials equipped with butyl rubber septa in liquid N_2 and stored at –80 °.

4.2.1.4.Purification of CoFeSP used for ATPase Activity Measurements

CoFeSP used in the ATPase activity assay was prepared as communicated by Sebastian Götzl (Strukturbiologie / Biochemie, Humboldt Universität zu Berlin).

First, the small subunit of CoFeSP, CfsB, was purified from 10 g *E. coli* BL21(DE3) / pPKacsD cells in three chromatographic steps as described before for complete CoFeSP. 13 g cells transformed with the plasmid pPKacsC were resuspended in 50 mM Tris/HCl, pH 8.0 containing 2 mM DTT. After 15 min sonication, the cell lysate was centrifuged for 1.5 h at 35,000 rpm and 10 °C. The supernatant was discarded and the pellet containing the insoluble large subunit CfsA was successively washed with Tris-buffer containing 1 mM EDTA and then centrifuged until the supernatant had become colourless. The washed pellet was resuspended in 10 mL Tris-buffer containing 1 mM DTT and stored at –80 °C. 18 mg of pure CfsB in 2 mL 50 mM Tris-buffer containing 100 µM hydroxocobalamin were mixed with 2 mL of the pellet suspension. The mixture was diluted 2-fold with Tris-buffer containing 4 M urea and incubated for 15 min at 25 °C. After centrifugation at 12,000 rpm for 10 min, the supernatant was diluted and concentrated to decrease the concentration of urea to less than 0.1 M. 200 µM hydroxocobalamin were added and after 45 min incubation at room temperature size exclusion chromatography was performed (Superdex^{TM} 200 prep-grade, 120 mL, GE Health Care, equilibrated in buffer D). Fractions corresponding to the CoFeSP heterodimer were combined, concentrated, analysed (Materials and Methods 5.1 and 5.2) and frozen in liquid nitrogen.

5. Analytical Methods

5.1. SDS-Polyacrylamide Gel Electrophoresis (SDS-PAGE)

To analyse protein samples according to their size, SDS-Polyacrylamide Gel Electrophoresis (SDS-PAGE) described by Laemmli (*105*) was used.

Table 6: Composition of SDS-Polyacrylamide gels, solutions and buffers used for SDS-PAGE.

Resolving gel		Stacking gel	
12 or 15 % (w/v)	Acrylamide	6 % (w/v)	Acrylamide
375 mM	Tris/HCl, pH 8.8	125 mM	Tris/HCl, pH 6.8
0.1 % (w/v)	SDS	0.1 % (w/v)	SDS
0.08 % (w/v)	TEMED	0.08 % (w/v)	TEMED
0.05 % (w/v)	APS	0.05 % (w/v)	APS

Staining solution		Destaining solution	
0.025 % (w/v)	Coomassie Brilliant Blue G250	10 % (v/v)	Acetic acid
10 % (v/v)	Acetic acid		

4xSDS sample buffer		10xSDS running buffer	
200 mM	Tris/HCl, pH 6.8	1.92 M	Glycine
0.4 M	DTT	248 mM	Tris
8 % (w/v)	SDS	1 % (w/v)	SDS
40 % (v/v)	Glycerol		

Samples were mixed with SDS loading buffer and boiled at 100 °C. Unstained protein molecular weight marker (Thermo Fisher Scientific Biosciences GmbH) served as a size standard. For electrophoresis, a voltage of 80 V was applied to the gel which was increased after 20 min to 120 V. Gels were stained by incubation in warm staining solution followed by destaining solution for several hours.

5.2. Determination of Protein Concentration

The concentration of proteins was determined by the method described by Bradford (*106*). Bradford and BSA solutions used for the preparation of standard curves were supplied by BioRad. In the case of the RACo variant Δ100 the protein concentration was calculated via the absorption at 280 nm applying the calculated theoretical extinction coefficient (ε_{280} = 31,860 $M^{-1}cm^{-1}$) (*108*).

5.3. Iron Quantification

To quantify protein bound iron the method described by Fish (*107*) was applied.

100 µL of a RACo sample was mixed with 100 µL 1 % (w/v) HCl and incubated for 10 min at 80 °C. When cooled down to room temperature, 500 µL 7.5 % (w/v) ammonium acetate, 100 µL 4 % (w/v) ascorbic acid and 100 µL 2.5 % (w/v) SDS and 100 µL 1.5 % (w/v) ferene were added sequentially. The reaction mixture was centrifuged at 14,000 rpm for 10 min and the absorbance at 593 nm was measured against water.

The amount of iron within the protein sample was calculated from a standard curve obtained by measuring known iron concentrations between 2 and 20 µM Fe.

5.4. Analytical Size Exclusion Chromatography

For the investigation of the complex formation between RACo and CoFeSP and their variants analytical size exclusion chromatography was performed using either a Superdex^{TM} 200 prep-grade gel filtration column (dimension 16 × 600 mm, GE Healthcare) or a Superdex S 150/5 column (dimension 5 x 150 mm, GE Healthcare) inside a glove box. Equimolar concentrations of the proteins (generally 25 or 45 µM) were incubated 10 min at room temperature and injected onto the gel filtration column equilibrated in 50 mM Tris/HCl, pH 8.0, 150 mM NaCl and additives as following.

To test the influence of nucleotides on complex formation 5 mM ATP or 5 mM ADP in the presence of 50 mM $MgCl_2$ were added to the protein sample and buffer. Redox-state

dependent complex formation of RACo and CoFeSP was determined by pre-incubation of RACo with the different redox states of CoFeSP (Co(II)-CoFeSP, Co(I)-CoFeSP and CH_3-Co(III)-CoFeSP), respectively, before load onto the column. To prepare Co(I)-CoFeSP the protein was incubated at least for 20 minutes with 1 mM Na-dithionite (DT) and the running buffer was supplemented with 1 mM DT. CH_3-Co(III)-CoFeSP was prepared by reconstitution of CoFeSP during purification with methyl-cobalamin. Individual peak fractions from each gel filtration experiment were collected and analysed by SDS-PAGE (Materials and Methods 5.1). The programme ImageMaster™ 2D Platinum v7.0 (GE Healthcare) was used for densitometry analysis of the SDS gels.

The elution volumes of the peaks were transformed into molecular weights using a standard curve (Appendix Figure 52) calculated from known standard proteins in the running buffer: 4 mg⁄mL lactate dehydrogenase (140 kDa), 4 mg⁄mL conalbumin (75 kDa), 4 mg⁄mL ovalbumin (43 kDa), and 4 mg⁄mL ribonuclease (13.7 kDa).

5.5. Isothermal Titration Calorimetry

The dissociation constants of the complex between RACo and Co(II)-CoFeSP, Δ100-RACo and Co(II)-CoFeSP and the RACoS398-mutants and Co(II)-CoFeSP were determined by ITC. ITC experiments were performed at 25 °C inside a glove box (LabStar, Braun) using a VP-ITC Micro Calorimeter (Microcal LLC). Storage buffers of the proteins were exchanged to 50 mM Tris/HCl, pH 8.0 containing 150 mM NaCl using Superdex^{TM} 200 prep-grade gel filtration column to remove remaining reducing agent from purification. Experiments were performed with 100 - 150 µM of RACo, RACoΔ100 or RACo-S398A or C, and 10 – 15 µM Co(II)-CoFeSP. Data were processed with supplier´s software assuming a one-site binding model (Microcal Origin).

6. Enzyme Activity Assay

6.1. NTPase Activity Assay

6.1.1. Malachite Green Assay

ATPase activity was determined by detecting the amount of inorganic phosphate (P_i) released during ATP hydrolysis by RACo using a modified malachite green-ammonium molybdate (MGAM) assay (*109*). The released P_i can be quantified by the absorbance of the phosphomolybdate-malachite green complex at 630 nm.

Table 7: Stock solutions and buffer of the MGAM-ATPase assay.

Stock solutions			Buffer A	
A	0.0812 % (w/v)	Malachite green	100 mM	Tris/HCl, pH 7.6
B	2.32 % (w/v)	Polyvinylalcohol	150 mM	KCl
C	5.72 % (w/v)	Ammonium molybdate	10 mM	$MgCl_2$
D		ddH_2O		
E	34 % (w/v)	Sodium citrate		
mix		2A + 1B +1C + 2D		

The MGAM solution was prepared freshly prior to use by mixing the stock solutions in the ratios given in Table 7. The dark brown solution turned golden yellow after approximately 30 min incubation at room temperature. The assay was performed under oxic conditions.

Generally, 10 or 15 µM RACo were incubated with 5 mM Mg-ATP in buffer A at different temperatures (RT, 37°C, 45°C, 50°C and 55°C, respectively). A complex sample was prepared by mixing 10 µM RACo and 10 µM CoFeSP. Every 15 or 20 min a sample of 25 µL was taken, diluted with 75 µL ddH_2O and 800 µL of the MGAM-mix were added. The calorimetric reaction was quenched with 100 µL Na-citrate and the assay mix was incubated for 15 min at room temperature before the absorption at 630 nm was measured. The amount of released phosphate by RACo was calculated from a standard curve (Appendix Figure 50) prepared from 1 to 9 nmol KH_2PO_4 plotted against the absorption at 630 nm. The absorbance of the sample was corrected by subtracting the absorbance of the corresponding control sample without protein.

One unit of activity (U) was defined as one µmol P_i released per minute. The specific activities of enzyme were designated in mU $(mg_{protein})^{-1}$ (equation 4).

$$1mU = 1\frac{\Delta nP_i[nmol]}{\min \times mg_{Protein}} \quad (4)$$

6.1.2. Coupled ATPase Assay

Table 8: Reaction mix and buffer used in the coupled ATPase activity assay.

Reaction mix		Buffer A	
9.9 U	LDH	100 mM	HEPES, pH 7.5
6.8 U	PK	150 mM	K-acetate / KCl
2 mM	Phosphoenolpyruvate	10 mM	Mg-acetate / $MgCl_2$
0.16 mM	NADH		
0.2 - 2 µM	Protein		

Beside the MGAM ATPase assay, a coupled assay with pyruvate kinase (PK) and lactate dehydrogenase (LDH) was used to follow the hydrolysis of ATP catalysed by wild type and the active site mutants of RACo (equation 5). The steady state kinetic constants, K_m and k_{cat}, were determined with this method (*110*).

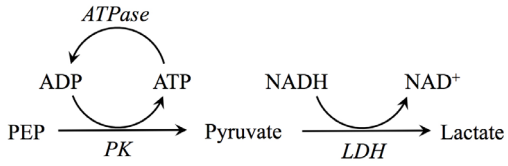

(5)

The reaction mixture was prepared in buffer A and contained either 200 nM or 2 µM of the wild type or the mutants of RACo. To test the influence of the presence of CoFeSP on the ATPase activity of RACo, the two proteins (2 µM each) were incubated for 10 minutes before the reaction was started. After blanking 0.16 mM of NADH was added and the reaction was initiated by addition of ATP. The consumption of NADH by LDH, corresponding to the ATPase activity of the enzyme, was followed spectroscopically by the decrease of absorption at 340 nm at 25 °C (Agilent 8453 photodiode array spectrophotometer with Peltier element). By varying the concentration of ATP from 0-9 mM the steady-state kinetic constants K_m and V_{max} were determined by applying the Michaelis-Menten equation (GraFit 5). One unit of ATPase activity was defined as one µmole of ADP produced per minute (equation 6) and was

calculated from the consumption of NADH by LDH using the extinction coefficient of NADH at 340 nm (ε_{340} = 6220 $M^{-1}cm^{-1}$).

$$1mU = \left[\frac{dn(ADP)}{\min \times mg_{Protein}} \right] = \frac{\Delta n(NADH)[nmol]}{\min \times mg_{Protein}} \quad (6)$$

6.2. ATP-Dependent Reductive Activation Assay

Table 9: Buffer of the reductive activation assay.

Buffer A	
100 mM	Tris/HCl, pH 8.0
150 mM	KCl
10 mM	$MgCl_2$
2 mM	DTT

The electron transfer assay was performed at a constant temperature of 25 °C under anoxic conditions inside a glove box using a photospectrometer equipped with a Peltier element (Agilent 8453 diode array photometer). The reaction mixtures contained equimolar amounts of the two proteins (usually 2.5 µM) in buffer A. The reaction was performed in 1 cm path-length cuvettes sealed with a butyl rubber septum and slight N_2 overpressure was applied. The reduction of the activator by DTT was followed by the decrease of absorption of characteristic bands for the [2Fe2S] cluster at 350, 410 and 460 nm. The baseline was defined when reduction of RACo was complete. Addition of ATP by a syringe initiated the reduction of Co(II)-CoFeSP to Co(I)-CoFeSP. The development of active Co(I)-species was followed by monitoring the increase of absorption at 390 nm and the decrease at 475 nm (*94*). Spectra were recorded every 5 – 10 s.

The electron transfer assay was also performed with the active sites mutants of RACo applying concentrations of 10 µM of both proteins in the reaction mixture as described above for the wild type.

7. Spectroscopy

7.1. UV-VIS Spectroscopy

UV-vis spectra of RACo wild type and mutants as well as of CoFeSP were measured on an Agilent 8453 photodiode array spectrophotometer. All measurements were performed anaerobically at 25 °C using quartz cuvettes with 1 cm path length. The UV-vis spectrum of 4 µM RACo (as-isolated) in 50 mM Tris/HCl, pH 8.0, 150 mM NaCl was recorded. To obtain reduced RACo, 2 mM dithiothreitol were added and complete reduction was achieved after approximately 20 min.

7.2. Resonance Raman Spectroscopy

Resonance Raman Spectroscopy was performed in cooperation with Wiebke Meister and Prof. Dr. Peter Hildebrandt (Institut für Chemie, Technische Universität Berlin) to investigate the influence of complex formation on the environment of the cofactors. Results of this cooperation have been published (*111*) .

7.2.1. Sample Preparation for Resonance Raman Spectroscopy

Samples were prepared anaerobically by concentrating the stock protein solutions (in 50 mM Tris/HCl, pH 8.0, 150 mM NaCl) to a final concentration of 1 mM. Vivaspin 500 concentrators with 30,000 MWCO for CoFeSP variants and 50,000 MWCO for RACo variants were used. When both protein variants were mixed, the samples were incubated for 15 min before concentrated using Vivaspin 500 spin concentrators with 100,000 MWCO (Sartorius stedim biotech GmbH). Reduced Co(I)-CoFeSP was prepared by adding 0.5 M DT to the sample.

A 3 µL drop of the sample solutions was placed onto a quartz holder and directly immersed in liquid nitrogen. The holders were subsequently transferred into the cryostat of the device.

7.2.2. Resonance Raman Spectroscopy of RACo and CoFeSP Variants

Measurements were carried out using the 413 nm line of a Krypton ion laser (Coherent Innova 300c) connected to a single-stage spectrograph (Jobin Yvon, LabRam 800 HR) and a liquid-nitrogen-cooled back-illuminated CCD detector. To focus the laser beam a Nikon 20× objective (N.A. 0.35) in a working distance of 20 mm was used. A laser power of 5 mW was applied to the sample and acquisition times ranged from 60 to 150 s according to the spectral quality of the samples. Signal / noise ratio was improved by averaging 4–30 single spectra. RR spectra were measured at approximately 80 K (Resultec/Linkam cryostat) under constant nitrogen stream on the sample.

7.2.3. Electron Paramagnetic Resonance Spectroscopy (EPR)

EPR was performed in cooperation with Dr. Friedhelm Lendzian and Prof. Dr. Peter Hildebrandt (Institut für Chemie, Technische Universität Berlin). Results have been published (*111*) .

7.2.4. Sample Preparation for EPR Spectroscopy

EPR samples of RACo and Co(II)-CoFeSP were prepared by dilution of the protein stock solutions to a final concentration of 300 µM in 50 mM Tris/HCl, pH 8.0, 150 mM NaCl. A complex sample was prepared by mixing both proteins in the presence of 300 mM DTT followed by incubation for 15 min. Co(I)-CoFeSP was obtained by incubation of the protein with 300 mM DT. The samples were transferred into EPR sample tubes. The tubes were gas-tight sealed and exported from the glove box and immediately frozen in liquid nitrogen.

7.2.5. EPR Spectroscopy of CoFeSP and the RACo:CoFeSP Complex

EPR measurements were performed at 9.3 GHz on a Bruker EMX Plus spectrometer connected to a high sensitivity cylindrical mode resonator (Bruker Super-high-Q-cavity ER 4122 SHQE). The spectra were recorded at a field modulation of 100 kHz and 10 G. Temperature was set with a cryostat (Oxford ITC4, Oxford ESR 900 helium flow) to 100 K to detect Co(II) and / or reduced [2Fe2S] and to 10 K for reduced [4Fe4S]. Background spectra of each set of experimental conditions were measured and used as correction for the protein spectra.

8. Redox Titration of RACo, CoFeSP and the RACo:CoFeSP Complex

Redox titrations were performed in the laboratory of Prof. Dr. Peter Hildebrandt together with Dr. Friedhelm Lendzian (Institut für Chemie, Technische Universität Berlin).

The buffer of the protein stock solutions was exchanged to 100 mM CAPSO, pH 9.5 using PD10 columns (GE Healthcare) to extend the negative potential range of sodium dithionite. RACo, Co(II)-CoFeSP and RACo-Co(II)FeSP-complex samples with a final concentration of 130 µM in 2 mL buffer were prepared. The samples were evacuated and flushed with argon in order to remove hydrogen.

The titration was performed inside a glove box under an atmosphere of nitrogen with oxygen concentrations below 10 ppm (VAC 101965 OMNILAB). A mediator mix covering a midpoint potential range from +80 to -550 mV was prepared by mixing 50 µM of phenazine methosufate, toluidine blue, methylene blue, indigocarmine, anthrachinone-2-sulfonate, phenosafranine, safranine T, deiquat, methylviologen and triquat, respectively,. The mediator mix was resuspended in the sample and DT was added stepwise. Potentials were measured with an Ag-AgCl electrode. Equilibrium was reached when the measured potential drift was less than 2 mV per minute. For each potential exactly 80 µL of the protein solution was transferred to an EPR tube. The tube was sealed and extroduced from the glove box. The samples were immediately frozen and stored in liquid nitrogen. EPR spectra were measured according to Materials and Methods 7.3.2. and the intensities of every species were plotted against the corresponding potentials. The potentials measured with the Ag-AgCl electrode were corrected by the potential of the redox electrode determined with quinhydrone. Data

have been fitted to a single-electron process (z = 1) according to the Nernst equation where E^{θ}_{red} is the standard half cell reduction potential, R= 8.314 J K^{-1} mol^{-1} is the universal gas constant and F = 9.648×10^{4} C mol^{-1} is the Faraday constant (equation 7).

$$E_{\mathrm{Re}d} = E^{\Theta}{}_{red} - \frac{RT}{zF}\ln\frac{c_{\mathrm{Re}d}}{c_{Ox}} \qquad (7)$$

9. Crystallisation

9.1. Crystallisation of the RACo:CoFeSP Complex

All crystallisation experiments were set up under anoxic conditions with a 95 % N_2/ 5 % H_2 atmosphere and oxygen concentrations below 1 ppm. The sitting drop vapour diffusion method was used for initial screening. Crystals were obtained from various screens appearing after a period of several months. All crystallisation conditions contained PEG 3350 and low salt concentrations. The crystals were transferred into cryoprotective buffer consisting of the reservoir solution and 10 % (v/ v) 2*R*,3*R* butanediol as cryoprotectant and flash cooled with liquid nitrogen.

9.2. Data Collection

Diffraction data were collected on beamlines 14.1 and 14.2 at the Helmholtz Zentrum Berlin (BESSYII) (*112*). Collected data were indexed and processed with X-ray Detector Software (XDS) (*113*) to a resolution of 2.5 Å. The crystal belonged to space group P1 with cell parameters a = 67.13, b = 128.18, c = 163.37, α = 77.61, β = 82.25, γ = 88.76. Calculation of the Matthew's coefficient suggested a solvent content of 43 % and four molecules per asymmetric unit using a molecular size of 150 kDa per complex molecule.

9.3. Structure Determination, Refinement and Graphical Representation

Phase determination was carried out by molecular replacement with structures of the single compounds of the complex, using RACo (PDB 3ZYY) (*102*) and CoFeSP (2YCL) (*94*) as search models. Initially, CoFeSP was used as a search model and the RACo structure was applied as a secondary search with the fixed solution from the first replacement using either Phaser of the CCP4i programme suite (*114*) or the Phenix packages (*115*). A model of the structure was built according to the observed electron density map and the sequence of the single proteins using the programme COOT (*116*). The structure was further refined with REFMAC5 (CCP4i) (*114*) and REFINE of the Phenix package (*115*) to final R_{work} and R_{free} of 20.4 % and 25.6 %, respectively. Statistics for refinement are summarised in Appendix Table 22. Graphical presentations of the final model and of all other protein structures showed in this thesis were created using the programme PyMol (*117*).

III. RESULTS AND DISCUSSION

1. Cloning, Mutagenesis and Expression

1.1. RACo

The gene CHY_1224, an uncharacterised gene (*orf7*) located in the gene cluster coding for the structural genes of the reductive acetyl-CoA pathway (Figure 11), was amplified by PCR from the genomic DNA of *Carboxydothermus hydrogenoformans* Z-2901 and cloned into pETDuet1 and pET28a vector (Novagen) by Dr. Jae-Hun Jeoung (Strukturbiologie / Biochemie, Humboldt Universität zu Berlin). The resulting constructs were named pPKCoDuet1 and pPKCo28a, respectively. The construct pPKCoDuet1 was first used for native purification. Protein purified from pPKCo28a contained a non-cleavable His-tag.

To simplify the purification as well as to increase the purity of RACo and to have a cleavable affinity tag, the plasmids pPKCoDuet1 and pPKCo28a were modified by inserting a cleavage site for Tobacco Etch Virus (TEV) protease as described in Materials and Methods 3.2. These constructs were used for purification as well as templates for mutagenesis. The active site mutants D212, D377, E404, and T380 were created from pPKCoDuet1-TEV. For RACoΔ100 and the S398 mutants pPKCo28aTEV served as template. All mutated constructs were obtained as described (Materials and Methods 3.2) and the successful insertion of the desired mutation(s) was confirmed by sequencing (Eurofins MWG Operon, Ebersberg, Germany). Plasmids were transformed into *Escherichia coli* BL21(DE3) and expressed as described in Materials and Methods 3.5 and 4.1.1.

1.2. CoFeSP

The plasmid pPKCD was kindly provided by Sebastian Götzl (Strukturbiologie / Biochemie, Humboldt Universität zu Berlin) and was used as template for modifications and mutations of CoFeSP. The deletion variants Δ_N60-CoFeSP and Δ_C128-CoFeSP as well as C25P-CoFeSP were obtained from the original plasmid as described in Materials and Methods 3.3. All constructs were confirmed by sequencing (Eurofins MWG Operon, Ebersberg, Germany).

CoFeSP and its variants were expressed in *Escherichia coli* BL21(DE3) cells (see Materials and Methods 3.5 and 4.1.2).

2. Purification of Proteins

2.1. Purification of RACo, RACo Mutants and Δ100-RACo

2.1.1. Purification without Affinity Tag

The reductive activator of CoFeSP was purified natively in a three-step purification. Ion-exchange chromatography (IEC), followed by hydrophobic interaction chromatography (HIC) and size exclusion chromatography (SEC) were applied sequentially.

In a standard native purification, 50 – 80 mg of RACo were obtained from 20 – 30 g cells (wet weight). According to the primary structure of the *orf7* gene product, the dimeric protein binds one [2Fe-2S] cluster per monomer. The amount of protein bound iron ranged from 50 to 71%.

2.1.2. Purification Using a Removable Affinity Tag

Wild type and the different variants of RACo, e.g. RACoΔ100, the active site mutants and S398A/C were isolated based either on a two-step (mutants D121A-, D377A-, E404A- and S398A/C-RACo) or three-step purification including immobilised metal affinity chromatography (IMAC) and size-exclusion chromatography (SEC). For wildtype-RACo a three-step purification including affinity chromatography (IMAC), ion-exchange chromatography (IEC) and size-exclusion chromatography (SEC) was performed (Appendix Figure 49). Due to the removable His_6-tag an overnight incubation of fractions containing RACo with TEV protease was included to the standard purification protocol. To check the occupancy of the [2Fe2S] cluster the iron content of the protein batch was determined (Materials and Methods 5.3). RACo obtained by this purification strategy bound between 47 and 84 % of iron.

Figure 13 shows a SDS-PAGE analysis of RACo samples prepared as described above.

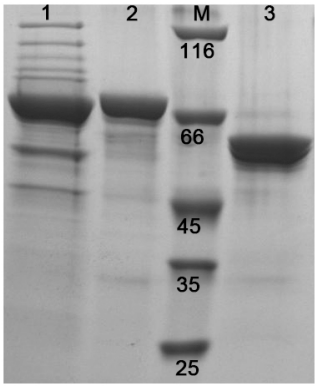

Figure 13: SDS-PAGE analysis of RACo samples. The final activator fraction after three purification steps was loaded onto a 12% (w/v) SDS gel to analyse protein purity. 20 µg of every sample were loaded. Lane 1: natively purified RACo; lane 2: RACo purified via affinity chromatography; lane 3: Δ100-RACo. Lane M contains a molecular mass marker with the indicated sizes in kilodalton.

2.2. Purification of CoFeSP and CoFeSP Variants

CoFeSP, Δ_N60-CoFeSP, Δ_C128-CoFeSP as well as the mutant C25P-CoFeSP were purified without chromatography tag applying a four-step purification protocol. The purification included two IEC steps, one HIC step followed by SEC chromatography (Materials and Methods 4.2.1.3). Approximately 50 – 100 mg of CoFeSP were purified from 20 g cells (wet weight) in a standard purification. In the case of the C25P-mutant only 10 mg were obtained. The yield of the variants Δ_N60-CoFeSP and Δ_C128-CoFeSP was 25 and 85 mg, respectively.

An SDS-PAGE analysis of CoFeSP and the variants ΔN60-CoFeSP, ΔC107-CoFeSP is shown in Figure 14.

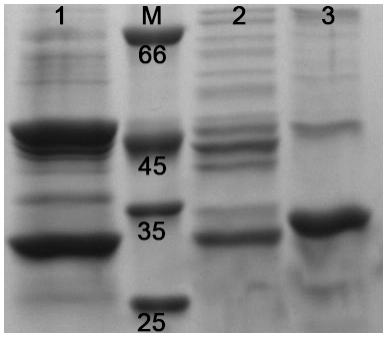

Figure 14: SDS-PAGE analysis of CoFeSP samples. The final CoFeSP fraction after native purification of CoFeSP (lane 1), Δ_C128-CoFeSP (lane 2) and Δ_N60-CoFeSP (lane 3) are shown. About 20 µg of protein were loaded onto a 12% (w/v) SDS gel. Lane M contains a protein marker with sizes indicated in kilodaltons.

3. Biochemical Characterisation of RACo

3.1. UV-Vis Spectroscopy of RACo

The primary structure of the *orf7* gene product contains a [2Fe-2S] cluster binding motif (C-X5 -C-X2 -C-Xn –C) and the crystal structure of the protein showed that it contained a plant-type ferredoxin [2Fe2S] cluster bound to its N-terminus (Figure 13A). This domain shares sequence identities with these ferredoxins of 28-30 % and displays the typical β-grasp topology with a β-sheet consisting of five β-strands and one α-helix. The [2Fe2S] cluster is bound near the surface (Figure 15A).

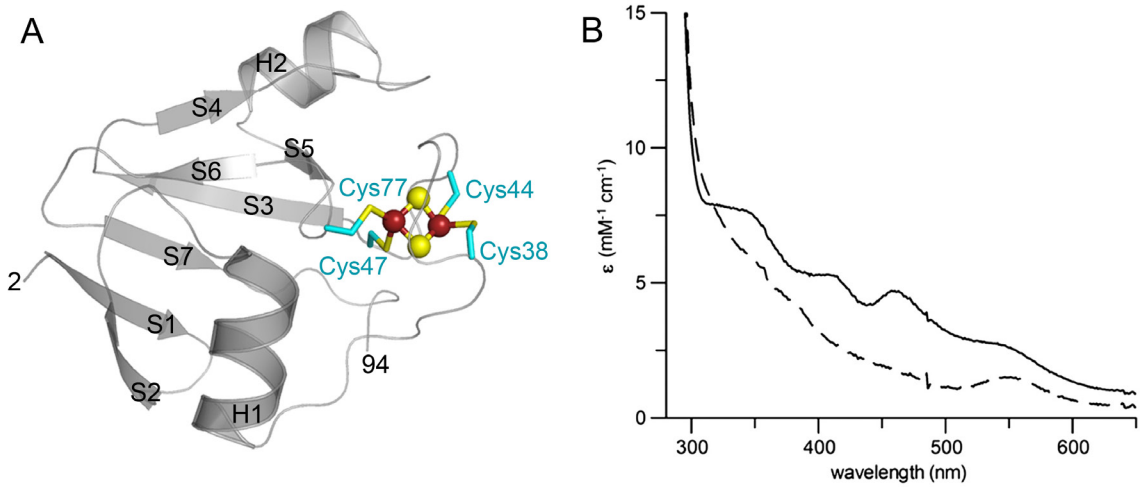

Figure 15: Structure and UV-Vis spectrum of the plant-type ferredoxin [2Fe2S] cluster bound to the N-terminus of RACo. (A) The N-terminal domain is shown as grey cartoon. Strands and helices are labelled. Cysteine residues coordinating the iron atoms (red spheres) are shown as cyan sticks. Sulfurs are coloured in yellow. (B) The spectrum of as-isolated RACo (4 µM) is shown as solid line, the spectrum of reduced RACo as dashed line, respectively.

The UV-Vis spectrum of the (putative) as-isolated activator is characteristic for an oxidised cluster of this type (Figure 15B). Maxima at 350, 410 and 460 nm and a shoulder at 550 nm are clearly distinguishable (solid line). The cluster was bleached in the presence of 2mM DTT within 20 min (dashed line) due to one-electron reduction to its +1 state.

3.2. ATPase Activity of RACo

The *orf7* gene product shares a common central fold with members of the ASKHA protein family and in the crystal structure a interdomain cleft, where usually nucleotide-binding and hydrolysis occur was identified (Figure 12B and C) (*47, 48*).

The ATPase activity of RACo was analysed by two different methods (Materials and Methods 6). As the ATPase activity of RACo was not influenced by the presence of oxygen, most of the experiments were performed under oxic conditions.

3.2.1. Determination of the Specific ATPase Activity by the MGAM Assay

For a first determination of the specific ATPase activity of RACo a calorimetric method was used. The release of inorganic phosphate was detected via the absorbance of the phosphomolybdate-malachite green complex according to a modified protocol (Materials and Methods 6.1.1) (*109*).

For every sample a control without protein was measured to determine the auto-hydrolysis of ATP (Figure 16A, white circles). The absorbance of the sample was corrected by subtracting the absorbance of the corresponding control sample. From the change in absorption at 630 nm in certain time intervals the phosphate release per minute was calculated. All samples were measured in triplicate and average values and the corresponding standard deviations are given.

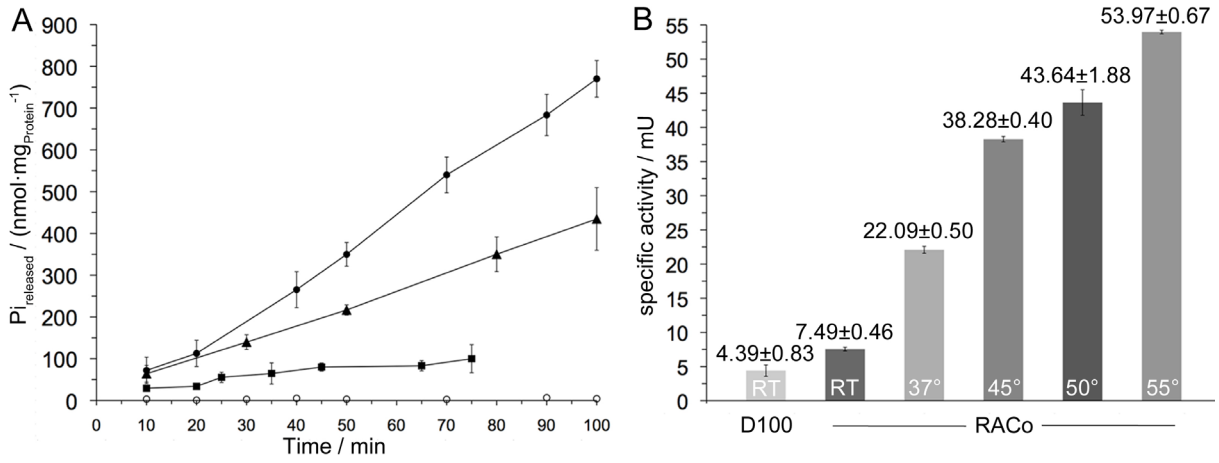

Figure 16: Specific ATPase activity of RACo determined by the MGAM assay. (A) Shown are the amounts of released phosphate per mg protein of RACo (filled circles), Δ100-RACo (filled triangles) and RACo with an N-terminal His-tag (filled squares). All samples were measured at room temperature. (B) Specific activities of RACo measured at different temperatures are given with standard deviations. The specific activity of Δ100-RACo (D100) was measured at room temperature.

At room temperature RACo (purified natively) displayed a specific activity of 7.49 ± 0.46 mU (Figure 16A, filled circles) corresponding to a k_{cat} of 0.51 ± 0.03 min^{-1}. The specific activity of Δ100-RACo was determined to be 4.49 ± 0.83 mU (Figure 16A, filled triangles) with a k_{cat} of 0.31 ± 0.06 min^{-1}. The specific ATPase activity of RACo with N-terminal His-tag was measured at 50°C. The protein showed a low activity of 1.87 ± 0.56 mU in contrast to an activity of 43.64 ±1.88 mU determined for RACo without tag at the same temperature (Figure 16A, squares). A dependency on the temperature was observed: increase in temperature resulted in an increase of the specific activity (Figure 16B).

3.2.2. Coupled ATPase Activity Assay

A coupled assay (Materials and Methods 6.1.2) was performed for the determination of the kinetic parameters of the ATPase activity of RACo. The coupled assay allows for continuous measurement and is, compared to the MGAM assay, less time-consuming.

The ATPase converts ATP to ADP, which is continuously regenerated in the reaction of phosphoenolpyruvate to pyruvate catalysed by phosphokinase. Pyruvate reacts to lactate

under consumption of NADH mediated by lactate dehydrogenase. The decrease of NADH can be followed directly by the decrease in absorption at 340 nm. The consumption of NADH and the conversion of ATP by the ATPase are directly coupled (*110*).

For the determination of the parameters K_m and V_{max} of RACo and the active site mutants the concentration of ATP in the assay was varied between 0 and 9 mM and rates were plotted against the concentration of the nucleotide. Data were fitted applying the Michaelis-Menten equation. Every sample was measured at least in triplicate.

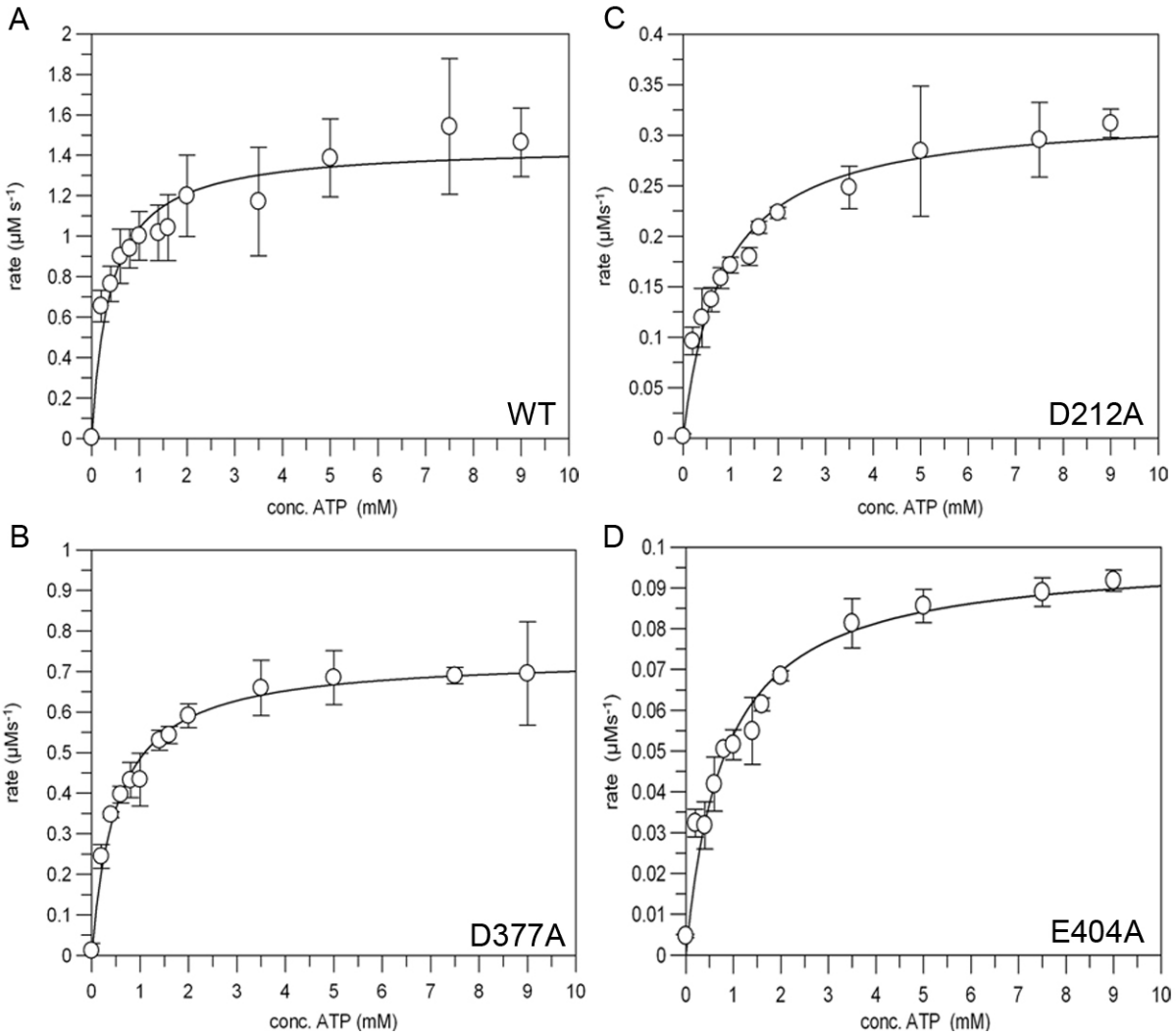

Figure 17: Steady-state kinetics of ATP hydrolysis. The steady-state kinetics of wild type (A) and the active site mutants of RACo D377A (B), (C) D212A and E404A (D) are shown.

Figure 17 displays the steady-state kinetics of ATP hydrolysis. Activity determined with this assay was dependent on the presence of Mg^{2+} and K^{+} ions in the buffer. The steady state kinetic constants of natively purified wild type RACo (panel A) and the active site mutants D377A (panel B), D212A (panel C) and E404A (panel D) were determined. The wild type shows the highest activity with a k_{cat} of 7.24 ± 0.30 s^{-1} and K_m of 0.39 ± 0.07 mM corresponding to a maximum reaction rate (V_{max}) of 6.4 ± 0.3 U $(mg_{Protein})^{-1}$. As expected, the active site mutants show lower catalytic activities than the (natively purified) wild type protein. E404A-RACo has an approximately 145-fold lower catalytic activity with a k_{cat} of 0.048 ± 0.002 s^{-1} and a slightly increased K_m of 0.81 ± 0.11 mM. The aspartate mutants D212A-RACo and D377A-RACo exhibit diminished catalytic rates with minor changes in the K_m values (D212A: k_{cat} = 0.16 ± 0.01 s^{-1}, K_m = 0.83 ± 0.10 mM; D377A: k_{cat} = 0.37 ±0.02 s^{-1} and K_m = 0.52 ± 0.04 mM).

The discrepancy between the activities obtained by the different assays is conspicuous. The assay conditions, however, differ in the composition of the buffer. The buffer first used in the coupled assay contains acetates (Table 8, Materials and Methods 6.1.2) that can be a substrate of acetate kinase, an enzyme found in almost all anaerobic bacteria and archaea acting in important pathways for acetyl-CoA synthesis (*118–120*). In *E. coli* acetate kinase is abundantly present, even if not grown on acetate (*121*). Acetate kinase catalyses the reaction of acetate to acetyl phosphate under consumption of ATP (*122*). Thus it is likely that impurities in the protein sample influenced the ATPase activity when acetate salts were present in the reaction. To check the impact of impurities (acetate kinase and other ATPases) on the activity, the assay was performed using the coupled assay in the absence of acetates as well as with protein samples of higher purity grade, e.g. RACo purified by a two-step or three-step purification protocol including Ni-IMAC (see Materials and Methods 4.2.1.2). RACo prepared by this protocol exhibits a decrease in the overall ATPase activity; activities are also lower in the presence of chloride salts (Figure 18).

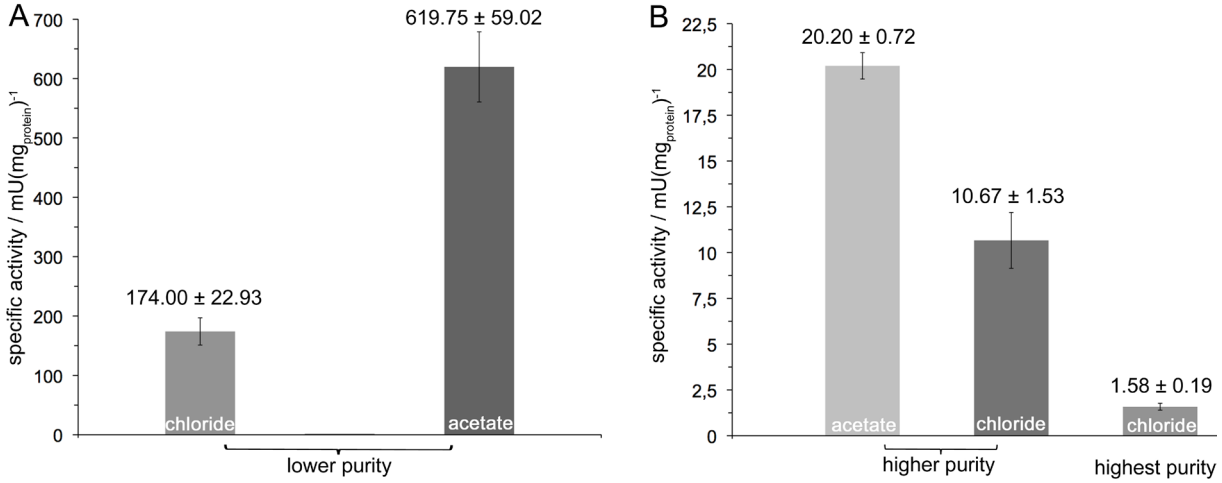

Figure 18: Comparison of activities determined in the presence of different ions and with RACo of distinct purity grade. Displayed are the specific ATPase activities of RACo determined by the coupled assay in the presence of acetate or chloride for natively purified protein (lower purity) (A) and protein purified in a two (higher purity) or three-step (highest purity) protocol including IMAC (B). All measurements were carried out at least in triplicate. Error bars indicate standard deviations.

In the presence of acetate, natively purified RACo displays a specific ATPase activity of 6.4 ± 0.3 U $(mg_{Protein})^{-1}$ or 0.620 ± 0.59 U $(mg_{Protein})^{-1}$ depending on the purification batch. The specific activity in the presence of chlorides of natively purified protein decreased to 174 ± 22.93 mU $(mg_{Protein})^{-1}$ indicating that beside acetate kinases further impurities displaying ATPase activity were present (Figure 18A). In contrast, samples of RACo prepared by a two-step purification including affinity chromatography (Materials and Methods 4.2.1.2) showed activities of 20.20 ± 0.72 mU $(mg_{Protein})^{-1}$ in the presence of acetate and 10.67 ± 1.53 mU $(mg_{Protein})^{-1}$ in the presence of chlorides. Protein obtained by a three-step purification including IMAC (Materials and Methods 4.2.1.2), displayed a minor specific activity of 1.58 ± 0.19 mU $(mg_{Protein})^{-1}$ (Figure 18B). Determination of the steady-state kinetic constants applying non-linear regression analysis following the Michealis-Menten equation was not possible anymore due to low rates in ATP hydrolysis. These values are now in better agreement to the activities determined by the malachite green assay. The colorimetric assay quantifying the amount of phosphate released by the reaction of the ATPase was also performed with acetate in the buffer and increased activities were measured for natively purified protein. This demonstrates that the ATPase activity of different RACo batches is highly influenced by impurities with mainly (acetate) kinase activity.

It has been shown that the ATPase activity of the activator of 2-hydroxyisocaproyl-CoA dehydratase from *Clostridium difficile* increases from 1.5 mU (mgProtein)$^{-1}$ up to 50 mU (mgProtein)$^{-1}$ in the presence of the partner protein dehydratase indicating that electron transfer takes place in the protein-protein complex (52, 123). The Fe-protein of nitrogenase belongs to a class of nucleotide-switch proteins. It does not exhibit intrinsic ATPase activity in the absence of the FeMo-protein, though (18, 124). ATP hydrolysis is only observed in the presence of the partner protein indicating that ATP hydrolysis and electron transport are efficiently coupled in the nitrogenase complex.

The influence of the presence of the biological partner, CoFeSP, on the specific ATPase activity of RACo was investigated. For the experiment highly pure CoFeSP has been mandatory as the determination of the specific ATPase activity is highly dependent on the purity of the proteins used in the assay. As shown for RACo, natively purified protein exhibits high activities deriving from impurities. Therefore, a distinct strategy was used for the purification of CoFeSP (Materials and Methods 4.2.1.4). The specific activity of the CoFeSP preparation, determined by the coupled assay, was 0.35 ± 0.21 mU (mgProtein)$^{-1}$. When CoFeSP and RACo were present in the reaction, the activity increased to 38.12 ± 5.44 mU (mgProtein)$^{-1}$ (coupled assay) and 46.41 ± 2.84 mU (mgProtein)$^{-1}$ (MGAM assay) (Figure 19). The approximately 25-fold increased activity cannot be explained as simply as the sum of the single activities and indicates that RACo´s affinity towards ATP and / or hydrolysis rate is higher in the complex.

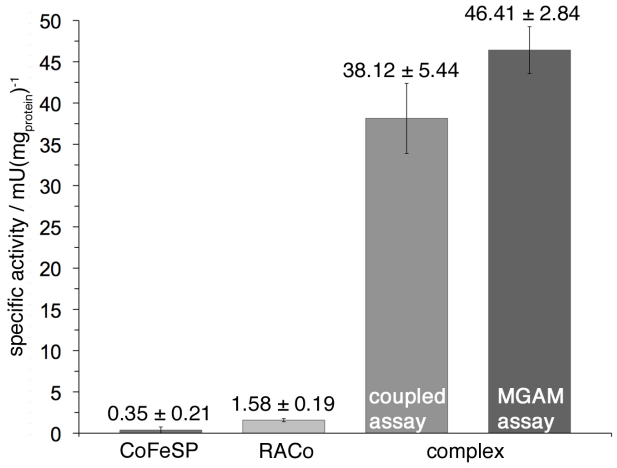

Figure 19: Comparison of the ATPase activities of CoFeSP, RACo and the RACo:CoFeSP complex. Activities were determined by the coupled assay applying 2 µM of protein and 1 mM of ATP. The activity of the complex was additionally determined by the MGAM assay with 10 µM of each protein and 5 mM of ATP.

3.3. Redox Titration of RACo Combined with EPR

In cooperation with Dr. Friedhelm Lendzian the redox potential of the cluster bound to RACo was determined by titration of the protein with Na-sodium dithionite. The titration was performed under anoxic conditions under an atmosphere of nitrogen and samples for EPR spectroscopy were taken at every potential step (Materials and Methods 8) and measured as described in Materials and Methods 7.2.5. The intensities of the EPR signals of the [2Fe2S] cluster bound to RACo at defined potentials were determined (Figure 20A). Relative intensities of the EPR signals were plotted against the corresponding potentials and fitted to a single-electron Nernstian process (Figure 20B).

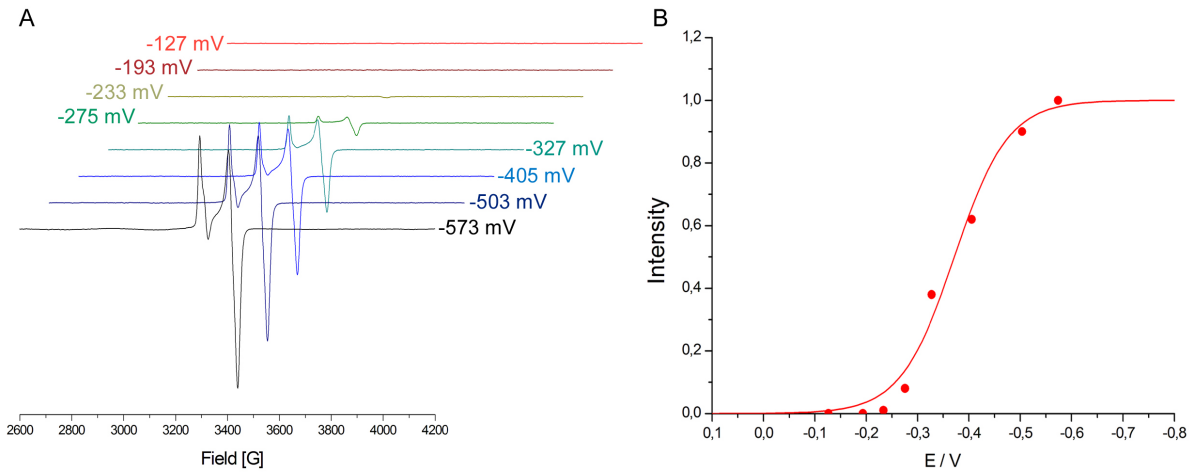

Figure 20: Redox titration of RACo. (A) EPR spectra of samples taken at given potentials recorded at 100 K. (B) Relative intensities of the EPR signals of the [2Fe2S] cluster were plotted as a function of the equilibrium redox potentials. The least-square fit to the Nernst-equation for n=1 with a midpoint potential of -371 mV is displayed as a solid line.

The redox potential determined from the data was –371 mV. The number of electrons in this one-electron reduction is 0.47 and is probably an effect of inhomogeneity of the protein sample and reflects the actual iron content of the purification batch.

The midpoint potential of the [2Fe2S] cluster of RACo is similar to the potential of another RACE protein (–330 ± 20 mV), namely the activating enzyme of the vanillate- and veratrol-*O*-demethylases of *Acetobacterium dehalogenans* (*17*) and is comparable to the midpoint potential of other plant-type ferredoxins (*125, 126*).

4. Characterisation of the Interactions between RACo and CoFeSP

4.1. ATP-Dependent Reductive Activation of CoFeSP by RACo

An ATP dependent activation of the corrinoid containing enzyme by RACE proteins was shown for the veratrol-*O*-demethylase of *Acetobacterium dehalogenans* (*16, 17, 73, 74*) and for RamA, isolated from *Methanosarcina barkeri* involved in the activation of the monomethylamine corrinoid protein, MtmC (*15*). Based on these experiments an electron transfer assay for CoFeSP and its putative activator was developed (Materials and Methods 6.2).

4.1.1. Electron Transfer between the Wildtypes of RACo and CoFeSP

For the above-mentioned activating enzymes a strong reducing agent is needed for the reduction of the FeS clusters. As CoFeSP is reduced by Ti(III)-citrate (*94*), another reducing agent for the reduction of the [2Fe2S] cluster of RACo was required. The addition of 2 mM DTT was sufficient to reduce the [2Fe2S] cluster of RACo but neither the cobalamin nor the [4Fe4S] cluster of CoFeSP. The reduction of the [2Fe2S] cluster was tracked by the bleaching of the bands at 350, 410 and 460 nm (Figure 15B, dashed line and Figure 23A). When the reduction was complete after 10 – 20 minutes, electron transfer from $[2Fe2S]^{1+}$ to Co(II)-CoFeSP was initiated by the addition of ATP (Figure 21A). The conversion of Co(II) to Co(I) was monitored by the decrease of the absorption at 475 nm. A distinct band at 390 nm evinced the formation of the Co(I) species (Figure 21B). Important to note is that upon electron transfer the [2Fe2S] returned to its +2 state influencing the absorption at 475 nm. The electron transfer from RACo to CoFeSP strictly depends on the presence of ATP and equimolar concentrations of the activator. No reduction was observed when catalytic amounts of RACo were applied in the assay as the slow reduction of the [2Fe2S] cluster by DTT is the limiting step in this single turnover experiment.

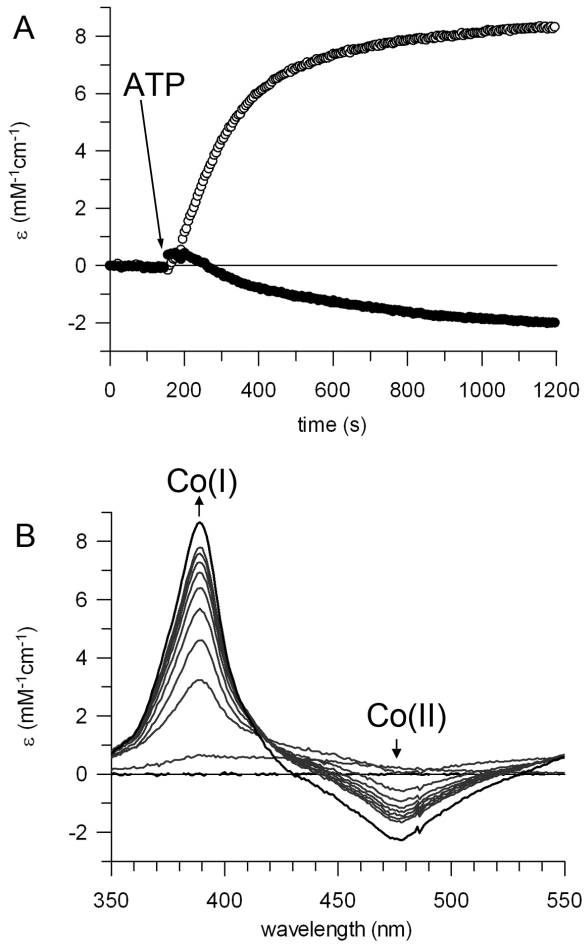

Figure 21: ATP-dependent electron transfer from RACo to CoFeSP. (A) The changes in absorption are induced by ATP addition as can be seen from the time-dependent change in extinction at 390 nm (white circles) and 475 nm (black circles). (B) The transfer of the electron from the reduced [2Fe2S] cluster of RACo to Co(II)-CoFeSP can be followed by UV-vis-spectroscopy and is indicated by the decrease in absorption at 475 nm (Co(II)-signal) and the increase of the signal at 390 nm (Co(I)-peak).

The electron transfer rate constants were determined by single-exponential fits. The catalytical rate of a typical assay reaction (initiating the transfer of the electron by addition of 1 mM ATP) was 1.27 ± 0.23 min^{-1} corresponding to a specific electron transfer activity of RACo of 18.62 ± 3.44 mU $(mgProtein)^{-1}$. When the reaction was performed with 0.5 mM ATP, the catalytical rate decreased to 0.51 ± 0.09 min^{-1} resulting in a specific activity of 7.47 ± 1.28 mU $(mgProtein)^{-1}$. All measurements were carried out at least in triplicate.

Figure 22 shows exemplary ET experiments with 1 and 0.5 mM ATP added. Preliminary experiments had already demonstrated the dependency of the electron transfer rate on the ATP concentration (Appendix Figure 52).

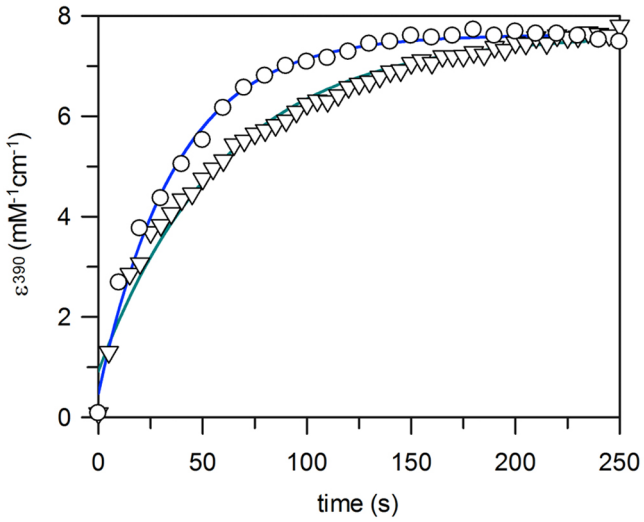

Figure 22: Dependency of the ET on the ATP concentration. Exemplary changes in the extinction at 390 nm upon reduction of CoFeSP by RACo initiated by 1 mM (white circles) and 0.5 mM (white triangles) ATP are shown. Experimental data points were fit to single-exponential equation to calculate the corresponding rate constants. Fitting curves are presented in blue (1 mM ATP) and green (0.5 mM ATP). The catalytice rate of ET initiated by the addition of 1 mM ATP was calculated to be 0.932 min^{-1}. The same experiment with 0.5 mM ATP resulted in a catalytic rate of 0.494 min^{-1}.

Usually, RACo activated approximately 70 % of CoFeSP present in the reaction. The yield of Co(I)-CoFeSP was dependent on the cobalamin content of the different purification batches of CoFeSP. At constant concentrations of Co(II)-CoFeSP, increased concentrations of RACo did not result in a significant increase of the Co(I)-CoFeSP signal.

The reductive activation activity of RACo (0.3 nkat mg^{-1} in the presence of 1 mM of ATP) is comparable to the corrinoid reduction activities of other RACE proteins (*74*). A reduction activity of 0.3 nkat mg^{-1} was reported for the corrinoid-dependent methylamine methyltransferases of *M. barkeri* (*15*) and Dhaf_2573 of *D. hafniense* DCB-2 activated the corrinoid protein Dhaf_4611 with 0.5 nkat mg^{-1} (*73*).

As the catalytic rates of the ATPase reaction (in the absence of acetate) and of the electron transfer are in the same range, both processes are presumptively coupled.

4.1.2. Electron Transfer Assay Performed with Mutants of RACo and CoFeSP

The electron transfer assay was also performed with the active site mutants D212A-, D377A- and E404A-RACo to check whether the transfer of the electron is dependent on ATP binding or ATP hydrolysis. Figure 23 shows exemplarily the spectra of the reduction of the mutant D377A-RACo (Figure 23A) and ATP-induced electron transfer. No ATP-induced reduction of CoFeSP by the active site mutant(s) D121A, D377A and E404A was detectable. However, re-oxidation of the [2Fe2S] cluster was observed (Figure 23B) upon ATP addition. Dithiothreitol seems to be the electron acceptor as implied by the change in absorption at 315 nm. The excess of DTT in the reaction resulted in a slow re-reduction of the cluster (not shown).

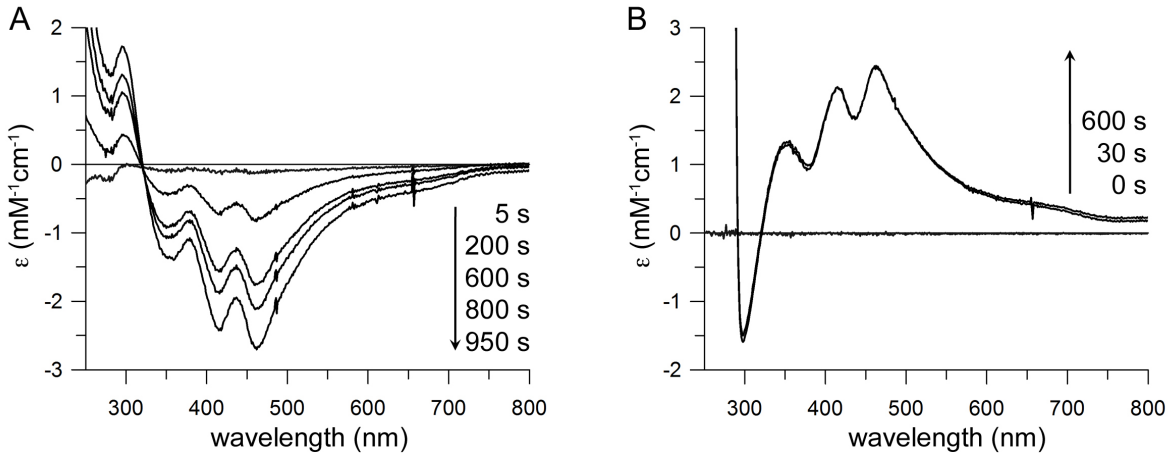

Figure 23: Electron transfer assay performed with the active site mutant D377A. (A) The reduction of 10 µM of the RACo mutant D377A in the presence of 10 µM CoFeSP and 2 mM DTT was followed by UV-vis spectroscopy. The decrease in absorption at 350, 410 and 460 nm and increase at 315 nm display the electron transfer from DTT to the [2Fe2S] cluster. (B) Addition of 1 mM of ATP caused the re-oxidation of the reduced cluster. Electron transfer from the [2Fe2S] cluster of RACo to Co(II)-CoFeSP was not detected.

The ATPase activity measurements did not reveal whether the mutation of single residues of the active site had changed the binding and / or hydrolysis behaviour of the protein (Results and Discussion 3.2.2) and it is hard to conclude if the activities of wildtype and mutants really differ. The modification of the nucleotide-binding site definitely influences the electron transfer ability of RACo (Figure 23) indicating that mutagenesis of specific residues within the nucleotide-binding site bias the function as electron transferase.

The ET assay was performed with the CoFeSP variants Δ_N60-CoFeSP and Δ_C128-CoFeSP as well as with apo-CoFeSP (not B12-reconstituted). No electron transfer between RACo and CoFeSP lacking its N-terminal [4Fe4S]-binding domain (Δ_N60-CoFeSP) was observed. Furthermore, in the presence of apo-CoFeSP and Δ_C128-CoFeSP, spectral changes indicating that the electron was transferred to the [4Fe4S] cluster of CoFeSP (in the absence of the corrinoid) were not detected neither. In all experiments reoxidation of the [2Fe2S] cluster of RACo was monitored.

The mutant C25P-CoFeSP, presumably binding a [3Fe4S] cluster, was prepared (Materials and Methods 3.3.2) to investigate the role of the FeS cluster in the conduit of the electron from the reduced [2Fe2S] of RACo to the cobalamin bound to CoFeSP. The alteration of the cluster theoretically increases the redox potential and should abort the electron flow if it was part of the conduit (*99*). The assay was performed with C25P-CoFeSP as described for wildtype CoFeSP. Reduction of the cobalamin was observed with a catalytical rate of 1.09 ± 0.12 min^{-1} (Figure 24). As the catalytical rates are almost the same and the yield of Co(I) in both cases was approximately 65 %, it is rather implausible that the [FeS] cluster bound to CoFeSP is part of the conduit of electrons from the [2Fe2S] cluster to the cobalamin.

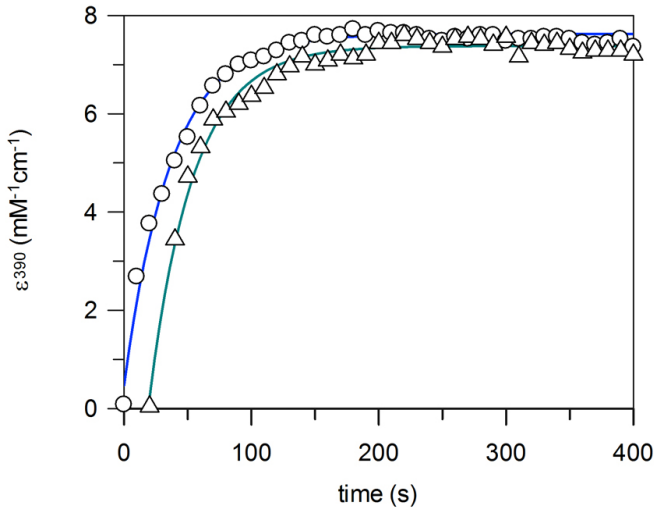

Figure 24: Comparison of electron transfer mediated by RACo to wild type CoFeSP and the C25P mutant of CoFeSP. The changes in extinction at 390 nm of wildtype CoFeSP (circles) and of the C25P mutant (triangles) upon reduction by RACo are shown. The fitting curves are shown in blue (wildtype) and green (mutant).

All results demonstrate that RACo is able to transfer one electron from its [2Fe2S] cluster to the cobalamin of Co(II)-CoFeSP in an ATP-dependent process (Figure 21) The data of the C25P mutant do not indicate for a role of the [4Fe4S] cluster of CoFeSP during the reduction of the cobalamin as suggested by Menon (*99, 100*).

The results described in this chapter clearly establish the *orf7* gene product as the reductive activator of CoFeSP. The scheme of the reductive acetyl-CoA pathway of *C. hydrogenoformans* can therefore be extended by the "reductive activation" mediated by RACo (Figure 25).

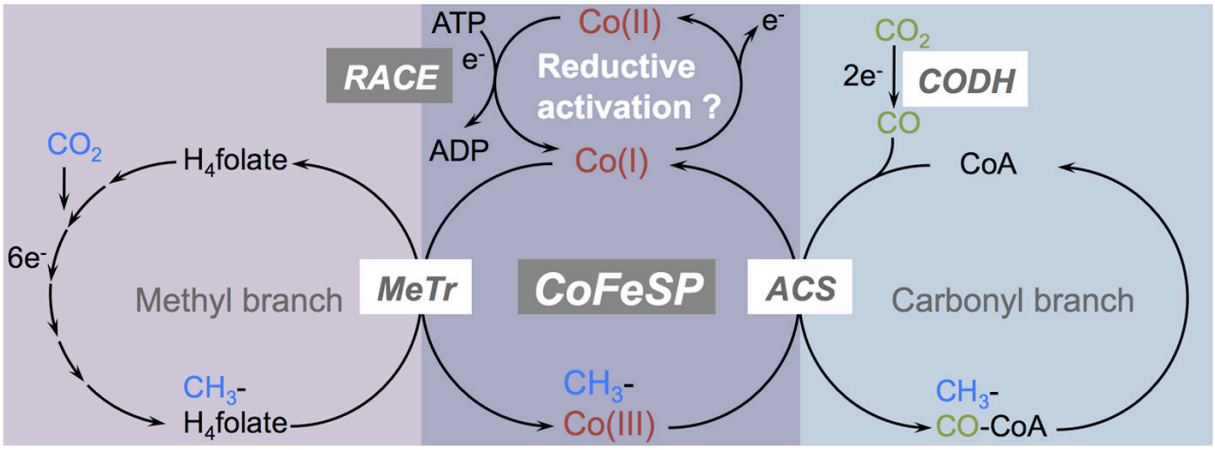

Figure 25: Reductive acetyl-CoA pathway of *C. hydrogenoformans* including the reductive activation of CoFeSP by RACo. In case of incidental oxidation of Co(I)-CoFeSP to Co(II)-CoFeSP one electron is transferred by RACo in an ATP-consuming reaction. Reactivated Co(I)-CoFeSP can then return to the catalytic cycle and is ready to accept the methyl group from methyltransferase.

4.2. Complex Formation between CoFeSP and Its Reductive Activator RACo

4.2.1. Redox State-Dependent Complex Formation

Analytical size exclusion chromatography was used for the first investigation of the interactions of RACo and CoFeSP (Materials and Methods 5.4)

The single proteins display clearly distinguishable peaks with defined elution volumes on a Superdex^{TM} 200 gel filtration column. The oligomeric state of RACo in solution was determined to be a homodimer with a molecular mass of 158 kDa corresponding to an elution volume of 68.3 mL. CoFeSP is a heterodimer composed of the two subunits CfsA and CfsB. With an elution volume of 77.5 mL the molecular mass was calculated to be 78 kDa (Figure 26A). An additional peak was observed, when both proteins were incubated in equimolar amounts in buffer containing 2 mM DTT and loaded onto the column. The elution volume of 60.3 mL corresponds to a molecular mass of 280 kDa (Figure 26B, solid line). The peak fractions were collected and analysed by SDS-PAGE. The fractions of the first peak clearly display three bands corresponding to RACo (68 kDa as monomer) and CoFeSP (with 48 kDa for CfsA and 34 kDa for CfsB) (Figure 26E). Densitometric analysis of the SDS gel indicates that one RACo molecule forms a complex with one CoFeSP molecule. Assuming a 2:2:2 stoichiometry of CfsA, CfsB and RACo in solution, the molecular size of the complex determined by gel filtration, is in perfect agreement with the calculated theoretical molecular mass of 300 kDa. This indicates that RACo forms a stable complex with the inactive Co(II)-CoFeSP – but leaves the question if the activator distinguishes between the inactive state and the two active states of CoFeSP. To test the affinity of RACo towards the different redox states of CoFeSP, RACo was incubated with reduced Co(I)-CoFeSP (prepared by incubation for 15 min with 1 mM DT) and run on a gel filtration column in the presence of 1 mM DT. Peaks for the single proteins, but no complex peak, were recorded (Figure 26B, dashed line). When methylated CH_3-Co(III)-CoFeSP, the second active form of CoFeSP was incubated with RACo, a small complex fraction was obtained (Figure 26B, dotted line), which possibly derived from photolysis of the light sensitive bond between the CH_3 group and the cobalt.

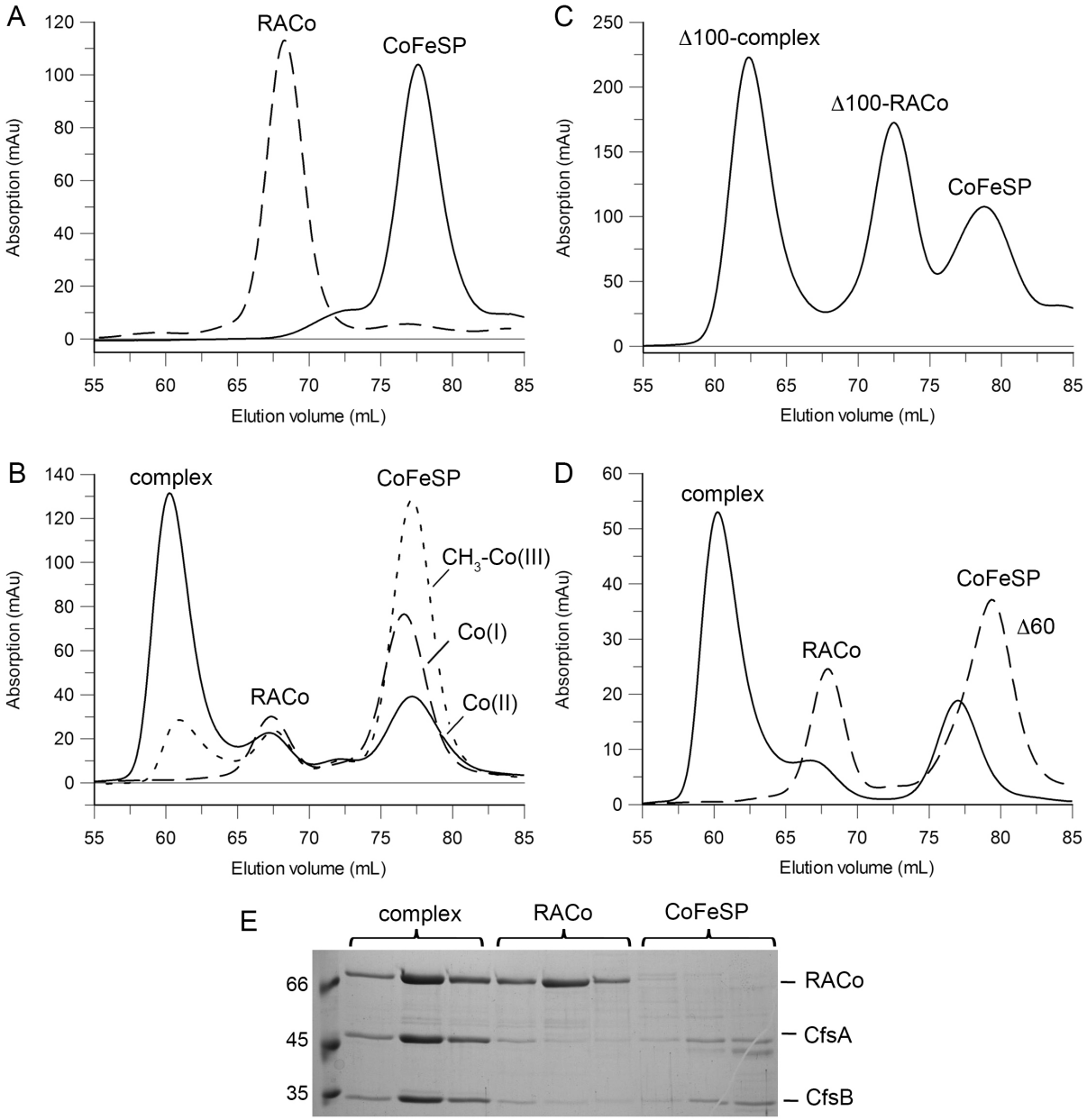

Figure 26: Complex formation between RACo and CoFeSP. (A) Individual elution profiles of RACo (29 µM) and CoFeSP (11 µM). The RACo peak corresponds to a homodimer of 158 kDa. The heterodimer CoFeSP has an apparent mass of 86 kDa. (B) Complex formation in dependence of the redox state of CoFeSP. RACo was mixed with the three possible redox states of CoFeSP: Co(II)-CoFeSP (solid line), Co(I)-CoFeSP (dashed line) and CH_3-Co(III)-CoFeSP (dotted line). (C) Elution profile of Δ100-RACo mixed with Co(II)-CoFeSP. Due to the smaller molecular size of Δ100-RACo the complex peak is shifted to 62.4 mL corresponding to a molecular mass of 241 kDa. (D) Comparison of complex formation between wild type Co(II)-CoFeSP and Δ60- Co(II)-variant with RACo. No complex peak is observed when Δ60-CoFeSP was incubated with RACo. (E) SDS-PAGE analysis of the main peak fractions of RACo incubated with Co(II)-CoFesP (B, solid line). The first lane shows the molecular mass marker with the molecular masses given in kilodaltons. Peak fractions and corresponding protein bands are labelled.

The [2Fe2S] cluster of RACo is the electron donor in the reactivation of CoFeSP. To test whether it is also important for the formation of the complex the entire N-terminal [2Fe2S] cluster domain and a part of the long linker were removed (Figure 13A) to obtain Δ100-RACo (Materials and Methods 3.2.1). When Co(II)-CoFeSP was incubated with Δ100-RACo (elution volume 72.5, 113 kDa) a peak at an elution volume of 62.4 mL corresponding to the Δ100-RACo:CoFeSP complex with a molecular mass of 241 kDa was observed (Figure 26C).

Like RACo, CoFeSP harbours its [4Fe4S] cluster at its N-terminus in a flexible domain (Figure 10). The deletion variant Δ_N60-CoFeSP, lacking the whole [4Fe4S] cluster-binding domain, was tested for complex formation with RACo, but no complex was formed (Figure 26D). In contrast to the [2Fe2S] domain of RACo the [4Fe4S] domain of CoFeSP seems to contribute to the stabilisation of the protein-protein complex.

Further the influence of nucleotides upon complex formation was tested. The proteins were incubated in buffer containing either 5 mM ATP or ADP and loaded onto a Superdex S 150／5 analytical column (dimension 5 × 150 mm, GE Healthcare) equilibrated in buffer containing 5 mM of the nucleotide. The presence of nucleotide did not affect the complex formation (Figure 27). In a second approach the necessity for DTT was tested and a sample without DTT was loaded onto the column. However, complex formation was observed under all conditions (Figure 27).

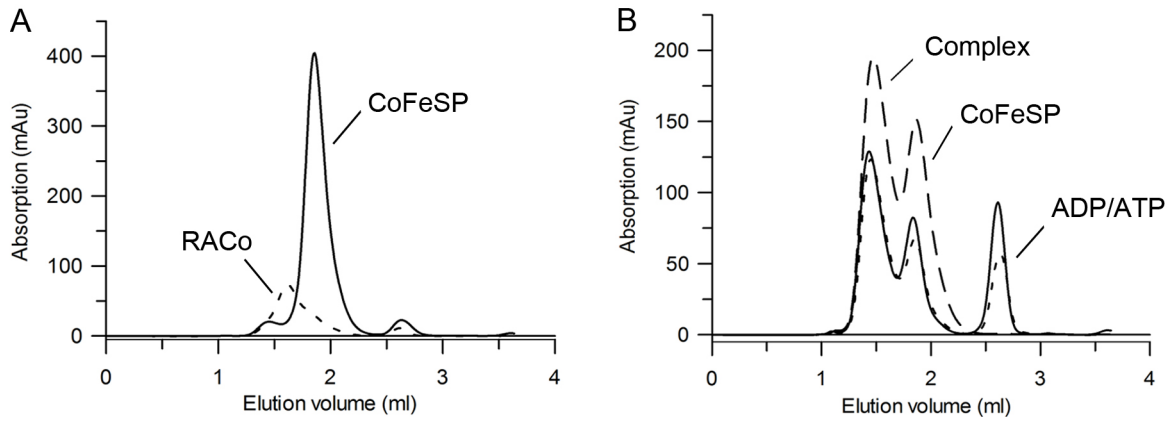

Figure 27: Complex formation in the presence of nucleotide. (A) Elution profiles of the individual proteins in the presence of 2 mM DTT. Experiments were performed on a Superdex S 150/5 column (dimension 5 x 150 mm). RACo were eluted at 1.61 mL (dashed line) and CoFeSP at 1.86 mL (solid line), respectively. (B) Elution profile dependence on the redox state of activator and the presence of ADP or ATP. In the absence of DTT in the running buffer, the oxidised state of the activator formed a complex with Co(II)-CoFeSP (dashed line, EV 1.46 mL). Irrespective of the presence of ADP (solid line, EV 2.64 mL) or ATP (dotted line, EV 2.65 mL), the complex specific peak was observed.

From the analytical size exclusion experiments one can conclude that the redox state of the activator has no impact on complex formation as the absence or presence of DTT did not have any effect on the formation of the additional complex peak. The presence or absence of nucleotide does not affect the interactions of the two proteins. The N-terminal domain of CoFeSP seems to play a role in the stabilisation of the complex as no complex formation was observed between Δ60-CoFeSP and RACo. In contrast, complex formation between Δ100-RACo and CoFeSP was detected irrespectively of the absence of the N-terminal of RACo.

Complex formation observed in these experiments, is not affected by the presence of nucleotides and marks a crucial difference to the complexes found in nitrogenase or dehydratase. In nitrogenase the nucleotide-binding acts as a switch for complex association and dissociation (*21, 35*) and conformational changes of the activator induced by nucleotide-binding enhance complex formation in dehydratases (*44, 50–52*).

Complex formation depends strictly on the redox state of the cobalamin cofactor bound to CoFeSP. The high substrate affinity of RACo towards inactive Co(II)-CoFeSP combined with the low affinity for the product Co(I)-CoFeSP has not been observed in any other ATP-dependent activation system. Redox-state dependent complex formation seems to be a

feasible strategy to assure uni-directional electron flow from the [2Fe2S] cluster bound to RACo and the cobalamin cofactor of CoFeSP.

4.2.2. Determination of the Dissociation Constant of the RACo:CoFeSP Complex

Redox-dependent complex formation between RACo and CoFeSP was solely qualitatively determined by analytical size exclusion chromatography (previous paragraph), while the determination of the binding / dissociation constant of the complex was performed by protein-protein isothermal titration calorimetry with different RACo variants. Co(II)-CoFeSP was titrated inside a glove box (under an atmosphere of nitrogen with $[O_2]<0.5$ ppm) either with wild type RACo or Δ100-RACo. Protein solutions were prepared and experiments were performed as described in Materials and Methods 5.5.

Figure 28 shows the raw measured heat changes as a function of time in the upper panel. The corresponding normalised measured heats of injections are illustrated in the panels below. The parameters were calculated using supplier's software assuming a one-site binding model.

The dissociation constants K_D determined for the RACo:CoFeSP complex and the Δ100-RACo:CoFeSP complex are comparable. For the "complete" complex a K_D of 18.1 ± 2.8 nM was obtained (Figure 28A). The K_D of the complex lacking the [2Fe2S] cluster domain of RACo was calculated to be 6.7 ± 0.8 nM (Figure 28B). The different complex samples exhibit very similar dissociation constants. As analytical gel filtration already has indicated, the N-terminal domain of RACo does not contribute to the stabilisation of the complex formed between the activator and CoFeSP.

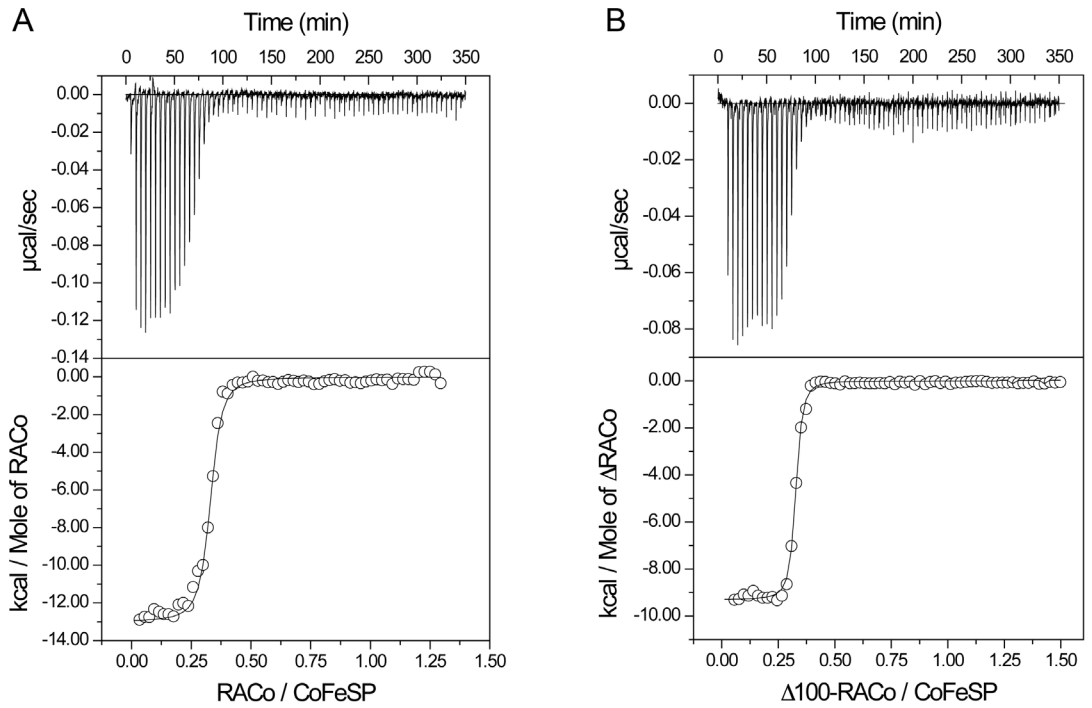

Figure 28: ITC data of the titration of RACo (A) and Δ100-RACo (B) to CoFeSP. Shown are the binding isotherms with exothermic heat change (upper) and the fit of the integrated enthalpic changes to a one-site binding model. Dissociation constants K_D are 18.1 ± 2.8 nM for RACo and 6.7 ± 0.8 nM for Δ100-RACo. Protein concentrations used in the titrations were 100 µM for RACo and Δ100-RACo and 10 µM for Co(II)-CoFeSP.

The stoichiometries of all titrations are far below 1 indicating that not all molecules form a complex. Stoichiometry depends on the protein concentration. The low stoichiometries most probably reflect the concentration of "active" species in the titration.

ITC was performed to quantify the affinity of RACo and Co(II)-CoFeSP to each other. The dissociation constants in a low nanomolar range describe strong interactions between the two partners and confirm the formation of a stable complex between Co(II)-CoFeSP and its activator RACo. Interprotein electron transfer (Results and Discussion 4.1) presumably occurs within the RACo:CoFeSP complex. The low catalytic rates of the activation of CoFeSP by RACo indicate that catalytic amounts of RACo slow down the electron transfer.

4.3. Influence of Complex Formation on the Cofactors

The RACo:CoFeSP complex contains three metallo cofactors that are supposed to be sensitive to changes in their direct environment upon complex formation. Resonance Raman (RR) and electro paramagnetic resonance (EPR) spectroscopy were conducted to investigate the environmental changes due to interactions between RACo and CoFeSP. These spectroscopic experiments were carried out in the laboratory of Prof. Dr. Peter Hildebrandt (Institut für Chemie, Technische Universität Berlin) and the results from this cooperation (Results and Discussion 4.3.1 and 4.3.2) have been published (*111*).

4.3.1. Resonance Raman Spectroscopy

Resonance Raman spectroscopy was used to investigate specific structural changes in the periphery of the cofactors of RACo ([2Fe2S] cluster) and Co(II)-CoFeSP (corrinoid and [4Fe4S] cluster) deriving from interactions of the two proteins upon complex formation.

For the RR measurements performed by Wiebke Meister (Institut für Chemie, Technische Universität Berlin) samples of RACo, Co(II)-CoFeSP, RACo:Co(II)-CoFeSP complex, Δ100-RACo, Δ100-RACo:Co(II)-CoFeSP complex, Co(I)-CoFeSP, Δ_N60-Co(II)-CoFeSP and Δ_C107-Co(II)-CoFeSP with and without RACo were prepared as described in Materials and Methods 7.2.1. The protein variants, each lacking one of the cofactor carrying domains, were used to facilitate the assignment of the signals to the different cofactors.

The spectra shown in Figure 29 illustrate the frequency range of the C=C stretching modes of the corrin macrocycle of CoFeSP since the spectrum of RACo does not contain any peak in the range between 1450 and 1650 cm^{-1} (Figure 29A). Three bands in the region between 1450 and 1650 cm^{-1} can be assigned to cobalamin (*127–130*). Oxidised Co(II)-CoFeSP gives signals at 1604, 1543 and 1498 cm^{-1} (Figure 29C). The C=C stretching modes depend on the oxidation state of the cobalt ion and a small downshift of 4 – 5 cm^{-1} in the spectrum of reduced Co(I)-CoFeSP (Figure 29B) could be observed. Interactions with RACo do indeed influence the corrin macrocycle as the spectrum of the complex sample (Figure 29D) illustrates. Complex formation results in an upshift from 1604 to 1607 cm^{-1} and from 1543 to

1545 cm^{-1}. A 2 cm^{-1} downshift is apparent for the band at 1498 cm^{-1}. Neither the [2Fe2S] cluster nor the [4Fe4S] cluster display RR bands in this range as the spectra of the complex lacking the [2Fe2S] cluster with the same signal patterns demonstrate (Figure 29E). Identical shifts of the cobalamin peaks indicate that the complex formed between Δ100-RACo and CoFeSP has the same electronic structure of the corrin macrocycle as the complex between RACo and CoFeSP. No peaks are found in the spectrum of CoFeSP lacking the C-terminal cobalamin-binding domain but containing the N-terminal bound [4Fe4S] cluster (Figure 29F).

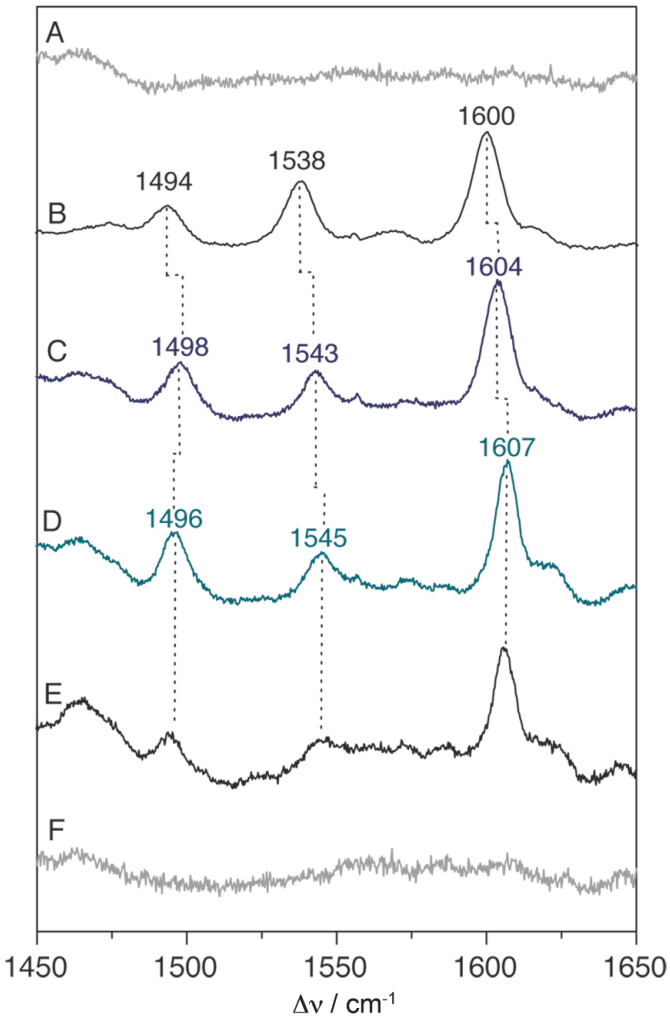

Figure 29: Resonance Raman spectra in the frequency range of 1450 – 1650 cm^{-1}. RR spectra obtained with 413 nm excitation of RACo. (A), Co(I)-CoFeSP (B), Co(II)-CoFeSP (C), RACo:Co(II)-CoFeSP (D), Δ100-RACo:Co(II)-CoFeSP (E) and Δ_C106-CoFeSP (F). The frequency range of the C=C stretching modes of the corrin macrocycle of CoFeSP is displayed. Shifts are indicated by dashed lines and wave numbers of the peaks characteristic for the corrinoid are given.

The frequency range between 280 and 400 cm^{-1} is assigned solely to the [FeS] clusters (Figure 30) since the spectra of the deletion mutants Δ100-RACo and Δ60-CoFeSP do not display any features in this region (Figure 30A and E). Five peaks at 288, 320, 327, 344 and 390 cm^{-1}, respectively, characterise the spectrum of RACo binding the [2Fe2S] cluster (Figure 30B). The spectrum of the [4Fe4S] cluster of CoFeSP shows three peaks at 335, 346 and 359 cm^{-1} (Figure 30D). The complex sample displays a mixture of both (Figure 30C). The spectrum of free Co(II)-CoFeSP (Figure 30D) and free RACo (Figure 30B) were subtracted from the complex spectrum and an effect on the [FeS] clusters due to the interactions between the two proteins can be excluded as the resulting spectra display the spectra of the free proteins (Figure 31).

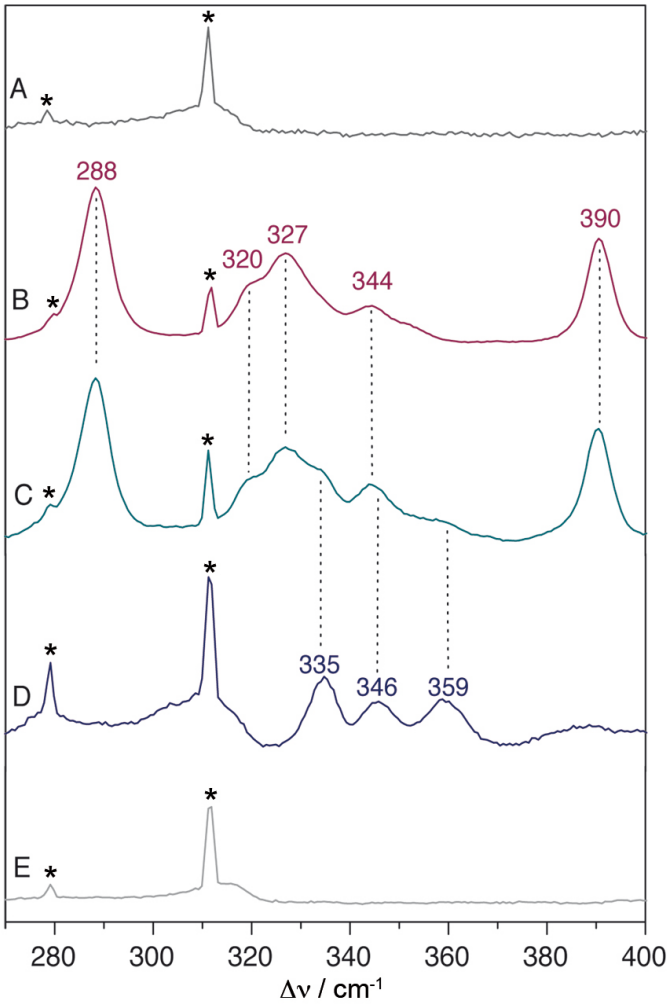

Figure 30: RR spectra of the [FeS] cluster frequency range. Spectra of Δ100-RACo (A), RACo (B), the RACo:Co(II)-CoFeSP complex (C), Co(II)-CoFeSP (D) and Δ60-Co(II)-CoFeSP, obtained with 413 nm excitation. The frequency range of the fundamentals of the [FeS] centres is shown. Asterisks mark peaks deriving from non-lasing emission lines of the Kr^{+} ion laser.

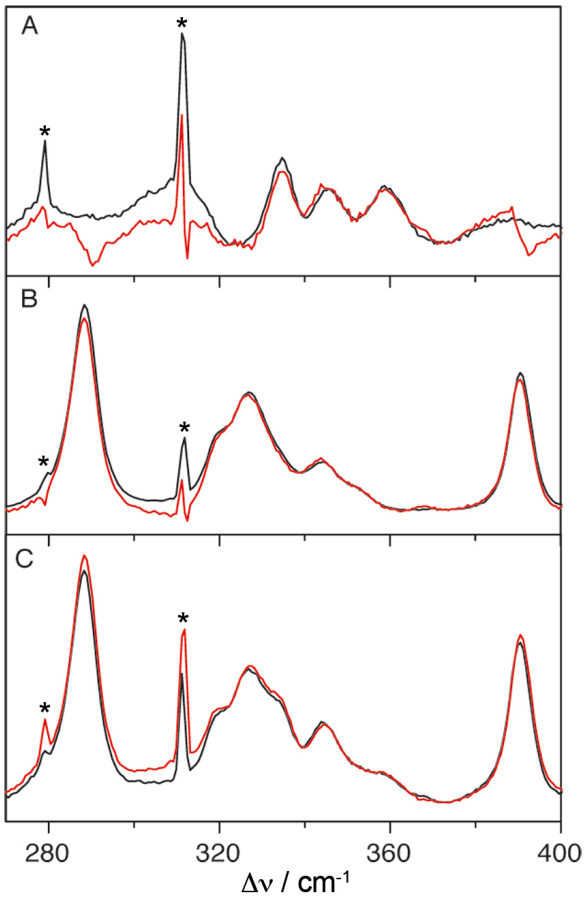

Figure 31: Difference spectra. (A) Comparison of the difference spectrum "complex – RACo" (red) and Co(II)-CoFeSP (black). (B) Spectrum of RACo (black) and the difference spectrum "complex – Co(II)-CoFeSP" (red). (C) Complex spectrum (black) and sum spectrum "RACo + Co(II)-CoFeSP" (red). All spectra were obtained with 413 nm excitation and display the range of the [FeS] cluster. Asterisks label peaks deriving from non-lasing emission lines of the Kr^{+}-ion laser.

Resonance Raman spectroscopy revealed perturbation of the (electronic) structure of the corrin macrocycle upon complex formation between CoFeSP and RACo. As the absence of the [2Fe2S] cluster binding domain in the Δ100-RACo:CoFeSP complex resulted in the same upshifts compared to the spectrum of free CoFeSP, it is clear that the alteration in the structure of the corrin ring is not a consequence of interactions with this domain.

The results obtained in these experiments demonstrate that the interactions between RACo and CoFeSP bias the cobalamin cofactor but none of the [FeS] clusters.

4.3.2. EPR Spectroscopy of CoFeSP and the RACo:CoFeSP Complex

In addition to RR spectroscopy, EPR spectroscopy was performed to visualize the alterations on the cobalamin cofactor observed in the RACo:CoFeSP complex. Samples were prepared as described in Materials and Methods 7.2.4 and EPR spectra were measured (Materials and Methods 7.2.5) by Dr. Friedhelm Lendzian (Institut für Chemie, Technische Universität Berlin). The obtained EPR spectra have been published (*111*).

Cobalamin in its Co(II) state is EPR active and the EPR spectrum of Co(II)-CoFeSP shows a broad pattern of eight lines resulting from hyperfine interactions of the unpaired electron and the cobalt nucleus, in the region of 2,500 to 3,800 G (Figure 32a). The spectrum is typical for Co(II)-cobalamin in its base-off conformation found in corrinoid iron/sulfur proteins (*67, 68, 130*).

The spectrum was compared with a spectrum of a sample containing Co(II)-CoFeSP and RACo in the presence of DTT (Figure 32b). The cobalt signal of the complex sample is sharper and better resolved on the low-field than is the one of CoFeSP alone. The dominant signal at 3,250 to 3,500 G in the complex spectrum is assigned to the EPR active $[2Fe2S]^{1+}$ cluster bound to RACo.

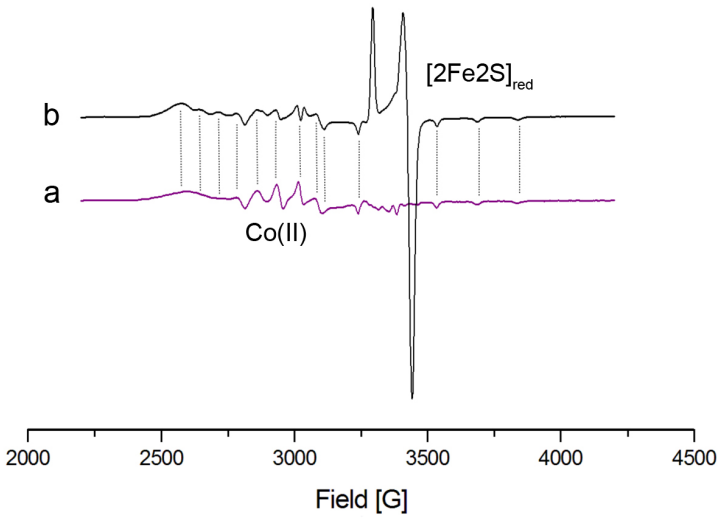

Figure 32: EPR spectra of Co(II)-CoFeSP (a) and the RACo:Co(II)-CoFeSP complex (b). The broad low-amplitude signals between 2,500 and 3,800 G are assigned to the corrinoid cofactor. In the complex sample these signals are sharper and better resolved indicating well-defined ligand-Co interactions. The dominant signal in the complex spectrum (b) derives from the reduced [2Fe2S] cluster of RACo. Corresponding signals of corrinoid of free Co(II)-CoFeSP and complex are labelled.

The better resolution of the Co^{2+} signal reflects a change in the cobalamin coordination and supports the results obtained by resonance Raman spectroscopy. The weak, loose interaction with the water ligand observed in the crystal structure of CoFeSP (Figure 10) (*94*) seems to be lost and replaced by a strong interaction with an axial ligand, possibly allocated by RACo.

4.3.3. Redox Titration of CoFeSP and the RACo:CoFeSP Complex Combined with EPR

The electron transfer from the [2Fe2S] cluster of RACo to the cobalamin of CoFeSP is energetically an uphill process against an electrochemical gradient. Midpoint reduction potentials of the cofactors of CoFeSP of *M. thermoacetica* were determined to be –504 mM for the cobalamin and –523 mM for the [4Fe4S] cluster, respectively (*68*). The midpoint potential of the [2Fe2S] cluster of RACo was assessed to be –371 mV (Results and Discussion 3.3) and is in a line with the activating enzyme of veratrol-*O*-demethylase (*17*). The midpoint reduction potential of the corrinoid protein of veratrol-*O*-demethylase increases from below –450 mV to –320 mV in the presence of the activating enzyme enabling the transfer of one electron from the [2Fe2S] cluster to the corrinoid (*16, 17*).

To gain insights how complex formation influences the redox behaviour of the cofactors, in addition to the redox titration of RACo (Results and Discussion 3.3), titrations of CoFeSP and the RACo:CoFeSP complex were performed in cooperation with Dr. Friedhelm Lendzian (Institut für Chemie, Technische Universität Berlin).

Samples were prepared and treated as described in Materials and Methods 8. EPR spectra were recorded at 100 K to detect signals of the (reduced) [2Fe2S] cluster and (oxidised) cobalamin or at 10 K for the detection of the (reduced) [4Fe4S] cluster of CoFeSP. All spectra were corrected by subtracting reference buffer spectra. The EPR intensities were normalised to one for all EPR active species, e.g. the signal of Co(II) at the most positive potential was assumed to represent 100 % of the cobalamin present in the sample. The [FeS] clusters are EPR silent in the 2+ state and the intensities at the lowest potentials were used for normalisation. The corrected intensities were plotted against the potentials of sampling and curves were fitted applying the Nernst-equation of a single-electron process.

The results of the redox titration of CoFeSP are illustrated in Figure 33. The single spectra of the different potential steps at 100 K (A), at 10 K (B) and the corresponding Nernst plots (C) are shown.

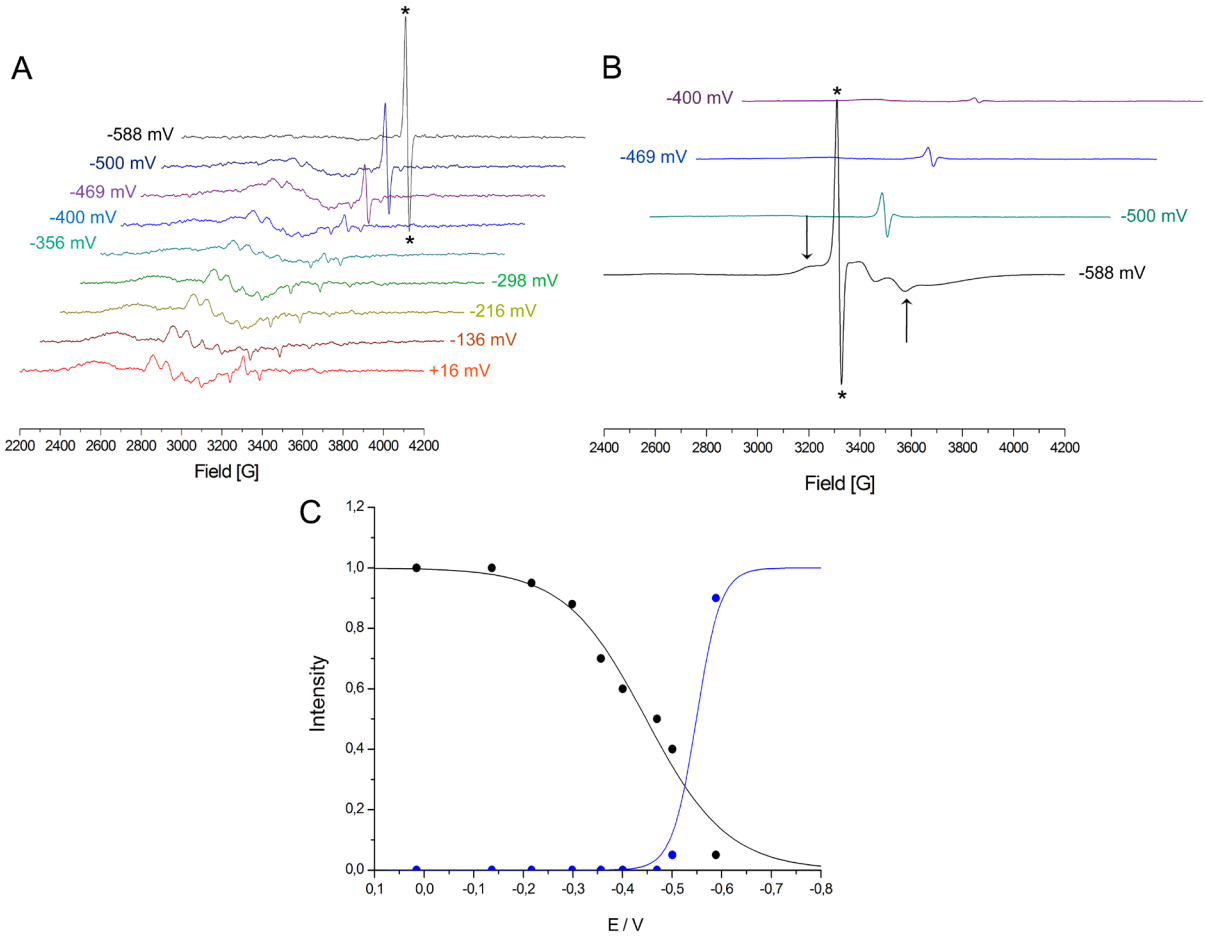

Figure 33: Redox titration combined with EPR of CoFeSP. (A) EPR spectra of CoFeSP recorded at 100 K. The signal of the mediators is labelled with an asterisk. (B) Spectra of the [4Fe4S] cluster taken at 10 K. The signal assigned to the cluster is marked with a black arrow; the mediator signal is labelled with an asterisk. (C) Nernst plots of the cofactors of CoFeSP. The Nernst fit of the cobalamin (black) results in a midpoint potential of –447 mV (n = 0.30). For the [4Fe4S] cluster (blue) the midpoint reduction potential was calculated to be –549 mV (n = 1, fixed).

The midpoint potential of the Co(I)/Co(II) couple was calculated to be –447 mV. According to the result of the Nernst-fit only 30 % (n=0.30) of the cobalamin was reduced. The plot of the [4Fe4S] cluster faces the problem that a strong intensity was only obtained at the lowest potential when already 0.9 spins / protein were reached. For the fitting the value of n had to be set to one. The midpoint potential from the fit was calculated to be –549 mV.

The midpoint potentials determined for CoFeSP of *C. hydrogenoformans* are comparable to those reported for CoFeSP of *M. thermoacetica* and *M. thermophila* (*67, 68*). The negative potential of the [4Fe4S] cluster even emphasises more the mysterious role of this metal centre.

A sample of both proteins in equimolar concentrations was titrated with DT and EPR spectra were recorded as for the single proteins (Materials and Methods 8). The spectra recorded at 100 K (A) and 10 K (B) and the corresponding Nernst plots (C) are presented in Figure 34.

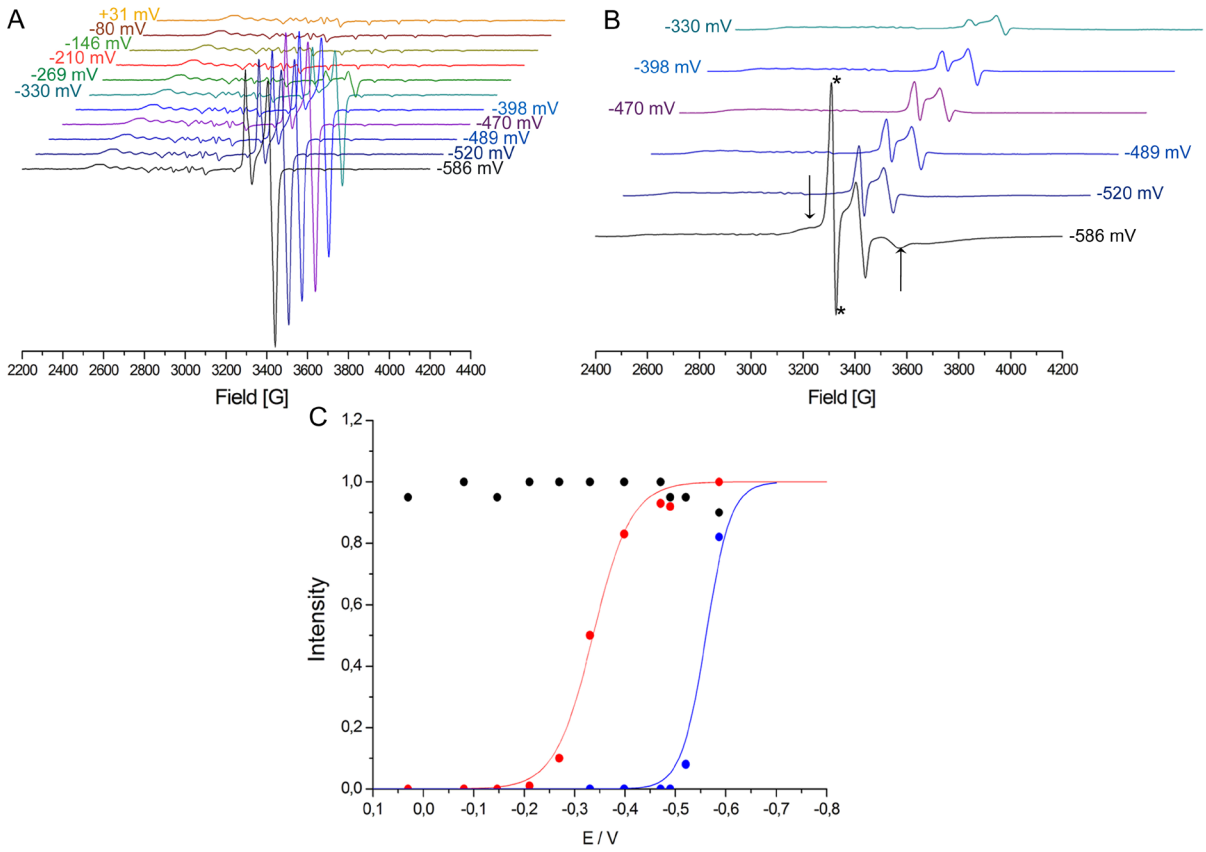

Figure 34: Redox titration combined with EPR of the RACo:CoFeSP complex sample. (A) Spectra of the complex sample measured at 100 K. The Co(II)-corrin signals are well conserved over the whole potential range. The signal of the reduced [2Fe2S] cluster of RACo arises at a potential of –269 mV. (B) EPR spectra recorded at 10 K. The signal of the reduced [4Fe4S] cluster (black arrows) is significant only at the most negative potential. The signal of the [2Fe2S] cluster is less strong at this temperature. The strong signal in the low potential range arises from the mediator mix and is labelled with an asterisk. (C) Nernst plots of the cofactors present in the complex. The potentials are plotted against the intensities and the curves were fitted according to the Nernst equation assuming for all cofactors a one-electron reaction. For the [2Fe2S] cluster of RACo (red) a midpoint potential of –337 mV (n = 0.64) was calculated. The [4Fe4S] cluster of CoFeSP (blue) has a midpoint potential of –560 mV (n = 1, fixed). The cobalamin of CoFeSP (black) is not reduced and the Co(II) state is observed over the whole potential range.

As in the free protein the redox potential of the FeS cluster of CoFeSP is rather negative (–560 mV) and a strong signal was only observed at the lowest potential. No dramatic changes in the redox behaviour of RACo were observed as the midpoint potential of the [2Fe2S] cluster in the complex (–337 mV) and the midpoint potential of uncomplexed RACo (–371 mV, Results and Discussion 3.3) are similar. The variation remained within the experimental error limits. Complex formation affected the cobalamin cofactor exclusively. In the complex sample, hardly any transition from the EPR active to the EPR silent Co(I) species was observed.

The Co(II) state was highly stabilised and the cofactor seems to be specially protected by the interactions with RACo. Even at the lowest potential reached during titration 90 % of the cobalamin remained oxidised. This result is oppositional to RACo´s original task as reductive activator. The reduction of Co(II)-CoFeSP to the active Co(I)-CoFeSP should be facilitated by the interaction with RACo.

As the midpoint reduction potential of the [2Fe2S] was not affected by complex formation the strategy for the electron transfer seems to be different to other ATP dependent activators where the protein-protein interactions mainly bias the electron donating centre adapting a potential as negative as the one of the acceptor site. Complex formation between the Fe-protein and the MoFe-protein of nitrogenase lowers the midpoint potential of the reductase by about –200 mV via the desolvation of its negatively charged [4Fe–4S] cluster (*131, 132*) as also suggested for radical dependent β,α-dehydratases (*133–135*). RACE proteins seem to modulate the midpoint potential of the corrinoid but in contrast to the activating enzyme of the veratrol-*O*-demetylase (*16, 17*), RACo decreases the midpoint potential of the cobalamin.

5. Crystal Structure of the RACo:Co(II)-CoFeSP Complex at 2.5 Å Resolution

For the crystallisation of the protein-protein complex fractions from several gel filtration experiments (Results and Discussion 4.2) were pooled and concentrated (Materials and Methods 9.1). Commercially available screens were used for the initial screening. Over a period of 18 months crystals (Figure 35) grew in 27 conditions, mainly of the Index and PEG-Ion screen (Hampton Research). All conditions contained PEG3350 with pH ranging from 5.5 to 8.5. Crystals of all conditions were tested for diffraction. Generally, crystals diffracted to 7 Å or lower except for one, which diffracted to 3.3 Å and could be indexed. Another crystal from a 13 months old plate even diffracted to 2.5 Å and data were processed with XDS (*113*). The crystal belonged to space group P1 with cell parameters a = 67.13, b = 128.18 and c = 163.37, α = 77.61, β = 82.25 and γ = 88.76. Calculation of the Matthew's coefficient suggested four molecules per asymmetric unit considering a molecular size of 150 kDa per complex molecule. The structure was solved by molecular replacement using the known structures of the complex components, RACo (PDB 3ZYY) (*102*) and CoFeSP (PDB 2YCL) (*94*) as replacement models. Statistics of data collection and refinement are summarised in Appendix Table 22.

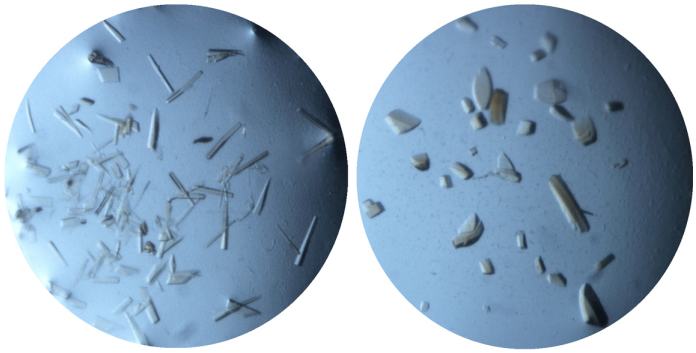

Figure 35: Crystals of the RACo:CoFeSP complex. Shown are two exemplary crystallisation drops. Crystals appeared after several months.

5.1. The Overall Structure of the RACo:CoFeSP Complex

In the asymmetric unit two copies of the RACo:CoFeSP complex were found. The physiological complex is composed of two RACo and CoFeSP molecules (Figure 26E and Figure 36) in perfect agreement with the 2:2:2 stoichiometry found in solution (see Results and Discussion 4.2.1).

The RACo homodimer is flanked at each side by a CoFeSP heterodimer which consists of two $(\beta/\alpha)_8$ barrel domains, the small subunit CfsB and the middle domain of CfsA. The N and C-terminal domains of the large subunit CfsA carry the cofactors: the N-terminal bound [4Fe4S] cluster and the cobalamin cofactor at the C-terminus (Figure 10). All domains of CoFeSP are visible in the complex structure (Figure 36), even the N-terminal domain, which was not resolved in a previously reported CoFeSP structure (*89*). RACo is composed of three domains (N-terminal [2Fe2S] binding domain, middle domain and C-terminal ASKHA domain). The N-terminal [FeS] cluster-binding domain of RACo is bound to the middle domain by a long linker (Figure 13A). In the complex structure this domain is not resolved in any of the four RACo molecules found in the asymmetric unit. The dissociation constant of 6.7 ± 0.8 nM of the Δ100-RACo:CoFeSP complex determined by ITC (Results and Discussion 4.2.2, Figure 28B) and the observed complex peak from gel filtration experiments (Results and Discussion 4.2.1, Figure 26C) showed that this domain does not contribute to the stabilisation of the complex. Most likely, there are no interactions with other domains of the protein-protein complex stabilising it. In the structure of free RACo a high flexibility was observed for the N-terminal domain and could only be modelled in one of the two monomers (Figure 13A). This flexibility seems to be retained in the complex.

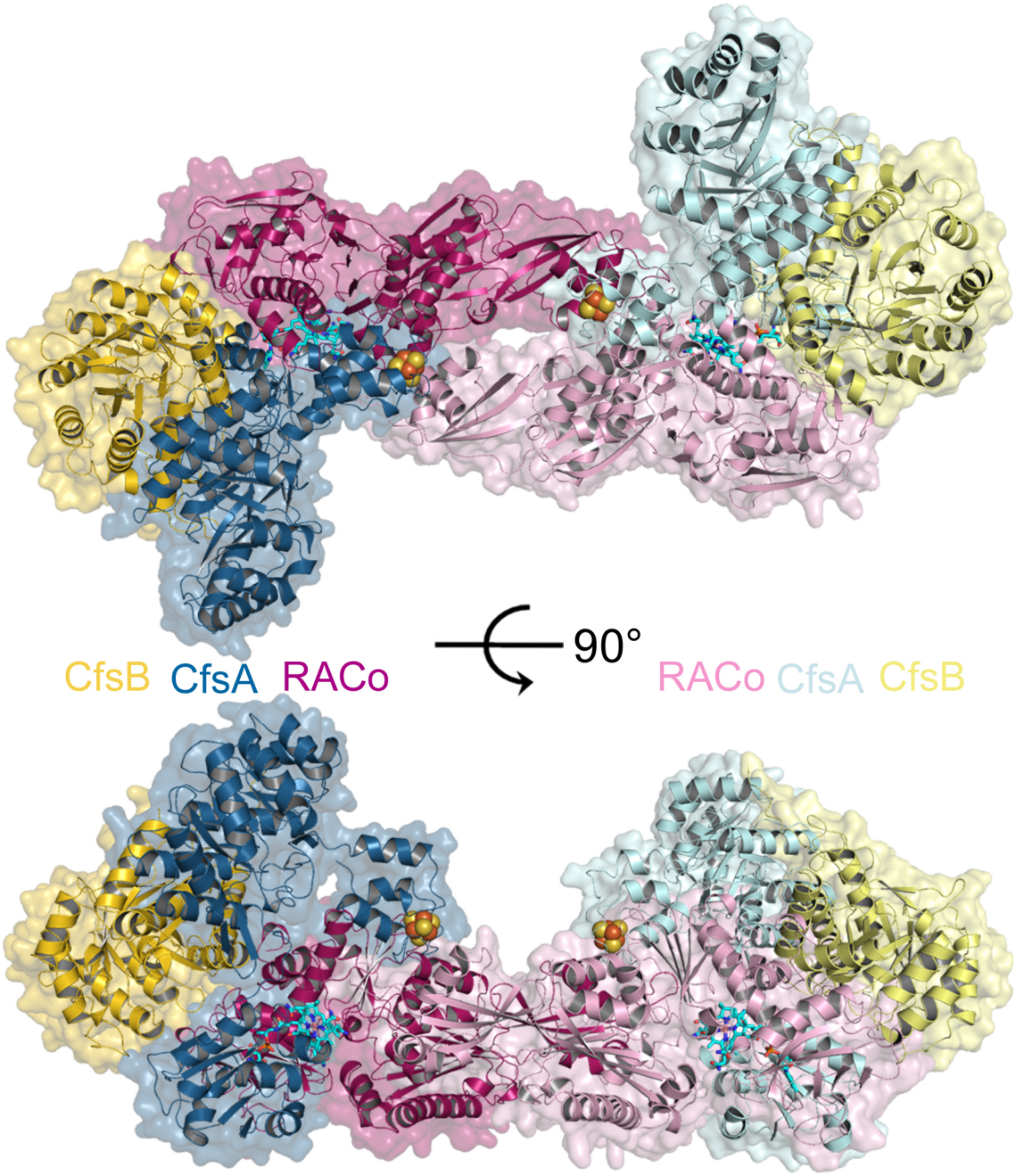

Figure 36: Overall crystal structure of the RACo:CoFeSP complex. The structure is represented as cartoon with the RACo homodimer at its core (dark and light pink). The large subunit of CoFeSP, CfsA, is coloured in dark and light blue. The small subunit, CfsB, is shown in yellow. The [4Fe4S] cluster of CoFeSP is depicted as spheres and the cobalamin is shown as cyan sticks. Additionally, the surface of the complex is shown.

Interactions between RACo and the N-terminal domain of CfsA as well as with the small subunit CfsB are found at the complex interfaces (Figure 37A and B). H-bonds and hydrophobic interactions are formed between a helix of CfsB and residues of the ASKHA domain of RACo (Figure 37C). The same helix is involved in the binding of MeTr to CoFeSP (*98*).

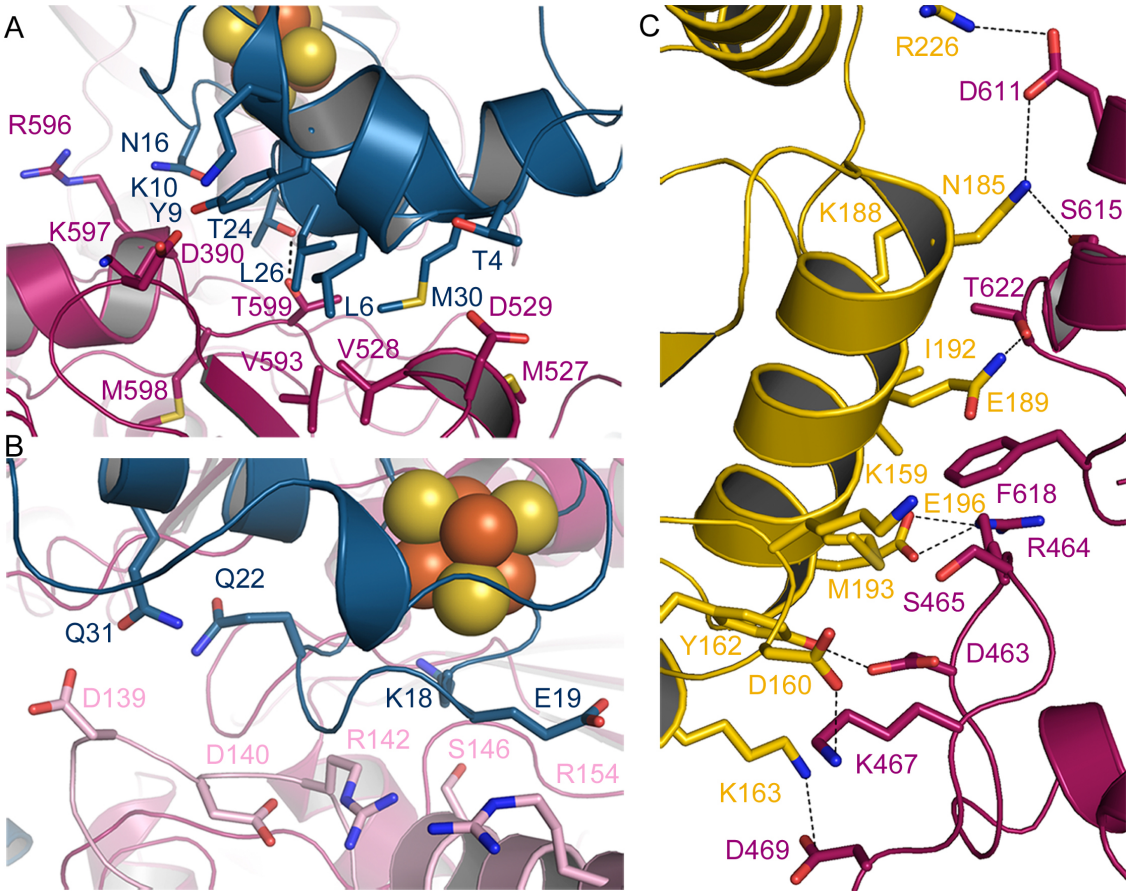

Figure 37: Interaction interfaces of the RACo:CoFeSP complex. (A) Interacting residues (shown as stick model) of the ASKHA domain of one RACo monomer (dark pink) with the N-terminal [4Fe4S] cluster-binding domain of CfsA (blue). (B) Residues of the middle domain of the second RACo monomer (light pink) interacting with the N-terminal domain of CfsA (blue). Iron and sulfur atoms of the cluster are presented as orange and yellow spheres, respectively. (C) The interaction interface of the small CoFeSP subunit (yellow) with the ASKHA domain of RACo (dark pink). Putative H-bonds are shown as dashed lines.

5.2. Domain Movements within CoFeSP

The relative positions of the two $(\beta/\alpha)_8$ barrel domains of CoFeSP are not affected by complex formation. However, the C-and N-terminal domains bound to the large subunit CfsA via flexible linkers (Figure 10) are displaced in the complex structure. The superimposition of uncomplexed CoFeSP (PDB 2YCL) (*94*) to the complex structure by the small subunit (r.m.s.d. = 0.336) reveals drastic domain movements and rotations around these linkers. The N-terminal domain containing the [4Fe4S] cluster of CoFeSP rotates by almost 90° and the cluster is translocated by 42 Å (Figure 38). Consequently many interactions with the RACo homodimer are formed and contribute to the stabilisation of the complex (Figure 37A and B).

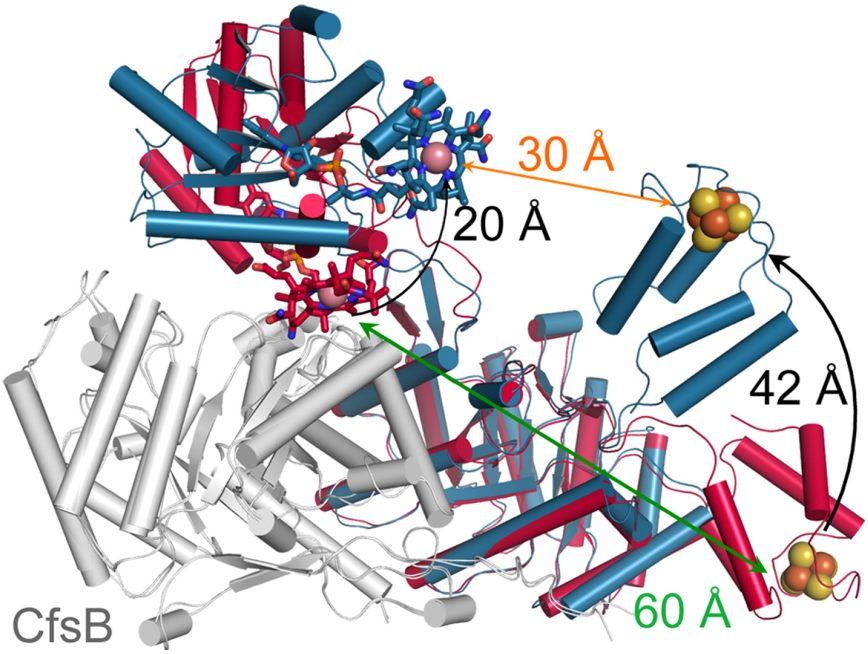

Figure 38: Domain movements of CoFeSP. Superimposition of free CoFeSP (red, PDB 2YCL) (*94*) and CoFeSP in complex with RACo (blue) by the small subunit CfsB. Distances between the cofactors are indicated by a green (free CoFeSP) and orange (complex) arrow.

As shown in Figure 37A and B residues of the middle domain of one RACo monomer and residues of the ASKHA domain of the other RACo monomer interact with the N-terminal domain of the large subunit of CoFeSP. Usually, the N-terminally bound [4Fe4S] cluster binding domain of CoFeSP is mobile (*89, 94*) and plays not only a crucial role in the stabilisation of the RACo:CoFeSP complex but also in the complex of CoFeSP and methyltransferase of *M. thermoacetica* which has been solved recently (*98*). Functionally, the

two complexes are unrelated but both crystal structures demonstrate that CoFeSP employs its flexible domains to interact with different protein partners (Figure 39A). “Dynamic domain juggling” in the methyl transfer complex is quantified by a displacement of 6.5 – 14.8 Å (*98*). In the activation complex this “domain juggling” induces movements of 20 – 42 Å compared to uncomplexed CoFeSP (Figure 39).

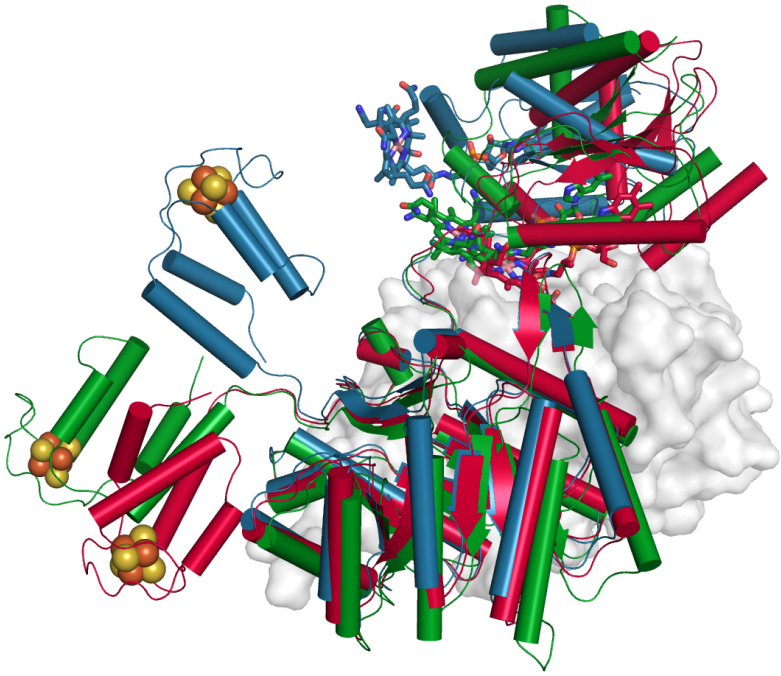

Figure 39: Domain flexibility of CoFeSP. Comparison of the relative positions of the flexible C-and N-terminal domain of CoFeSP in free CoFeSP of *C. hydrogenoformans* (red, PDB 2YCL) (*94*), CoFeSP bound to MeTr of *M. thermoacetica* (green, PDB 4DJD) (*98*) and CoFeSP bound to RACo (blue). All structures were aligned by superimposition to the small subunit, CfsB (white surface presentation).

The C-terminal domain of CfsA, carrying the cobalamin cofactor, moves by 20 Å and rotates by 45° around the linker connecting it to the $(\beta/\alpha)_8$ barrel domain. The cobalamin moves from its interaction interface with the small subunit towards the surface of RACo (Figure 36, Figure 39).

5.3. Coordination Environment of the Cobalamin

Like in free CoFeSP the cobalamin cofactor is bound "base-off" in the complex but nestled by several residues of the ASKHA domain of RACo (D246, T380, N381, S398, A399, N509 and R512). The hydroxyl group of a serine residue of RACo replaces the axial water ligand on the β-side of the corrin macrocycle with a Co–O distance of 2.5 Å while the interaction of the Co-ion and T374 is retained in the complex structure (Figure 40A). The corrin cycle is placed in a surface cavity of RACo with its ring fitting perfectly in this cobalamin-binding pocket (Figure 40B).

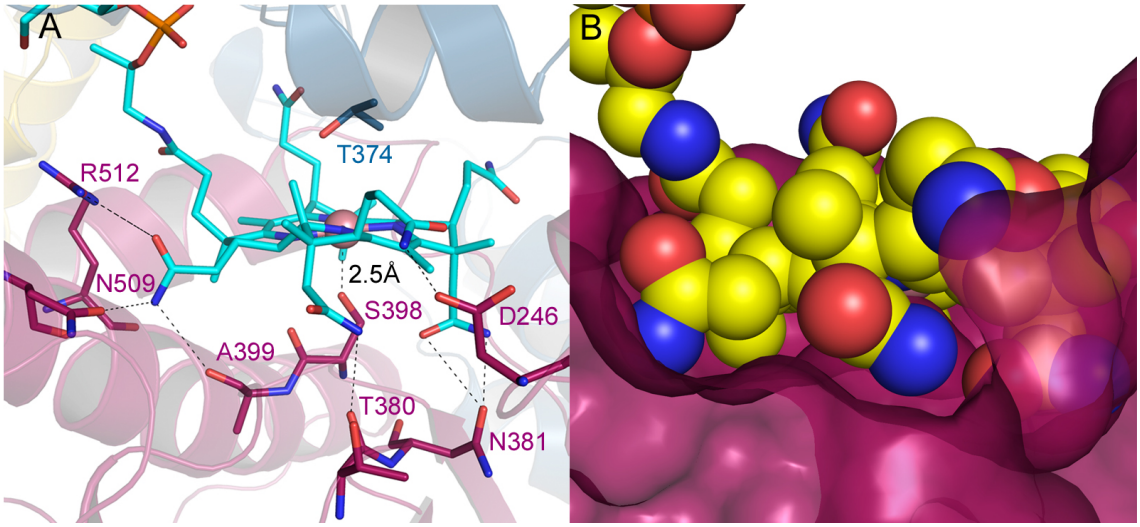

Figure 40: Environment of the cobalamin cofactor. (A) Interactions between the corrin ring (cyan stick model) and RACo (pink). The residues interacting with cobalamin are shown as sticks and interactions are denoted by black dashes. (B) Cobalamin (yellow spheres) confined in the corrin-binding pocket of RACo (pink surface).

The complex structure revealed a direct interaction of the Co-ion with a residue of RACo. The serine residue 398 was mutated to either alanine or cysteine (Materials and Methods 3.2.3) to investigate the influence of this residue on the dissociation constant of the RACo:CoFeSP complex by ITC (Materials and Methods 5.5). The Serine398 mutants of RACo have a lower affinity towards Co(II)-CoFeSP and the dissociation constants determined by ITC are 3.8. ± 0.5 µM for S398A and 16.9 ± 0.6 µM for S398C, respectively (Figure 41). These constants underline the importance of this residue in the selective redox-state-dependent partner recognition.

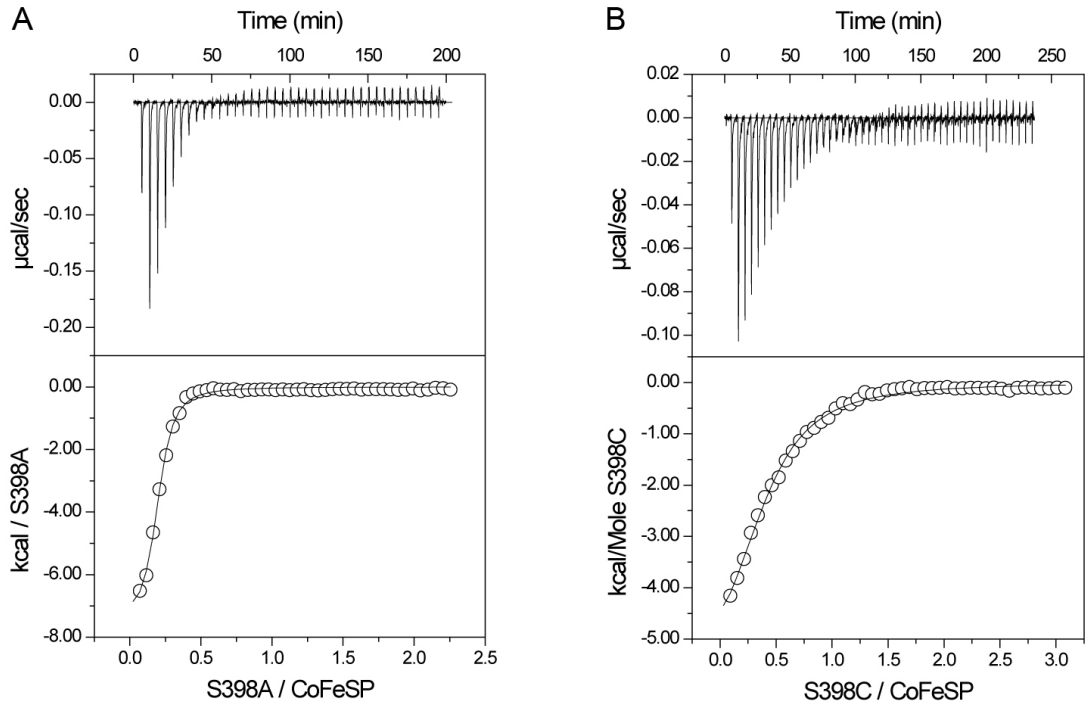

Figure 41: ITC data of the titration of CoFeSP with RACo-S398A (A) and RACo-S398C (B). Shown are the binding isotherms with exothermic heat changes and the fits of the integrated enthalpy changes to a one-site binding model. The dissociation constants K_D are 3.8. ± 0.5 µM for RACo-S398A and 16.9 ± 0.6 nM for RACo-S398C, respectively.

The complex structure demonstrates how the environment of the cobalamin cofactor is influenced by the interactions with RACo and explains the results obtained earlier by resonance Raman and EPR spectroscopy as well as the manipulated redox potential of the cobalamin (Results and Discussion 4.3).

In free CoFeSP the corrin macrocycle is positioned between CfsB and the C-terminal domain of CfsA (*89, 94*) and bound "base-off/His-off", i. e. the lower methoxybenzimidazolyl moiety does not coordinate the cobalt neither does a protein bound histidine residue (Figure 10B). On the upper face (β-side) of the corrin cycle, a water molecule coordinates the cobalt ion with a Co–O distance of 2.5 Å. On the lower face (α-side), Thr374 of the cap-helix is at 3.6 Å distance from the cobalt. The loose interactions are displayed in the EPR spectrum of as-isolated CoFeSP with a broad and less resolved signal in the low field side (Figure 32A). The active Co(I)-state is favoured by the base-off conformation and stabilised by around 100 mV compared to base-on or His-on cobalamins (*68*). The redox potential of –450 mV, determined by redox titration (Figure 33), is in good agreement with the coordination environment found in free CoFeSP.

The decrease of the midpoint potential of the Co(II)/Co(I) couple in the RACo:CoFeSP complex from –450 to a potential below –600 mV (Figure 34) certainly derives from the interactions with the protein matrix of RACo, especially with Ser398. Co(II)-cobalamins prefer a penta-coordination and the structure demonstrates how the Co(II)-state is stabilised by a strong axial ligand (Figure 40A) (*136*). The redox-dependent complex formation can now be explained by the coordination chemistry of the cobalamin (Figure 42) (*136*). A direct interaction of Ser398 and the cobalt ion is only reasonable in the inactive Co(II) state. While the active Co(I) state prefers tetracoordination without axial ligands, the active CH_3-Co(III) state binds a methyl group, which cannot easily be replaced by the hydroxyl group of the serine residue.

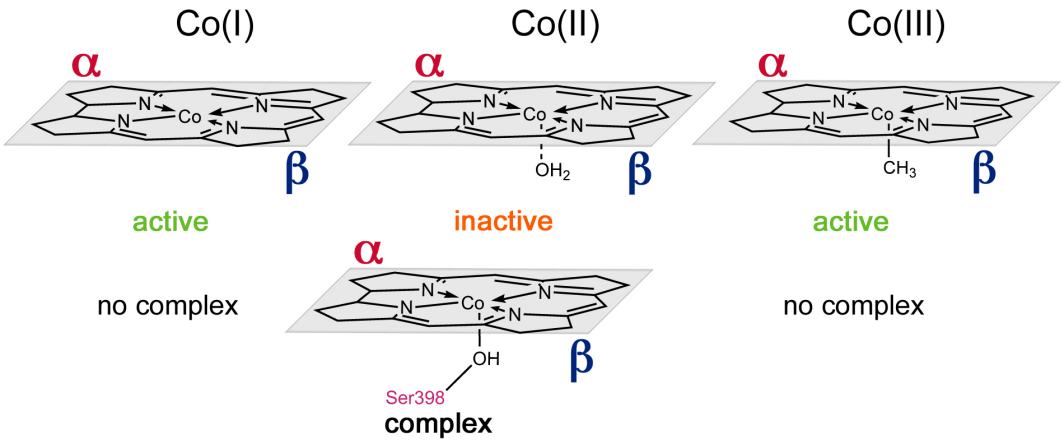

Figure 42: Coordination chemistry of the cobalamin. The favoured coordination of the different cobalamin redox states is presented. States, active in the reductive acetyl-CoA pathway, are labelled in green, whereas the inactive state is marked in orange. The tendency of the different states to form a complex with RACo is indicated.

Strengthening of the interaction with an axial ligand was indicated by the EPR spectrum of a complex sample and was manifested by sharper signals compared to the cobalamin signals of uncomplexed CoFeSP where a loose interaction to an axial water ligand is displayed (Figure 32). An impact on the redox potential upon complex formation had already been implied by resonance Raman spectroscopy. Changes observed in the RR spectra are assigned to the redox-state sensitive C=C stretching modes. Frequency downshifts are usually explained by an increase of electron density on the metal ion and concurrent weakening of the C=C bonds as observed in the spectrum of reduced CoFeSP (Figure 29B). Upshifts are expected for oxidation and were described for the Co(II)/Co(III) couple at 1543 and 1604 cm^{-1} (*127*). The

upshifts from 1543 to 1545 cm^{-1} and from 1604 to 1607 cm^{-1} in the complex spectrum (Figure 29D) should not derive from incidental oxidation to the Co(III)-state but could display the stabilisation of the Co(II) state.

The Co(II) state is stabilised by burying the corrin moiety inside a surface pocket of RACo (Figure 40). To position the corrin cycle into the pocket, CoFeSP performs a displacement of two complete domains (Figure 38 and Figure 39). Adaption of different conformations during the catalytic cycle was proposed and discussed earlier (*89*). The manifoldness of CoFeSP in adapting different conformations depending on the interaction partner has to be enlarged and replenished by an activation conformation found in the RACo:CoFeSP complex (Figure 43).

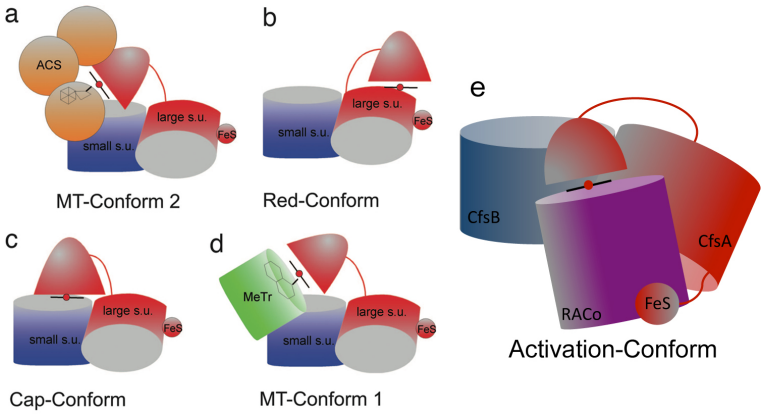

Figure 43: Overview of the different CoFeSP conformations. MT-Conform 1 (a) and 2 (d) describe the conformation during methyl group transfer when CoFeSP interacts with ACS or MeTr, respectively. The Cap-Conform (c) is the inactive Co(II)-state as observed in as isolated CoFeSP (*89, 94*). Red-Conform (b) represents the conformation during the suggested activation of Co(II)-CoFeSP under participation of its FeS cluster (99, *100*). Conformations a-d are taken from *Svetlitchnaia et al.* (*89*). A new conformation, the activation-Conform (e) as part of the activation complex with RACo, has been included in the reaction scheme.

5.4. Conformational Changes on RACo

Complex association commonly induces conformational changes on at least one protein involved. In all ATP dependent activation systems described so far, conformational changes have been mainly observed on the ATPases. Additionally to the domain rearrangements described for CoFeSP, conformational changes on RACo are evident.

RACo is assigned to the ASKHA protein family since the large C-terminal domain resembles the typical core fold with a βββαβαβα topology (*47, 48*). Many members of the ASKHA family exist in two conformations. Commonly, binding of the (sugar) substrate, the nucleotide, a metal ion or a combination of the different ligands trigger protein motion (*48, 137–139*). The binding of the nucleotide to the open conformation of actin and hsc70 for example solely induces conformational changes and provokes the closure of the binding site (*140, 141*).

The crystal structure of RACo represents with a phosphate bound in the narrow cleft between the two subdomains of the ASKHA domain a closed conformation (Figure 12 and Figure 44, blue). The comparison of the structures of complexed and free RACo upon superimposition of the middle domains (r.m.s.d. = 0.342) demonstrates that the narrow cleft has opened upon complex formation (Figure 44, purple). Residues of this domain are displaced by up to 16 Å. Two generic helices are rotated by 19 and 25 °, respectively (Figure 44A). As a consequence of the conformational changes observed on RACo, H-bonds and salt bridges are formed between these residues and CfsB (Figure 37C) and the corrin macro cycle (Figure 40A). Surface presentations of the two conformers visualise the opening of the nucleotide-binding site in the cleft between the subdomains I and II of the ASKHA domain. Displacement of subdomain II results in the formation of the corrin-binding pocket in which the corrin macrocycle perfectly suits (Figure 44B).

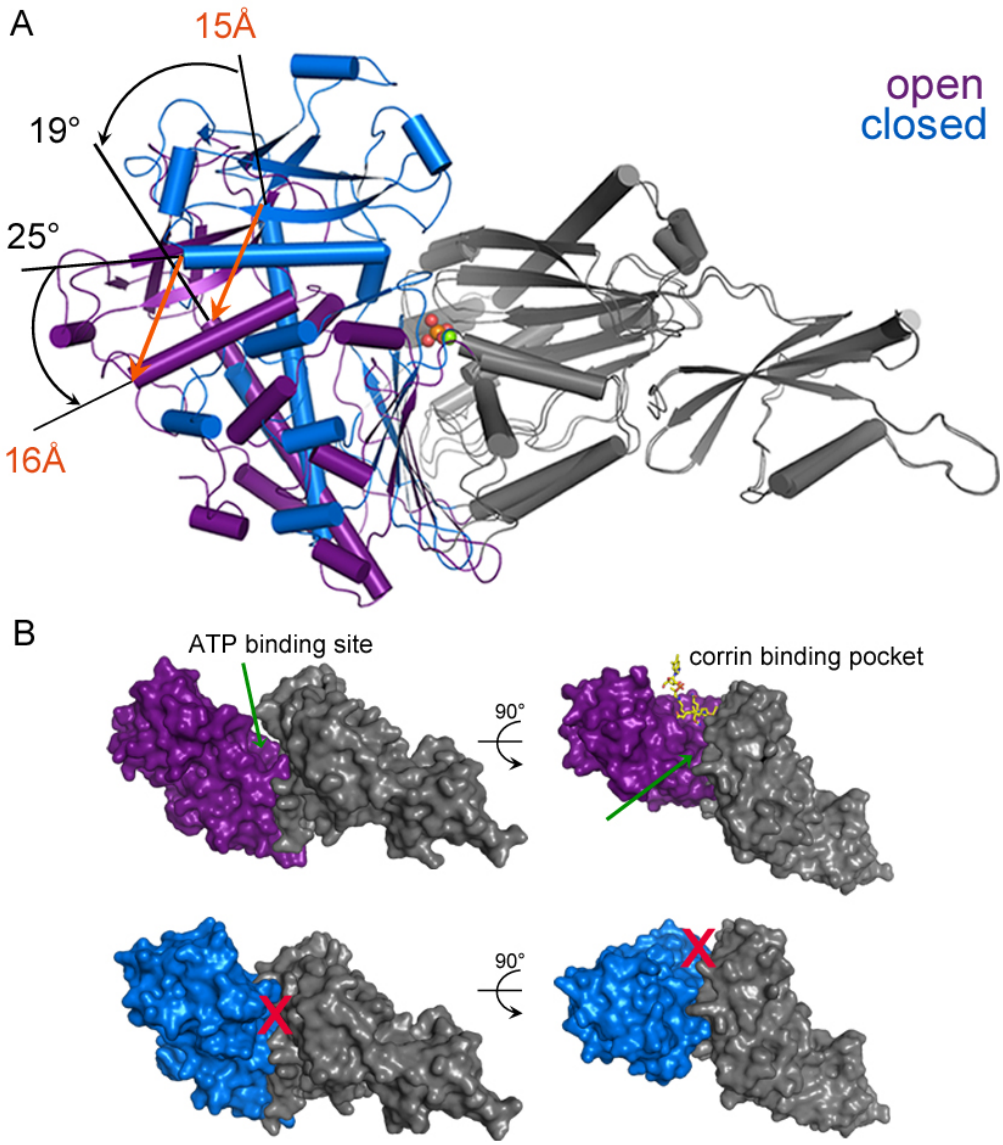

Figure 44: Conformational changes on RACo upon complex formation. (A) Free RACo (blue, PDB 3ZYY) (*102*) superimposed to CoFeSP-bound RACo (purple) by the middle domain (residues 125-205). Only subdomain II is coloured; parts of the structure not affected by the interaction with CoFeSP are illustrated in grey. The Mg^{2+} and PO_4^{3-} bound in free RACo are shown as spheres. Orange arrows highlight the displacement of two generic helices. (B) Closed and open conformation of the ASKHA domain of RACo. Surface presentation of the activator of CoFeSP in the RACo:CoFeSP complex (above) and of free activator (below) in two orientations. The open cleft representing the nucleotide-binding site and the open corrin-binding pocket (with cobalamin depicted as yellow sticks) are indicated. The closed cleft and pocket are marked with a red X.

The activator of 2-hydroxyisocaproyl-CoA dehydratase from *Clostridium difficile* also belong to the ASKHA fold protein family and exist in a closed and an open conformation (Figure 45A) (*50*). Superimposition of the two states of the activator of 2-hydroxyisocaproyl-CoA dehydratase by domain II revealed a relocation of domain I. Helix 1 is displaced by 19 Å

increasing the angle between domain I and II by 40° (Figure 45B) (*50*). The dislocation and rotation within the ASKHA domain of RACo and the activator of 2-hydroxyisocaproyl-CoA dehydratase are similar. Nevertheless, both conformations of the latter were observed in the absence of the dehydratase.

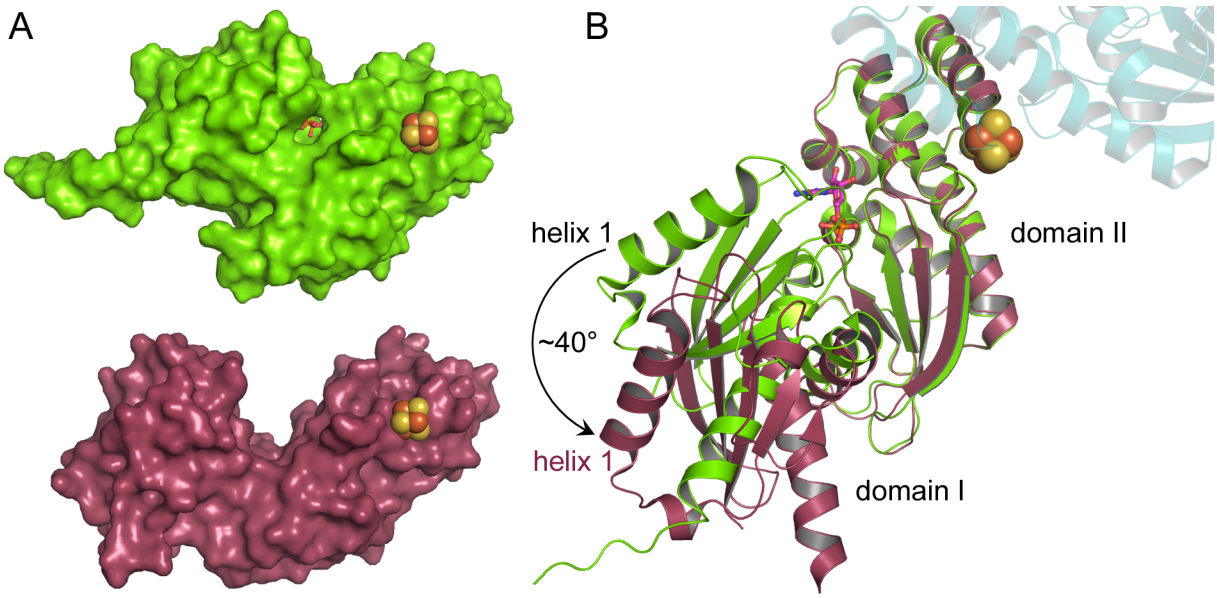

Figure 45: Closed and open conformation of the activator of (*R*)-2-hydroxyisocaproyl-CoA dehydratase. (A) Surface presentation of the activator of (*R*)-2-hydroxylisocaproyl-CoA dehydratase with ADP bound representing the closed conformation (green, PDB 4EHT) and the open, e.g. nucleotide free state (red, PDB 4EIA) (*50*). ADP bound to the closed conformation is shown as stick model, the [4Fe4S] cluster is illustrated as spheres (sulfur atoms in yellow, iron atoms in orange). (B) Superimposition of the monomers of the closed and open conformation based on C_α atoms of domain II. The monomers are shown as ribbon and are coloured as in (A). ADP (bound to the closed conformation) is illustrated as sticks and the FeS cluster as spheres. The second monomer of the closed state is hinted in light blue. The figure was prepared and modified from *Knauer et al.* (*50*).

The dislocation of the ASKHA domain allows for the creation of the corrin-binding pocket, which is too narrow for the corrin cycle to fit in in the closed conformation (Figure 46).

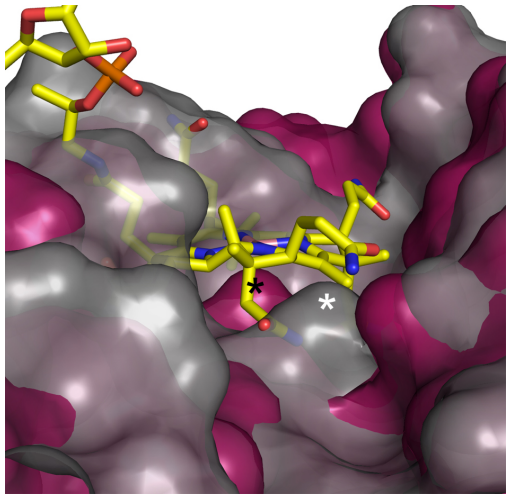

Figure 46: Closed and open corrin-binding pocket. The corrin ring of the cobalamin cofactor (yellow stick model) and the binding pocket of RACo in the open conformation (pink surface presentation) show a nearly perfect fit as illustrated in Figure 40B. In the closed conformation (PDB 3ZYY (*102*), grey surface) the pocket is not wide enough to accommodate the corrin ring and it is partially covered. The serine 398 coordinating directly the cobalt ion in the complex is marked with an asterisk (white in RACo, black in the complex).

The conformational changes on RACo result in the loss of a β-strand within the ASKHA domain (residues 547-549) interacting with a β-strand of the linker domain (residues 110-112) (Figure 47A). The lacking "fixation" (Figure 47B) could be an explanation why this domain is highly disordered in the complex and provides an even higher mobility resulting in a bigger operating range of the electron donor domain.

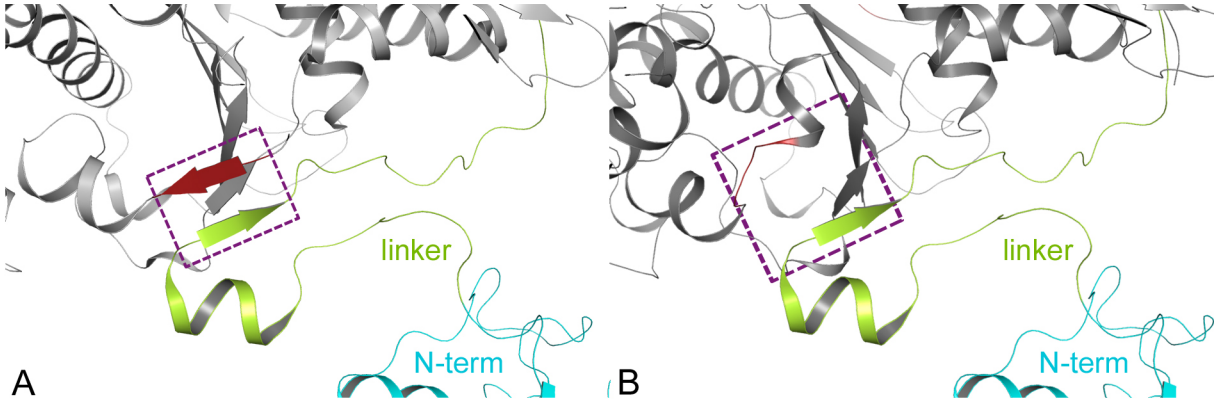

Figure 47: Loss of the interaction between two β-strands may result in higher flexibility of the linker domain. (A) The interaction of a β-strand of the linker domain (green cartoon) and a β-strand (red) of the ASKHA domain observed in the RACo structure (PDB 3ZYY) (*102*). (B) In the RACo:CoFeSP complex, this interaction is lost due to the opening of the ASKHA domain. Shown is the linker domain of the single RACo structure. The residues forming the β-strand are coloured as in (A).

IV. CONCLUSION

Scheme of the Mechanism of the Reductive Activation of CoFeSP by RACo

Based on the results obtained in this study (Results and Discussion 3, 4 and 5), a mechanism for the reductive activation of CoFeSP by RACo can be drawn (Figure 48).

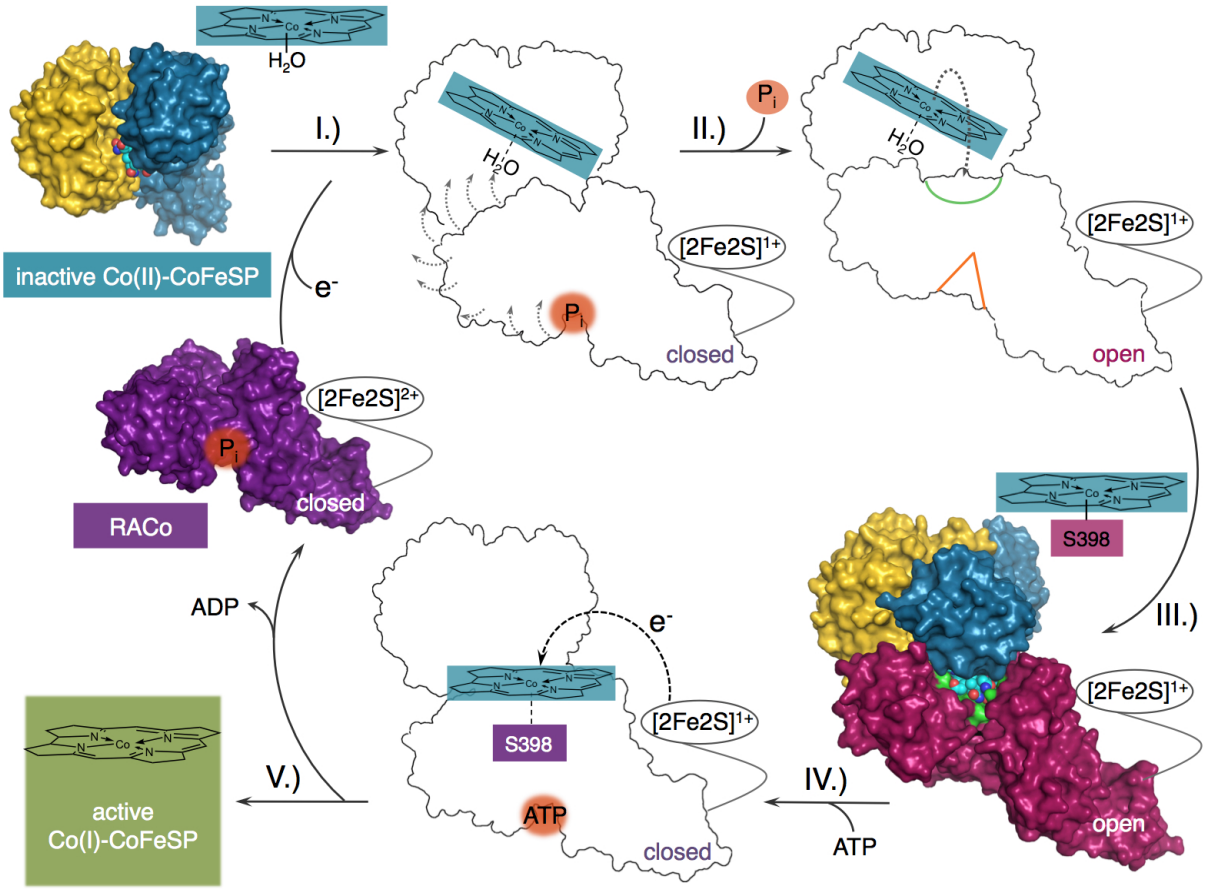

Figure 48: Proposed mechanism of the ATP-dependent reductive activation of CoFeSP by its activator RACo. Available protein structures (PDB 2YCL (*94*) and 3ZYY (*102*)) are shown as surfaces, whereas contour plots illustrate theoretical intermediary states not captured in crystal structures. The coordination of the cobalamin cofactor in every state is sketched; the open corrin-binding pocket is illustrated with green, an orange triangle indicates the open ATP-binding site. Dashed lines demonstrate movements. The activation mechanism is described in detail in the text. For clarity, only the complex monomer is shown.

I.) A transient complex is formed between RACo in its closed conformation and the inactive resting state of CoFeSP.

II.) Conformational changes on RACo, i.e. switching from the closed to the open state, result in the expansion of the nucleotide-binding cleft. Simultaneously, the corrin-binding pocket is created.

III.) Upon complete formation of the binding pocket, the cobalamin-binding domain of CoFeSP adapts a new conformation (activation conform, Figure 43) and places the corrin ring into the corrin-binding pocket where it is engaged in a tight hydrogen bonding network including direct interaction between the cobalt ion and Ser398 of RACo. In the activation complex, Co(II) is highly stabilised and without energy input a reduction to the active Co(I) is not achieved.

IV.) Binding of ATP induces the closure of RACo, straightens the corrin pocket and results in a weakening of the interactions between the ASKHA domain of RACo and CfsB. As the corrin ring has been tightly fit into the pocket, it transiently adopts a square-planar geometry like it is favoured in the Co(I)-cobalamin. Water cannot replace the hydroxyl group of Ser398 as axial ligand since simply no space is provided. The [2Fe2S] cluster transfers its electron just in the right moment when ATP hydrolysis provides the energy needed to overcome the potential barrier and to break the complex completely.

V.) Active Co(I)-CoFeSP can now return to the catalytic cycle, and RACo in its closed conformation is prepared to reactivate another inactive Co(II)-CoFeSP.

It cannot be clearly concluded which event (I or II) during complex formation occurs first. As the corrin-binding pocket cannot be formed in RACo´s closed conformation and the opening is induced by interactions between CfsB and RACo (Figure 37C), it is more likely that conformational changes upon complex formation on the activator happens first, followed by bending over the cobalamin to its new “accommodation”.

The tight interactions between the corrin macrocycle and residues of the ASKHA domain of RACo, especially the direct interaction with Ser398 (Figure 40A), modulate the midpoint potential of the cobalamin cofactor and stabilise the inactive Co(II) state (Results and Discussion 4.3.3, Figure 40) supported also by a small dissociation constant (Results and Discussion 4.2.2, Figure 28). The dependency of the electron transfer reaction on ATP was shown (Results and Discussion 4.1) but it could not be proved whether nucleotide-binding or hydrolysis triggers the reduction. Definitely, energy input is mandatory to provoke the dissociation of the stable RACo:CoFeSP complex ($\Delta G_{binding}$ of – 44 kJ/mol); the hydrolysis of one molecule of ATP (approximately ΔG_{ATP} of – 48 kJ/mol) (*142*) or the binding in combination with conformational changes, have to promote the reactivation of CoFeSP.

Different models of electron transfer in nitrogenase like the "deficit spending" model suggest that ET is gated by conformational changes on the Fe-protein and that the hydrolysis of ATP induces complex dissociation (*35, 132*). Recently, Duval *et al.* (*43*) were able to complete the thermodynamic cycle of the Fe-protein during nitrogenase reduction and showed that interprotein ET is not directly coupled to the hydrolysis of ATP. Phosphate release and complex dissociation mark the last steps (*43*). Hence, ET in nitrogenase is driven by the free energy of ATP binding and protein-protein association. (*43, 132*). Compared to the Fe-protein both, the electron transfer (Results and Discussion 4.1.1) and the ATP hydrolysis rates (Results and Discussion 3.2) of RACo are low. The reductive activation of CoFeSP by RACo represents a "rescue" mechanism. Hence, it is just required occasionally and fast turnovers are less mandatory than during the reduction of one molecule of nitrogen by nitrogenase; the reaction depends on at least 8 successive cycles of complex association / dissociation, each transferring one electron and consuming two molecules of ATP (*12, 18, 23, 27*). Despite this variation, the elctron transfer between RACo and CoFeSP may also be controlled by the free energy of nucleotide binding and / or complex association, in compliance with nitrogenase.

Interactions of the two proteins do not alter the donor cluster as it is proposed for the activator of 2-hydroxy-isocaproyl-CoA-dehydratase (*135*) or the Fe-protein of nitrogenase (*131, 132*). The midpoint potential of the corrinoid protein of *O*-demethylase increases to a moderate midpoint potential, i.e. comparable to the one of the donor cluster, in the presence of the activating enzyme (*16, 17*). In contrast to nitrogenase or dehydratase, the donor cluster on RACo as well as the accepting cofactor on CoFeSP is bound to flexible domains. The FeMo-cluster of nitrogenase and the acceptor [4Fe4S] cluster in dehydratase are buried in the protein

and cannot be accessed directly (*24, 49*); direct modulation by the activator or reductase is precluded. Hence, the stabilisation of the Co(II) state in the RACo:CoFeSP complex is enabled by the modular architecture of both proteins. The modular protein methionine synthase in the reactivation conformation (juxtaposition of the cobalamin- and AdoMet-binding domains) is capable of altering the reduction potential of the Co(II)/Co(I) couple by elongation of the bond between the cobalt ion and its upper axial water ligand. Thus, reduction by flavodoxin is facilitated by the adaption of a 4-coordinate cobalamin (*143*). In the RACo:CoFeSP complex, ATP-binding may provoke the elongation of the bond between Ser398 and the Co-ion, destabilise the Co(II) state and favour the transition to the preferred Co(I)-geometry. This temporarily adapted square-planar Co(I)-like coordination may facilitate the reduction of cobalamin, like reported for MetH (*143*). Thereby the sensitive Co(I) state is protected by the tight fit of the corrin-binding pocket since no water molecule can compensate the loss of the axial protein ligand.

In the ATP-dependent electron transfer systems of nitrogenase, radical-dependent β,α-dehydratases and the related benzoyl- CoA reductases, the functional unit is the activator / reductase dimer. Contrary to these systems, the RACo monomer, each binding one [2Fe2S] cluster, acts as functional unit in the reductive activation of CoFeSP, which is also reflected in the stoichiometry of the ternary activation complex between one RACo dimer and two CoFeSP heterodimers (Results and Discussion 4.2 Figure 26 and 5.1, Figure 36).

In conclusion, oxidation-state-dependent partner recognition (Results and Discussion 4.2.1) combined with a manipulation of the electron accepting site (Results and Discussion 4.3 and 5.3) and balance of binding energies (Results and Discussion 4.2.2) represents a feasible way to gate the ATP-coupled electron transfer in the reductive activation of CoFeSP by its activator RACo.

V. OUTLOOK

The characterisation of the reductive activator of CoFeSP, RACo, operating in the reductive acetyl-CoA pathway of *Carboxydothermus hydrogenoformans*, has extended the general knowledge about the functionality of RACE proteins. The structural and spectroscopic investigation of the activator:CoFeSP complex within this study have offered insights into the mechanism of the reductive activation of corrinoid enzymes.

Recently, Duval *et al.* were able to complete the thermodynamic cycle of the Fe-protein by determination of the rate constants of the four sequential steps during reduction of nitrogenase (*43*). A comparable kinetic study of the single events during the reductive activation of CoFeSP by RACo in combination with further studies on the active site mutants of RACo (Results and Discussion 3.2 and 4.1.2) could be helpful to solve the enigma of the role of ATP and confirm or refute the suggested ATP-dependent reactivation mechanism (Conclusion, Figure 48).

The increase of the cobalamin potential by the interaction with RACo (Results and Discussion 4.3.3) is in contrast to the nitrogenase / dehydratase system where conformational changes on the Fe-protein and the activator of dehydratase in the presence of a nucleotide cause changes on the redox potential of the reducing cluster (*131–135*). The midpoint potential of the [2Fe2S] cluster of RACo was determined in the absence of a nucleotide (Results and Discussion 3.3). Redox titration could be repeated with ATP or ATP-analogues to exclude modulations on the donor site.

In the structure of the RACo:CoFeSP complex the N-terminal domain of RACo and parts of the linker are unresolved (Results and Discussion, Figure 36), probably due to the high flexibility of the long linker domain or as a result of proteolysis during the long crystallisation process. Even though the domain does not contribute to the stability of the complex (Results and Discussion 4.2, 4.3.1 and 5.1), its position could shed light on how the electron is transferred to the cobalamin. The distance between the metals involved in the electron transfer from RACo to CoFeSP could be detected in pulsed electron–electron double resonance (PELDOR or DEER) experiments (*144*). Fluorescence resonance energy transfer (FRET) (*145*) enables the measurement of changes in molecular distances and could be performed to get further insights into the kinetics of domain movements (Results and Discussion 5.2 and 5.4) during the reductive activation of CoFeSP by RACo.

VI. REFERENCES

1. V. P. Skulachev, The laws of cell energetics. *Eur. J. Biochem.* **208**, 203–209 (1992).

2. F. Lipmann, Metabolic Generation and Utilization of Phosphate Bond Energy In *Advances in Enzymology and Related Areas of Molecular Biology* (John Wiley & Sons, Inc, 2006), pp. 99–162.

3. I. C., West P. Mitchell, Proton/sodium ion antiport in Escherichia coli. *Biochem. J.* **144**, 87–90 (1974).

4. V. P. Skulachev, Transmembrane electrochemical H^+-potential as a convertible energy source for the living cell. *FEBS Lett.* **74**, 1–9 (1977).

5. D. C. Rees, J. B. Howard, Structural bioenergetics and energy transduction mechanisms. *J. Mol. Biol.* **293**, 343–350 (1999).

6. A. L. Lehninger, D. L. Nelson, M. M. Cox, *Lehninger Principles of biochemistry* (W. H. Freeman, New York, Basingstoke, ed. 5, 2008).

7. P. Mitchell, Coupling of Phosphorylation to Electron and Hydrogen Transfer by a Chemi-Osmotic type of Mechanism. *Nature* **191**, 144–148 (1961).

8. R. E. Sharp, S. K. Chapman, Mechanisms for regulating electron transfer in multi-centre redox proteins. *Biochim. Biophys. Acta* **1432**, 143–158 (1999).

9. W. Buckel, R. K. Thauer, Energy conservation via electron bifurcating ferredoxin reduction and proton/Na^+ translocating ferredoxin oxidation. *Biochim. Biophys. Acta* **1827**, 94–113 (2013).

10. H. Huang, S. Wang, J. Moll, R. K. Thauer, Electron Bifurcation Involved in the Energy Metabolism of the Acetogenic Bacterium *Moorella thermoacetica* Growing on Glucose or H_2 plus CO_2. *J. Bacteriol.* **194**, 3689–3699 (2012).

11. A. Bar-Even, Does acetogenesis really require especially low reduction potential? *Biochim. Biophys. Acta* **1827**, 395–400 (2013).

12. L. C. Seefeldt, B. M. Hoffman, D. R. Dean, Mechanism of Mo-Dependent Nitrogenase. *Annu. Rev. Biochem.* **78**, 701–722 (2009).

13. W. Buckel, M. Hetzel, J. Kim, ATP-driven electron transfer in enzymatic radical reactions. *Curr. Opin. Chem. Biol.* **8**, 462–467 (2004).

14. M. Unciuleac, M. Boll, Mechanism of ATP-driven electron transfer catalyzed by the benzene ring-reducing enzyme benzoyl- CoA reductase. *Proc. Natl. Acad. Sci. U.S.A.* **98**, 13619–13624 (2001).

15. T. Ferguson, J. A. Soares, T. Lienard, G. Gottschalk, J. A. Krzycki, RamA, a Protein Required for Reductive Activation of Corrinoid-dependent Methylamine Methyltransferase Reactions in Methanogenic Archaea. *J. Biol. Chem.* **284**, 2285–2295 (2009).

16. A. Siebert, T. Schubert, T. Engelmann, S. Studenik, G. Diekert, Veratrol-O-demethylase of *Acetobacterium dehalogenans*: ATP-dependent reduction of the corrinoid protein. *Arch. Microbiol.* **183**, 378-384 (2005).

17. A. Schilhabel *et al.,* The Ether-Cleaving Methyltransferase System of the Strict Anaerobe *Acetobacterium dehalogenans*: Analysis and Expression of the Encoding Genes. *J. Bacteriol.* **191**, 588–599 (2009).

18. B. K. Burgess, D. J. Lowe, Mechanism of Molybdenum Nitrogenase. *Chem. Rev.* **96**, 2983–3012 (1996).

19. J. B. Howard, D. C. Rees, Nitrogenase: A Nucleotide-Dependent Molecular Switch. *Annu. Rev. Biochem.* **63**, 235–264 (1994).

20. J. B. Howard, D. C. Rees, Structural Basis of Biological Nitrogen Fixation. *Chem. Rev.* **96**, 2965–2982 (1996).

21. R. Y. Igarashi, L. C. Seefeldt, Nitrogen fixation: the mechanism of the Mo-dependent nitrogenase. *Crit. Rev. Biochem. Mol. Biol.* **38**, 351–384 (2003).

22. L. C. Seefeldt, B. M. Hoffman, D. R. Dean, Electron transfer in nitrogenase catalysis. *Curr. Opin. Chem. Biol.* **16**, 19–25 (2012).

23. R. N. Thorneley, D. J. Lowe, R. R. Eday, R. W. Miller, The coupling of electron transfer in nitrogenase to the hydrolysis of magnesium adenosine triphosphate. *Biochem. Soc. Trans.* **7**, 633–636 (1979).

24. D. C. Rees *et al.,* Structural basis of biological nitrogen fixation. *Philos. Trans. R. Soc. London Ser. A* **363**, 971–984 (2005).

25. A. F. Holleman, Holleman-Wiberg, E. Wiberg, N. Wiberg, *Lehrbuch der anorganischen Chemie* (de Gruyter, Berlin [u.a.], ed. 101, 1995).

26. L. E. Mortenson, R. N. F. Thorneley, Structure and Function of Nitrogenase. *Annu. Rev. Biochem.* **48**, 387–418 (1979).

27. R. V. Hageman, W. H. Orme-Johnson, R. H. Burris, Role of magnesium adenosine 5'-triphosphate in the hydrogen evolution reaction catalyzed by nitrogenase from *Azotobacter vinelandii*. *Biochemistry* **19**, 2333–2342 (1980).

28. H. Schindelin, C. Kisker, J. L. Schlessman, J. B. Howard, D. C. Rees, Structure of ADP·AlF_4^--stabilized nitrogenase complex and its implications for signal transduction. *Nature* **387**, 370–376 (1997).

29. F. A. Tezcan *et al.*, Nitrogenase Complexes: Multiple Docking Sites for a Nucleotide Switch Protein. *Science* **309**, 1377–1380 (2005).

30. M. Georgiadis *et al.,* Crystallographic structure of the nitrogenase iron protein from *Azotobacter vinelandii*. *Science* **257**, 1653–1659 (1992).

31. P. Strop *et al.,* Crystal Structure of the All-Ferrous $[4Fe\text{-}4S]^0$ Form of the Nitrogenase Iron Protein from *Azotobacter vinelandii*. *Biochemistry* **40**, 651–656 (2001).

32. E. F. Pai *et al.*, Refined crystal structure of the triphosphate conformation of H-ras p21 at 1.35 Å resolution: implications for the mechanism of GTP hydrolysis. *EMBO J.* **9**, 2351–2359 (1990).

33. J.-H. Jeoung, T. Giese, M. Grünwald, H. Dobbek, Crystal Structure of the ATP-Dependent Maturation Factor of Ni,Fe-Containing Carbon Monoxide Dehydrogenases. *J. Mol. Biol.* **396**, 1165–1179 (2010).

34. K. Scheffzek *et al.,* The Ras-RasGAP complex: structural basis for GTPase activation and its loss in oncogenic Ras mutants. *Science* **277**, 333–338 (1997).

35. K. Danyal, D. Mayweather, D. R. Dean, L. C. Seefeldt, B. M. Hoffman, Conformational Gating of Electron Transfer from the Nitrogenase Fe Protein to MoFe Protein. *J. Am. Chem. Soc.* **132**, 6894–6895 (2010).

36. T. Spatzal *et al.,* Evidence for Interstitial Carbon in Nitrogenase FeMo Cofactor. *Science* **334**, 940 (2011).

37. J. Kim, D. Rees, Structural models for the metal centers in the nitrogenase molybdenum-iron protein. *Science* **257**, 1677–1682 (1992).

38. O. Einsle *et al.*, Nitrogenase MoFe-Protein at 1.16 A Resolution: A Central Ligand in the FeMo-Cofactor. *Science* **297**, 1696–1700 (2002).

39. M. G. Duyvis, H. Wassink, H. Haaker, Formation and characterization of a transition state complex of *Azotobacter vinelandii nitrogenase*. *FEBS Lett.* **380**, 233–236 (1996).

40. C. C. Page, C. C. Moser, X. Chen, P. L. Dutton, Natural engineering principles of electron tunnelling in biological oxidation-reduction. *Nature* **402**, 47–52 (1999).

41. H. B. Gray, J. R. Winkler, Electron transfer in proteins. *Annu. Rev. Biochem.* **65**, 537–561 (1996).

42. K. Danyal, D. R. Dean, B. M. Hoffman, L. C. Seefeldt, Electron Transfer within Nitrogenase: Evidence for a Deficit-Spending Mechanism. *Biochemistry* **50**, 9255–9263 (2011).

43. S. Duval *et al.,* Electron transfer precedes ATP hydrolysis during nitrogenase catalysis. *Proc. Natl. Acad. Sci. U.S.A.* **110**, 16414–16419 (2013).

44. J. Kim, M. Hetzel, C. D. Boiangiu, W. Buckel, Dehydration of (R)-2-hydroxyacyl-CoA to enoyl-CoA in the fermentation of α-amino acids by anaerobic bacteria. *FEMS Microbiol. Rev.* **28**, 455–468 (2004).

45. J. Kim, D. J. Darley, W. Buckel, A. J. Pierik, An allylic ketyl radical intermediate in clostridial amino-acid fermentation. *Nature* **452**, 239–242 (2008).

46. W. Buckel *et al.,* Enzyme catalyzed radical dehydrations of hydroxy acids, Radical SAM Enzymes and Radical Enzymology. *Biochim. Biophys. Acta* **1824**, 1278–1290 (2012).

47. P. Bork, C. Sander, A. Valencia, An ATPase domain common to prokaryotic cell cycle proteins, sugar kinases, actin, and hsp70 heat shock proteins. *Proc. Natl. Acad. Sci. U.S.A.* **89**, 7290–7294 (1992).

48. J. H. Hurley, The sugar kinase/heat shock protein 70/actin superfamily: implications of conserved structure for mechanism. *Annu. Rev. Biophys. Biomol. Struct.* **25**, 137–162 (1996).

49. S. H. Knauer, W. Buckel, H. Dobbek, Structural Basis for Reductive Radical Formation and Electron Recycling in (R)-2-Hydroxyisocaproyl-CoA Dehydratase. *J. Am. Chem. Soc.* **133**, 4342–4347 (2011).

50. S. H. Knauer, W. Buckel, H. Dobbek, On the ATP-Dependent Activation of the Radical Enzyme (R)-2-Hydroxyisocaproyl-CoA Dehydratase. *Biochemistry* **51**, 6609–6622 (2012).

51. J. Kim, A. J. Pierik, W. Buckel, A Complex of 2-Hydroxyisocaproyl-Coenzyme A Dehydratase and its Activator from *Clostridium difficile* Stabilized by Aluminium Tetrafluoride-Adenosine Diphosphate. *Chem. Eur. J. of Chem. Phys.* **11**, 1307–1312 (2010).

52. J. Kim, D. Darley, W. Buckel, 2-Hydroxyisocaproyl-CoA dehydratase and its activator from *Clostridium difficile*. *FEBS J.* **272**, 550–561 (2005).

53. M. Boll, G. Fuchs, Benzoyl-Coenzyme A Reductase (Dearomatizing), a Key Enzyme of Anaerobic Aromatic Metabolism. ATP Dependence of the Reaction, Purification and Some Properties of the Enzyme from *Thauera Aromatica* Strain K172. *Eur. J. Biochem.* **234**, 921–933 (1995).

54. M. Boll, S. S. P. Albracht, G. Fuchs, Benzoyl-CoA Reductase (Dearomatizing), A Key Enzyme of Anaerobic Aromatic Metabolism. A Study of Adenosinetriphosphatase

Activity, ATP Stoichiometry of the Reaction and EPR Properties of the Enzyme. *Eur. J. Biochem.* **244**, 840–851 (1997).

55. B. Thiele, O. Rieder, B. T. Golding, M. Müller, M. Boll, Mechanism of Enzymatic Birch Reduction: Stereochemical Course and Exchange Reactions of Benzoyl-CoA Reductase. *J. Am. Chem. Soc.* **130**, 14050–14051 (2008).

56. R. V. Banerjee, R. G. Matthews, Cobalamin-dependent methionine synthase. *FASEB J.* **4**, 1450–1459 (1990).

57. C. W. Goulding, D. Postigo, R. G. Matthews, Cobalamin-Dependent Methionine Synthase Is a Modular Protein with Distinct Regions for Binding Homocysteine, Methyltetrahydrofolate, Cobalamin, and Adenosylmethionine. *Biochemistry* **36**, 8082–8091 (1997).

58. R. G. Matthews, Cobalamin-dependent methionine synthase. In *Chemistry and biochemistry of B12*. R. Banerjee, Ed. (1999) , pp. 681–706.

59. S. W. Ragsdale, The acetogenic corrinoid proteins. In *Chemistry and biochemistry of B12*. R. Banerjee, Ed. (1999), pp. 633–653.

60. K. Sauer, R. K. Thauer, The role of corrinoids in methanogens. In *Chemistry and biochemistry of B12*. R. Banerjee, Ed. (1999) , pp. 655–679.

61. G. Wohlfahrt, G. Diekert, Reductive dehalogenases. In *Chemistry and biochemistry of B12*. R. Banerjee, Ed. (1999), pp. 871–893.

62. R. G. Matthews, Cobalamin-Dependent Methyltransferases. *Acc. Chem. Res.* **34**, 681–689 (2001).

63. K. Sauer, R. K. Thauer, Methanol:coenzyme M methyltransferase from *Methanosarcina barkeri*. Zinc dependence and thermodynamics of the methanol:cob(I)alamin methyltransferase reaction. *Eur. J. Biochem.* **249**, 280-285 (1997).

64. van der Meijden, P, te Brommelstroet, B W, C. M. Poirot, van der Drift, C, G. D. Vogels, Purification and properties of methanol:5-hydroxybenzimidazolylcobamide methyltransferase from *Methanosarcina barkeri*. *J. Bacteriol.* **160**, 629–635 (1984).

65. F. Kaufmann, G. Wohlfarth, G. Diekert, O-demethylase from *Acetobacterium dehalogenans* - substrate specificity and function of the participating proteins. *Eur. J. Biochem.* **253**, 706–711 (1998).

66. F. Kaufmann, G. Wohlfarth, G. Diekert, O-demethylase from *Acetobacterium dehalogenans* - cloning, sequencing, and active expression of the gene encoding the corrinoid protein. *Eur. J. Biochem.* **257**, 515–521 (1998).

67. P. E. Jablonski, W. P. Lu, S. W. Ragsdale, J. G. Ferry, Characterization of the metal centers of the corrinoid/iron-sulfur component of the CO dehydrogenase enzyme complex from *Methanosarcina thermophila* by EPR spectroscopy and spectroelectrochemistry. *J. Biol. Chem.* **268**, 325–329 (1993).

68. S. R. Harder, W. P. Lu, B. A. Feinberg, S. W. Ragsdale, Spectroelectrochemical studies of the corrinoid/iron-sulfur protein involved in acetyl coenzyme A synthesis by *Clostridium thermoaceticum*. *Biochemistry* **28**, 9080–9087 (1989).

69. P. J. Daas, J. T. Keltjens, W. R. Hagen, van der Drift, C, The electrochemistry of 5-hydroxybenzimidazolylcobamide. *Arch. Biochem. Biophys.* **319**, 244–249 (1995).

70. Daas, P.H.J., Gerrits, K.A.A., Keltjens, J.T., van der Drift C., Vogels G.D., Involvement of an Activation Protein in the Methanol:2-Mercaptoethanesulfonic Acid Methyltransferase Reaction in *Methanosarcina barkeri*. *J. Bacteriol.*, 1278–1283 (1993).

71. M. H. Berman, A. C. Frazer, Importance of tetrahydrofolate and ATP in the anaerobic O-demethylation reaction for phenylmethylethers. *Appl. Environ. Microbiol.* **58**, 925–931 (1992).

72. T. Engelmann, F. Kaufmann, G. Diekert, Isolation and characterization of a veratrol:corrinoid protein methyl transferase from *Acetobacterium dehalogenans*. *Arch. Microbiol.* **175**, 376–383 (2001).

73. S. Studenik, M. Vogel, G. Diekert, Characterization of an O-Demethylase of Desulfitobacterium hafniense DCB-2. *J. Bacteriol.* **194**, 3317–3326 (2012).

74. H. D. Nguyen, S. Studenik, G. Diekert, Corrinoid activation by a RACE protein: studies on the interaction of the proteins involved. *FEMS Microbiol. Lett.* **345**, 31–38 (2013).

75. G. Fuchs, Alternative Pathways of Carbon Dioxide Fixation: Insights into the Early Evolution of Life? *Ann. Rev. Microbiol.* **65**, 631–658 (2011).

76. S. W. Ragsdale, Nickel and the carbon cycle. *J. Inorg. Biochem.* **101**, 1657–1666 (2007).

77. S. W. Ragsdale, E. Pierce, Acetogenesis and the Wood–Ljungdahl pathway of CO_2 fixation. *Biochim. Biophys. Acta* **1784**, 1873–1898 (2008).

78. S. W. Ragsdale, Life with Carbon Monoxide. *Crit. Rev. Biochem. Mol. Biol.* **39**, 165-195 (2004).

79. G. Fuchs, CO_2 fixation in acetogenic bacteria: Variations on a theme. *FEMS Microbiol. Lett.* **39**, 181–213 (1986).

80. Müller-Drake, V. Müller, F. Imkamp, A. Rauwolf, K. Küsel, H.L. Drake, Molecular and cellular biology of acetogenic bacteria. In *Strict and facultative anaerobes.* , pp. 251–281.

81. S. W. Ragsdale, Catalysis of Methyl Group Transfers Involving Tetrahydrofolate and B12 In *Folic Acid and Folates* (Elsevier, 2008), vol. **79,** pp. 293–324.

82. V. A. Svetlichny *et al., Carboxydothermus hydrogenoformans* gen. nov., sp. nov., a CO-utilizing Thermophilic Anaerobic Bacterium from Hydrothermal Environments of Kunashir Island. *Syst. Appl. Microbiol.* **14**, 254–260 (1991).

83. M. Wu *et al.,* Life in Hot Carbon Monoxide: The Complete Genome Sequence of *Carboxydothermus hydrogenoformans* Z-2901. *PLoS Genet.* **1**, e65 (2005).

84. A. M. Henstra, A. J. M. Stams, Deep Conversion of Carbon Monoxide to Hydrogen and Formation of Acetate by the Anaerobic Thermophile *Carboxydothermus hydrogenoformans*. *Int. J. Microbiol.* **2011**, 1–4 (2011).

85. V. Svetlitchnyi, C. Peschel, G. Acker, O. Meyer, Two Membrane-Associated NiFeS-Carbon Monoxide Dehydrogenases from the Anaerobic Carbon-Monoxide-Utilizing Eubacterium *Carboxydothermus hydrogenoformans*. *J. Bacteriol.* **183**, 5134–5144 (2001).

86. S. W. Ragsdale, Enzymology of the Wood-Ljungdahl Pathway of Acetogenesis. *Ann. N.Y. Acad. Sci.* **1125**, 129–136 (2008).

87. L. G. Ljungdahl, H. G. Wood, Total Synthesis of Acetate From CO_2 by Heterotrophic Bacteria. *Ann. Rev. Microbiol.* **23**, 515–538 (1969).

88. V. Svetlitchnyi *et al.,* A functional Ni-Ni-[4Fe-4S] cluster in the monomeric acetyl-CoA synthase from *Carboxydothermus hydrogenoformans*. *Proc. Natl. Acad. Sci. U.S.A.* **101**, 446–451 (2004).

89. T. Svetlitchnaia, V. Svetlitchnyi, O. Meyer, H. Dobbek, Structural insights into methyltransfer reactions of a corrinoid iron-sulfur protein involved in acetyl-CoA synthesis. *Proc. Natl. Acad. Sci. U.S.A.* **103**, 14331–14336 (2006).

90. J.-H. Jeoung, T. Giese, M. Grünwald, H. Dobbek, CooC1 from *Carboxydothermus hydrogenoformans* Is a Nickel-Binding ATPase. *Biochemistry* **48**, 11505–11513 (2009).

91. J.-H. Jeoung, H. Dobbek, n-Butyl isocyanide oxidation at the [NiFe4S4OH(x)] cluster of CO dehydrogenase. *J. Inorg. Biochem.* **17**, 167–173 (2012).

92. J.-H. Jeoung, H. Dobbek, Structural Basis of Cyanide Inhibition of Ni, Fe-Containing Carbon Monoxide Dehydrogenase. *J. Am. Chem. Soc.* **131**, 9922–9923 (2009).

93. J.-H. Jeoung, H. Dobbek, Carbon Dioxide Activation at the Ni,Fe-Cluster of Anaerobic Carbon Monoxide Dehydrogenase. *Science* **318**, 1461–1464 (2007).

94. S. Goetzl, J.-H. Jeoung, S. E. Hennig, H. Dobbek, Structural Basis for Electron and Methyl-Group Transfer in a Methyltransferase System Operating in the Reductive Acetyl-CoA Pathway. *J. Mol. Biol.* **411**, 96–109 (2011).

95. S. W. Ragsdale, P. A. Lindahl, E. Münck, Mössbauer, EPR, and optical studies of the corrinoid/iron-sulfur protein involved in the synthesis of acetyl coenzyme A by *Clostridium thermoaceticum*. *J. Biol. Chem.* **262**, 14289–14297 (1987).

96. S. I. Hu, E. Pezacka, H. G. Wood, Acetate synthesis from carbon monoxide by *Clostridium thermoaceticum*. Purification of the corrinoid protein. *J. Biol. Chem.* **259**, 8892–8897 (1984).

97. E. Pezacka, H. G. Wood, Role of carbon monoxide dehydrogenase in the autotrophic pathway used by acetogenic bacteria. *Proc. Natl. Acad. Sci. U.S.A.* **81**, 6261–6265 (1984).

98. Y. Kung *et al.,* Visualizing molecular juggling within a B12-dependent methyltransferase complex. *Nature* **484**, 265–269 (2012).

99. S. Menon, S. W. Ragsdale, Role of the [4Fe-4S] Cluster in Reductive Activation of the Cobalt Center of the Corrinoid Iron−Sulfur Protein from *Clostridium thermoaceticum* during Acetate Biosynthesis. *Biochemistry* **37**, 5689–5698 (1998).

100. S. Menon, S. W. Ragsdale, The Role of an Iron-Sulfur Cluster in an Enzymatic Methylation Reaction. Methylation of Co Dehydrogenase/Acetyl-Coa Synthase by the Methylated Corrinoid Iron-Sulfur Protein. *J. Biol. Chem.* **274**, 11513–11518 (1999).

101. H.-K. Loke, P. A. Lindahl, Identification and preliminary characterization of AcsF, a putative Ni-insertase used in the biosynthesis of acetyl-CoA synthase from *Clostridium thermoaceticum*, A Special Issue in Honor of William H. Orme-Johnson. *J. Inorg. Biochem.* **93**, 33–40 (2003).

102. S. E. Hennig, J.-H. Jeoung, S. Goetzl, H. Dobbek, Redox-dependent complex formation by an ATP-dependent activator of the corrinoid/iron-sulfur protein. *Proc. Natl. Acad. Sci. U.S.A.* **109**, 5235–5240 (2012).

103. H. E. Klock, E. J. Koesema, M. W. Knuth, S. A. Lesley, Combining the polymerase incomplete primer extension method for cloning and mutagenesis with microscreening to accelerate structural genomics efforts. *Proteins* **71**, 982–994 (2008).

104. M. J. S. Bommer, Accelerating the Discovery of Transaminase Biocatalysis. Dissertation, University College London (2008).

105. U. K. Laemmli, Cleavage of Structural Proteins during the Assembly of the Head of Bacteriophage T4. *Nature* **227**, 680–685 (1970).

106. M. M. Bradford, A rapid and sensitive method for the quantitation of microgram quantities of protein utilizing the principle of protein-dye binding. *Anal. Biochem.* **72**, 248–254 (1976).

107. W. W. Fish, Rapid colorimetric micromethod for the quantitation of complexed iron in biological samples. *Methods Enzymol.* **158**, 357–364 (1988).

108. E. Gasteiger, ExPASy: the proteomics server for in-depth protein knowledge and analysis. *Nucleic Acids Res.* **31**, 3784–3788 (2003).

109. P. A. Lanzetta, L. J. Alvarez, P. S. Reinach, O. A. Candia, An improved assay for nanomole amounts of inorganic phosphate. *Anal. Biochem.* **100**, 95–97 (1979).

110. J. E. Lindsley, Use of a real-time, coupled assay to measure the ATPase activity of DNA topoisomerase II. *Methods Mol. Biol.* **95**, 57–64 (2001).

111. W. Meister *et al.,* Complex Formation with the Activator RACo Affects the Corrinoid Structure of CoFeSP. *Biochemistry* **51**, 7040–7042 (2012).

112. U. Mueller *et al.,* Facilities for macromolecular crystallography at the Helmholtz-Zentrum Berlin. *J. Synchrotron Rad.* **19**, 442–449 (2012).

113. W. Kabsch, XDS. *Acta Crystallogr. D* **66**, 125–132 (2010).

114. M. D. Winn *et al.,* Overview of the CCP 4 suite and current developments. *Acta Crystallogr. D* **67**, 235–242 (2011).

115. P. D. Adams *et al.,* PHENIX, A comprehensive Python-based system for macromolecular structure solution. *Acta Crystallogr. D* **66**, 213–221 (2010).

116. P. Emsley, K. Cowtan, Coot, Model-building tools for molecular graphics. *Acta Crystallogr. D* **60**, 2126–2132 (2004).

117. L. L. Schrödinger, The PyMOL Molecular Graphics System, Version 1.3r1. (2010).

118. F. Lipmann, Enzymatic Synthesis of Acetyl Phosphate. *J. Biol. Chem.* **155**, 55–70 (1944).

119. K. A. Buss, C. Ingram-Smith, J. G. Ferry, D. A. Sanders, M. S. Hasson, Crystallization of acetate kinase from *Methanosarcina thermophila* and prediction of its fold. *Protein Sci.* **6**, 2659–2662 (1997).

120. I. A. Rose, M. Grunberg-Manago, S. R. Korey, S. Ochoa, Enzymatic Phosphorylation of Acetate. *J. Biol. Chem.* **211**, 737–756 (1954).

121. T. D. K. Brown, M. C. Jones-Mortimer, H. L. Kornberg, The Enzymic Interconversion of Acetate and Acetyl-coenzyme A in *Escherichia coli*. *J. Gen. Microbiol.* **102**, 327–336 (1977).

122. C. Ingram-Smith, S. R. Martin, K. S. Smith, Acetate kinase: not just a bacterial enzyme. *Trends Microbiol.* **14**, 249–253 (2006).

123. J. Kim, On the enzymatic mechanism of 2-hydroxyisocaproyl-CoA dehydratase from *Clostridium difficile*. Dissertation, Philipps-Universität Marburg (2004).

124. M. J. Ryle, L. C. Seefeldt, Hydrolysis of Nucleoside Triphosphates Other than ATP by Nitrogenase. *J. Biol. Chem.* **275**, 6214–6219 (2000).

125. R. Cammack *et al.,* Midpoint redox potentials of plant and algal ferredoxins. *Biochem. J.* **168**, 205–209 (1977).

126. K. Fukuyama, Structure and Function of Plant-Type Ferredoxins. *Photosyn. Res.* **81**, 289-301 (2004).

127. E. Mayer, Gardiner, D. J., Hester, R. E., Resonance Raman spectra of vitamin B12 and some cobalt corrinoid derivatives. *J. Chem. Soc., Faraday Trans. 2* **69**, 1350–1358 (1973).

128. S. Salama, T. G. Spiro, Visible and near-ultraviolet resonance Raman spectra of photolabile vitamin B12 derivatives with a rapid-flow technique. *J. Raman Spectrosc.* **6**, 57–60 (1977).

129. S. Dong, R. Padmakumar, R. Banerjee, T. G. Spiro, Co−C Bond Activation in B12-Dependent Enzymes: Cryogenic Resonance Raman Studies of Methylmalonyl-Coenzyme A Mutase. *J. Am. Chem. Soc.* **121**, 7063–7070 (1999).

130. T. A. Stich *et al.,* Spectroscopic Studies of the Corrinoid/Iron−Sulfur Protein from *Moorella thermoacetica*. *J. Am. Chem. Soc.* **128**, 5010–5020 (2006).

131. W. N. Lanzilotta, L. C. Seefeldt, Changes in the midpoint potentials of the nitrogenase metal centers as a result of iron protein-molybdenum-iron protein complex formation. *Biochemistry* **36**, 12976–12983 (1997).

132. I. V. Kurnikov, A. K. Charnley, D. N. Beratan, From ATP to Electron Transfer: Electrostatics and Free-Energy Transduction in Nitrogenase. *J. Phys. Chem. B* **105**, 5359–5367 (2001).

133. W. Buckel, Radical and electron recycling in catalysis. *Angew. Chem. Int. Ed.* **48**, 6779–6787 (2009).

134. W. Buckel, B. M. Martins, A. Messerschmidt, B. T. Golding, Radical-mediated dehydration reactions in anaerobic bacteria. *Biol. Chem.* **386**, 951–959 (2005).

135. M. Hans *et al.,* Adenosine Triphosphate-Induced Electron Transfer in 2-Hydroxyglutaryl-CoA Dehydratase from *Acidaminococcus fermentans*. *Biochemistry* **41**, 5873–5882 (2002).

136. B. Kräutler, Organometallic chemistry of B12 coenzymes. *Met Ions Life Sci* **6**, 1–51 (2009).

137. K. A. Buss *et al.,* Urkinase: Structure of Acetate Kinase, a Member of the ASKHA Superfamily of Phosphotransferases. *J. Bacteriol.* **183**, 680–686 (2001).

138. H. Nishimasu, S. Fushinobu, H. Shoun, T. Wakagi, Crystal structures of an ATP-dependent hexokinase with broad substrate specificity from the hyperthermophilic archaeon *Sulfolobus tokodaii*. *J. Biol. Chem.* **282**, 9923-9931 (2007).

139. M. Miki, T. Kouyama, Domain Motion in Actin Observed by Fluorescence Resonance Energy Transfer. *Biochemistry* **33**, 10171–10177 (1994).

140. S. M. Wilbanks, L. Chen, H. Tsuruta, K. O. Hodgson, D. B. McKay, Solution small-angle X-ray scattering study of the molecular chaperone Hsc70 and its subfragments. *Biochemistry* **34**, 12095-12106 (1995).

141. J. K. Chik, U. Lindberg, C. E. Schutt, The structure of an open state of beta-actin at 2.65 A resolution. *J. Mol. Biol.* **263**, 607-623 (1996).

142. R. A. Alberty, R. N. Goldberg, Standard thermodynamic formation properties for the adenosine 5'-triphosphate series. *Biochemistry* **31**, 10610–10615 (1992).

143. M. Koutmos, S. Datta, K. A. Pattridge, J. L. Smith, R. G. Matthews, Insights into the reactivation of cobalamin-dependent methionine synthase. *Proc. Natl. Acad. Sci. U.S.A.* **106**, 18527–18532 (2009).

144. M. Pannier, S. Veit, A. Godt, G. Jeschke, H.W. Spiess, Dead-time free measurement of dipole–dipole interactions between electron spins. *J. Magn. Reson.*, **142**, 331–340 (2000).

145. P. R. Selvin, Fluorescence resonance energy transfer. *Meth. Enzymol.* **246**, 300–334 (1995).

VII. APPENDIX

A. Appendix Tables

1. Cloning and Mutagenesis of RACo

Table 10: Primers used in cloning and mutagenesis of RACo.

Primer	Sequence 5´→ 3
Cloning of RACo (pPKCoDuet1 & pET28a)	
Orf7_fwd	CAG CCA TAT GGC AGA ATA TAA AGT TTT G
Orf7_rev	GCA CTC GAG TTA TTC TAC TGA AGG AAA TAG ATG
Deletion of N-terminal Domain (PIPE cloning into pET28aTEV)	
RACo100+_fwd	CTT GTA TTT CCA GGG CCA TTC TGG AGT TAT GAA TGA ATT AGA TTT AGC GG
RACo100+_rev	CGA CGG AGC TCG AAT TCG GAT CCG GAT CCT TAT TCT ACT GAA GGA AAT AGA TGC AAA TCG G
Active Site Mutants (QuickChange Method, pPKCoDuet1TEV)	
R_D212A_fwd	CTT TGG TTT AGC AAT TGC TAT TGG CAC CAC TAC TGT
R_D212A_rev	ACA GTA GTG GTG CCA ATA GCA ATT GCT AAA CCA AAG
R_T215A_fwd	TAG CAA TTG ATA TTG GCG CCA CTA CTG TTG TGG TGC AAT TG
R_T215A_rev	CAA TTG CAC CAC AAC AGT AGT GGC GCC AAT ATC AAT TGC TA
R_D377A_fwd	GAA ATA ACC CTA TTT ATC GCT ATC GGG ACA AAC GGA GAA ATG
R_D377A_rev	CAT TTC TCC GTT TGT CCC GAT AGC GAT AAA TAG GGT TAT TTC
R_T380A_fwd	ATT TAT CGA TAT CGG GGC AAA CGG AGA AAT GGT TCT TGG CAA
R_T380A_rev	TTG CCA AGA ACC ATT TCT CCG TTT GCC CCG ATA TCG ATA AAT
R_E404A_fwd	CAG CGG GTC CAG CGT TTG CAG GAA GCG GAA TTA AGC
R_E404A_rev	GTG CTT AAT TCC GCT TCC TGC AAA CGC TGG ACC CGC
Residues involved in cobalamin coordination (PIPE cloning into pET28aTEV)	
Orf7_fwd	CAG CCA TAT GGC AGA ATA TAA AGT TTT G
Orf7_rev	GCA CTC GAG TTA TTC TAC TGA AGG AAA TAG ATG
R_S398A_fwd	TGG CTT GTA ACT TGC GCC TGC **GCA** GCG GGT CCA GCG TTT GAA GGA AGC GG
R_S398A_rev	CCG CTT CCT TCA AAC GCT GGA CCC GC**T GC**G CAG GCG CAA GTT ACA AGC CA
R_S398C_fwd	TGG CTT GTA ACT TGC GCC TGC TGT GCG GGT CCA G**CG T**TT GAA GGA AGC GG
R_S398C_rev	CCG CTT CCT TCA A**AC G**CT GGA CCC GCA CAG CAG GCG CAA GTT ACA AGC CA

1.1 Deletion of the N-terminal Domain (Residues 1-100)

Table 11: PCR reaction mix for the deletion of the N-terminal domain of RACo.

Standard PCR reaction mix	Final concentration
Template	Variable, 2-10 ng
Fwd primer (5 µM)	0.5 µM
Rev primer (5 µM)	0.5 µM
dNTPs (10 mM)	200 µM
5-fold buffer for DNA Polymerase	1 fold
Phusion DNA Polymerase	1.0 units/50 µL PCR
Nuclease free water	Added to 50 µL

Table 12: Temperature programme for the deletion of the N-terminal domain of RACo.

Step	Temperature	Duration	
Initial Denaturation	98 °C	2 min	
Denaturation	98 °C	10 s	x35
Annealing	63 °C	10 s	
Extension	72 °C	22 s	

1.2 Active Site Mutants (QuickChange Method)

Table 13: Mutagenesis reaction mix used for the preparation of active site mutants of RACo.

Standard Mutagenesis reaction mix	Final concentration
Template	pPKCoDuet1-TEV, variable, 5 – 50 ng
Fwd primer (5 µM)	0.5 µM
Rev primer (5 µM)	0.5 µM
dNTPs (10 mM)	200 µM
10-fold buffer for DNA Polymerase	1 fold
PfuTurbo DNA Polymerase	2.5 units/µL
Nuclease free water	Added to final volume of 50 µL

Table 14: Temperature program for Quick Change Mutagenesis.

Step	Temperature	Duration	
Initial Denaturation	95 °C	0.5 min	
Denaturation	95 °C	0.5 min	x 12
Annealing	55 °C	1 min	
Extension	68 °C	6 min	
Final Extension	68 °C	10 min	

1.3 Mutation of Ser398 by combining PIPE cloning and QuickChange Method

Table 15: PCR reaction mix for the preparation of Ser398 mutants.

Standard PCR reaction mix	Final concentration
Template	Orf7, variable 1 and 5 ng
Fwd primer (5 µM)	0.5 µM
Rev primer (5 µM)	0.5 µM
dNTPs (10 mM)	200 µM
5-fold buffer for DNA Polymerase	1 fold
Phusion DNA Polymerase	1.0 units/50 µL PCR
Nuclease free water	Added to 50 µL

Table 16: Temperature programme used in the preparation of Ser398 mutants.

Step	Temperature	Duration	
Initial Denaturation	98 °C	30 s	
Denaturation	98 °C	10 s	x 25
Annealing	55 °C	30 s	
Extension	72 °C	1 min	
Final Extension	72 °C	10 min	

2. Cloning and Mutagenesis of CoFeSP

Table 17: Primers used in the cloning and mutagenesis of CoFeSP.

Primer	Sequence 5´→ 3
Deletion of C-terminal Domain of CfsA (PCR:Religate:Transform)	
acsCD_NM_fwd	GAA CAG AAA GTA ATC GTA TTG TAC ACG GCC
acsCD_MCNM_rev	TTA TTT CTG CGG GTC GGT GTA AAT GTT AAG T
Deletion of C-terminal Domain of CfsA (PCR:Religate:Transform)	
acsCD_MC_fwd	ATG CCA CCG GTA GCT TTA ATT AAA GTG GGT AAA G
pPKCD_rev	
Change in 4Fe4S-coordination (QuickChange Method)	
acsCD_C25P_fwd	GGT CAA CCA ACT **CCT** CTT GCT TTT GCC ATG CAA ATT GCC G
acsCD_C25P_rev	CGG CAA TTT GCA TGG CAA AAG CAA G**AG G**AG TTG GTT GAC C

2.1 Deletion of entire Domains of CfsA

Table 18: PCR reaction mix for the deletion of domains of CfsA.

Standard PCR reaction mix	Final concentration
Template	pPKCD, 1 and 10 ng
Fwd primer (5 µM)	0.5 µM
Rev primer (5 µM)	0.5 µM
dNTPs (10 mM)	200 µM
5-fold buffer for DNA Polymerase	1 fold
Phusion DNA Polymerase	1.0 units/50 µL PCR
Nuclease free water	Added to 50 µL

Table 19: Temperature program of the deletion of CfsA domains.

Step	Temperature	Duration	
Initial Denaturation	98 °C	2 min	
Annealing	68 °C	15 s	
Extension	72 °C	4 min	x 25
Final Extension	72 °C	10 min	

2.2 Site directed Mutagenesis of cysteines coordinating the [4Fe4S] cluster

Table 20: Mutagenesis reaction mix for [4Fe4S] cluster mutants.

Standard Mutagenesis reaction mix	Final concentration
Template	pPKCD, variable, 5 – 50 ng
Fwd primer (5 µM)	0.5 µM
Rev primer (5 µM)	0.5 µM
dNTPs (10 mM)	200 µM
10-fold buffer for DNA Polymerase	1 fold
PfuTurbo DNA Polymerase	2.5 units/µL
Nuclease free water	Added to final volume of 50 µL

Table 21: Temperature programme for mutagenesis of CoFeSP.

Step	Temperature	Duration	
Initial Denaturation	95 °C	1 min	
Denaturation	95 °C	0.5 min	
Annealing	55 °C	1 min	x 16
Extension	68 °C	9 min	

3. Statistics of Data collection and refinement of the RACo:CoFeSP complex

Table 22: Statistics of data collection and refinement of the complex structure. Highest resolution shell is shown in parenthesis

	RACo:CoFeSP complex
Data collection	
Space group	*P*1
Cell dimensions	
a, *b*, *c* (Å)	67.13, 128.18, 163.37
α, β, γ (°)	77.61, 82.25, 88.76
Resolution (Å)	30 – 2.53 (2.60 – 2.53)*
R_{sym}	0.092 (0.535)
I / sI	9.99 (2.60)
Completeness (%)	96.05 (88.26)
Redundancy	2.74 (2.70)
Refinement	
Resolution (Å)	30 – 2.53
No. reflections	168 978
R_{work} / R_{free}	0.2042 / 0.2559
No. atoms	40 235
Protein	38 562
Ligand/ion	396
Water	1277
B-factors	
Protein	29.60
Ligand/ion	22.36 (B_{12}), 38.68 (4Fe4S)
Water	28.90
R.m.s. deviations	
Bond lengths (Å)	0.011
Bond angles (°)	1.29

B. Appendix Figures

1. Modified purification of RACo

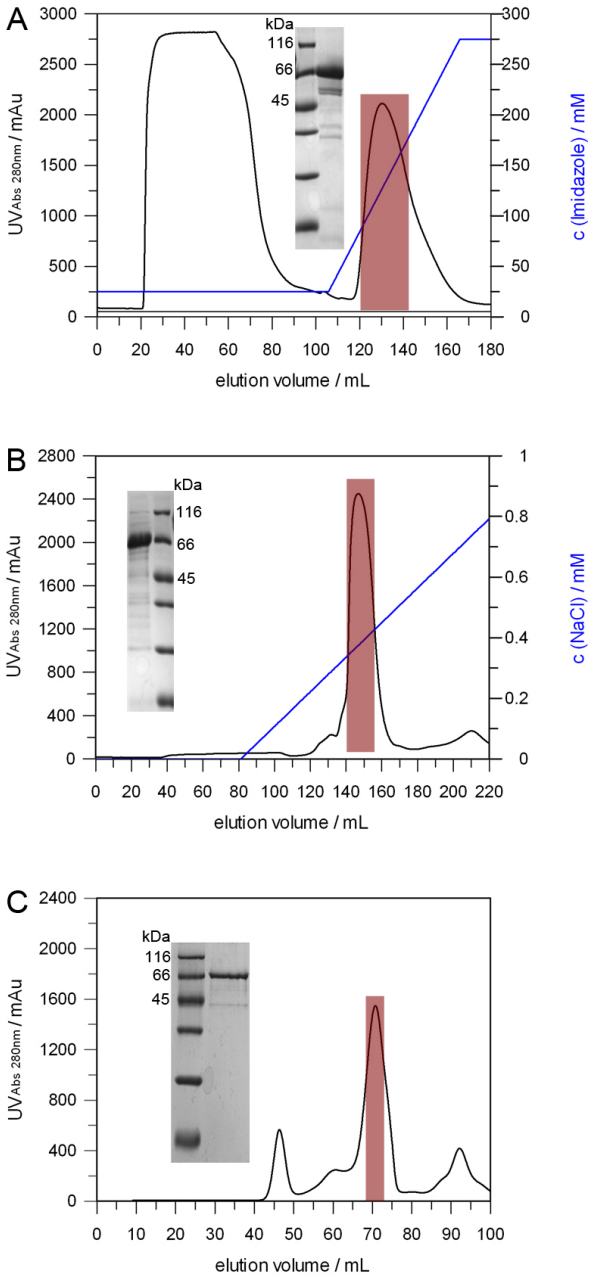

Figure 49: Chromatograms and SDS-PAGEs of the different purification steps of the modified RACo purification (Materials and Methods 2.1.2). (A) Elution profile of IMAC using Ni-SHP material and SDS-PAGE analysis of the pooled fractions (red box). (B) Chromatogram of the second purification step (IEC) and SDS-PAGE analysis of the combined fractions (red box). (C) After TEV-cleavage the fraction was loaded onto a S200 column for SEC. SDS-PAGE analysis of the final protein fraction is shown.

2. Standard curve used for the MGAM assay

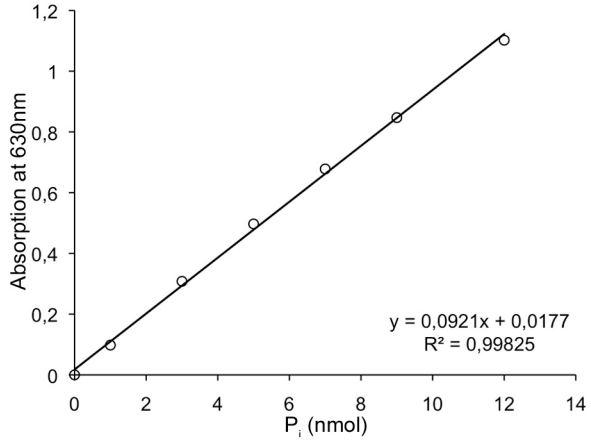

Figure 50: Standard curve for the calculation of the amount of released inorganic phosphate in the malachite green assay (Materials and Methods 6.1.1).

3. Standard curve used in analytical size exclusion chromatography

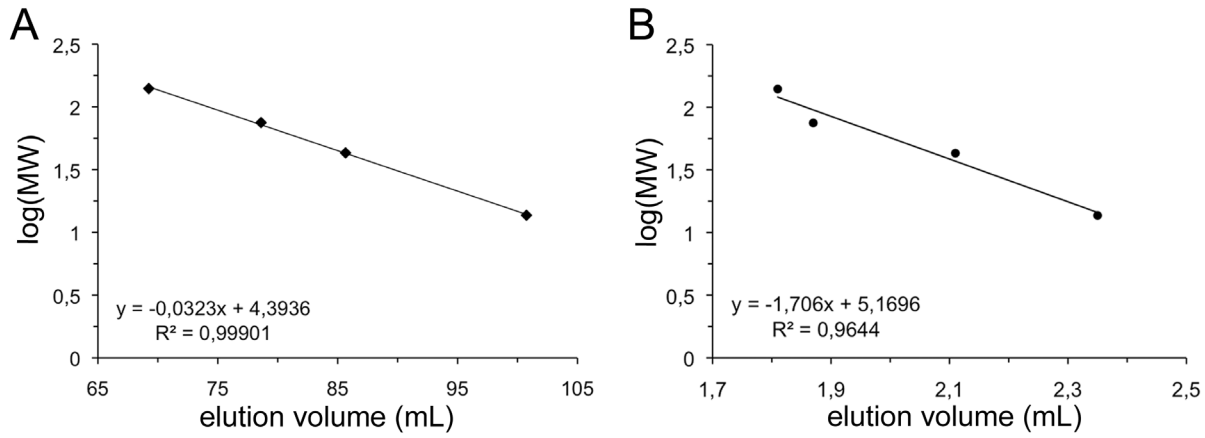

Figure 51: Standard curves used in analytical gel filtration (Materials and Methods 5.4). (A) Superdex^{TM} 200 prep-grade gel filtration column (120 mL, GE Healthcare). The logarithms of the molecular weights of several proteins were plotted against the corresponding elution volumes. As marker proteins 1 mg of Lactate Dehydrogenase (140 kDa, 69.2 mL), Conalbumin (75 kDa, 78.6 mL), Ovalbumin (43 kDa, 85.7 mL) and Ribonuclease (13.7 kDa, 100.7 mL) were loaded to the column and run in 50 mM Tris/HCl, pH 8.0, 150 mM NaCl, 2 mM DTT. (B) S200 5/150 (3 mL, GE Healthcare). As marker proteins 1 mg of Lactate Dehydrogenase (140 kDa, 1.81 mL), Conalbumin (75 kDa, 1.87 mL), Ovalbumin (43 kDa, 2.11 mL) and Ribonuclease (13.7 kDa, 2.35 mL) were loaded to the column and run in 50 mM Tris/HCl, pH 8.0, 150 mM NaCl, 2 mM DTT.

4. Dependency of the electron transfer rate on the ATP-concentration

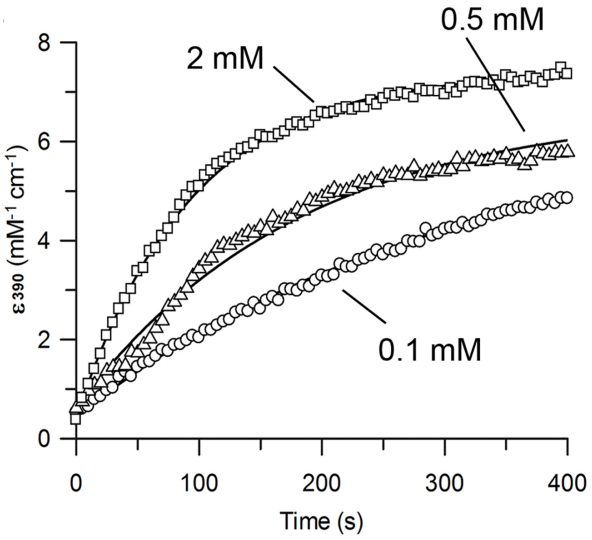

Figure 52: The rate of electron transfer depends on the ATP concentration. Observed rate constants for ET were determined by single-exponential fits were 0.089 min^{-1} with 0.1 mM ATP, 0.150 min^{-1} with 0.5 mM ATP, and 0.288 min^{-1} with 2 mM ATP.

VIII. LIST OF ABBREVIATIONS

Å	Ångström
ACS	Acetyl-CoA-Synthase
ADP	Adenosin-5´-diphosphate
AE	Activating Enzyme
APS	Ammoniumperoxodisulphate
ASKHA	Acetate and Sugar Kinases / Heat Shock protein 70/Actin
ATP	Adenosin-5´-triphosphate
BSA	Bovine serum albumin
Cb	Carbenicilin
CCP4	Collaborative Computational Project
Cfs	CoFeSP subunit
CODH	Carbonmonoxide Dehydrogenase
CoFeSP	Corrinoid/Iron-Sulfur Protein
CP	Corrinoid Protein
DEAE	Diethylaminoethyl
DT	Dithionite
DTT	Dithiothreitol
EPR	Electron Paramagnetic Resonance
ET	Electron Transfer
HEPES	4-(2-hydroxyethyl)-1-piperazine-ethanesulfonic acid
HIC	Hydrophobic Interaction Calorimetry
IEC	Ion Exchange Chromatography
IMAC	Immobilised Metal Affinity Chromatography
ITC	Isothermal Titration Calorimetry
k_{cat}	Catalytic rate constant
K_d	Dissociation constant
K_m	Michaelis constant
Km	Kanamycin
LB	Luria Bertani
MGAM	Malachite Green-Ammonium Molybdate
MetH	Methionine Synthase
MeTr / MT	Methyltransferase
mTB	modified Terrific Broth

NADH	Nicotinamide Adenine Dinucleotide, reduced form
NTP	Nucleoside-5´-triphosphate
OD_{600}	Optical density at 600 nm
Orf	Open Reading Frame
PAGE	Polyacrylamide gel electrophoresis
PCR	Polymerase chain reaction
PDB	Protein data bank
PEG	Polyethylene glycol
P_i	Inorganic phosphate
PIPE	Polymerase Incomplete Primer Extension
RACE	Reductive Activase of Corrinoid Enzymes
RACo	Reductive Activator of CoFeSP
r.m.s.d.	root-mean-square deviation
rpm	rotation per minute
RR	Resonance Raman
SDS	Sodium dodecyl sulphate
SEC	Size Exclusion Chromatography
SHE	Standard hydrogen electrode
SHP	Sepharose High Performance
TEMED	*N,N,N′,N′*-Tetra-methylethylenediamine
Tris	Tris-(hydroxymethyl)-aminomethane
U	Unit
UV-vis	Ultra-violet visible
v/v	volume per volume
w/v	weight per volum

IX. ACKNOWLEDGEMENTS

An erster Stelle danke ich Herrn Prof. Dr. Holger Dobbek, nicht nur für die Aufnahme in sein Labor und die Bereitstellung des spannenden Themas, sondern für das in mich gesetzte Vertrauen.

Prof. Dr. Erwin Schneider und Prof. Dr. Peter Hildebrandt möchte ich meinen Dank für die Übernahme der Gutachten aussprechen. Des Weiteren bedanke ich mich bei Prof. Dr. Thomas Eitinger, sowie bei dem Vorsitzenden der Prüfungskommission Prof. Dr. Christian Schmitz-Linneweber.

Dr. Jae-Hun Jeoung gilt mein ganz persönlicher Dank für die Einführung in das Thema und die Bereitstellung seiner Plasmide und Strukturdaten. Danke für die zahlreichen Diskussionen, Anregungen und die grenzenlose Unterstützung während der vergangenen vier Jahre.

Sebastian Götzl danke ich für die gemeinsamen PhD-Jahre und das Teilen seiner CoFeSP-Erfahrungen. Ein großes Dankeschön geht an Dr. Martin Bommer für seine Ideen rund um PIPE cloning und seine Geduld beim Versuch mir Kristallographie zu erklären. Danke für die regelmäßige Ablenkung vom Laboralltag in Form von Fahrradausflügen und Entdeckungstouren in und um Berlin.

Herzlicher Dank geht an Prof. Dr. Peter Hildebrandt, Dr. Friedhelm Lendzian und Wiebke Meister für die erfolgreiche(n) und entspannte(n) Kooperation(en).

Für das Korrekturlesen möchte ich mich bei Dr. Anja Pomowski und Dr. Jae-Hun Jeoung bedanken.

Herzlicher Dank geht an meine Laborkollegen Berta, Brinda, Christina, Jae-Hun, Jochen, Lilith, Martin, Olivia, Rainer, Sebastian, Silke, Stefan, Tobias, Tzong-Yuan und Yulia für die lockere Atmosphäre und die entspannte Zusammenarbeit. Ich werde die täglichen Kaffeepausen vermissen! Unvergessen bleiben zahlreiche Abendessen in wechselnder Runde. Olivia möchte ich für die herzliche Aufnahme und Einführung ins Bayreuther Labor und Leben danken.

Barbara Franke, Silke Steinborn, Rainer Dietrich, sowie den HiWis (Cornelia, Peer und Noam) danke ich für ihren Einsatz zum Überwinden von technischen und bürokratischen Hürden. Ein großes Dankeschön an Barbara für die selbstgebackenen Kekse, an Silke für die Versorgung mit hausgemachter Marmelade und an Rainer für das regelmäßige Auffüllen der Kaffee-und Gummibärchenvorräte. Ihr habt viele Tage versüßt!

Meinen Freunden: Dankeschön für eure aufmunternden Worte und die vielen unvergesslichen Momente, die wir teilen durften. Dankeschön an Caspar für die Unterstützung bei der Wohnungssuche in Berlin und das Weiterführen einer in Freiburg begonnen Tradition. Alma, Anja: Danke für euren Rückhalt und eure bedingungslose Freundschaft, die auch die große Entfernung überdauert!

Danken möchte ich meiner Familie, v.a. meiner Mutter, für die Unterstützung und Freiheit, die ich stets erfahren durfte. Un abrazo fuerte para mi familia española. Antonio, muchas gracias por todo.

X. SELBSTÄNDIGKEITSERKLÄRUNG

Hiermit erkläre ich, dass ich die vorliegende Arbeit selbstständig verfasst und keine weiteren als die angegebenen Hilfsmittel verwendet habe.

Berlin, den 16.12.2013 Sandra E. Hennig